EPRI | ELECTRIC POWER RESEARCH INSTITUTE

Low-Pressure Steam Turbine Corrosion Mechanisms and Interactions: State of Knowledge 2010



Low-Pressure Steam Turbine Corrosion Mechanisms and Interactions: State of Knowledge 2010

1020671

Final Report, July 2010

EPRI Project Manager
B. Dogan

DISCLAIMER OF WARRANTIES AND LIMITATION OF LIABILITIES

THIS DOCUMENT WAS PREPARED BY THE ORGANIZATION(S) NAMED BELOW AS AN ACCOUNT OF WORK SPONSORED OR COSPONSORED BY THE ELECTRIC POWER RESEARCH INSTITUTE, INC. (EPRI). NEITHER EPRI, ANY MEMBER OF EPRI, ANY COSPONSOR, THE ORGANIZATION(S) BELOW, NOR ANY PERSON ACTING ON BEHALF OF ANY OF THEM:

(A) MAKES ANY WARRANTY OR REPRESENTATION WHATSOEVER, EXPRESS OR IMPLIED, (I) WITH RESPECT TO THE USE OF ANY INFORMATION, APPARATUS, METHOD, PROCESS, OR SIMILAR ITEM DISCLOSED IN THIS DOCUMENT, INCLUDING MERCHANTABILITY AND FITNESS FOR A PARTICULAR PURPOSE, OR (II) THAT SUCH USE DOES NOT INFRINGE ON OR INTERFERE WITH PRIVATELY OWNED RIGHTS, INCLUDING ANY PARTY'S INTELLECTUAL PROPERTY, OR (III) THAT THIS DOCUMENT IS SUITABLE TO ANY PARTICULAR USER'S CIRCUMSTANCE; OR

(B) ASSUMES RESPONSIBILITY FOR ANY DAMAGES OR OTHER LIABILITY WHATSOEVER (INCLUDING ANY CONSEQUENTIAL DAMAGES, EVEN IF EPRI OR ANY EPRI REPRESENTATIVE HAS BEEN ADVISED OF THE POSSIBILITY OF SUCH DAMAGES) RESULTING FROM YOUR SELECTION OR USE OF THIS DOCUMENT OR ANY INFORMATION, APPARATUS, METHOD, PROCESS, OR SIMILAR ITEM DISCLOSED IN THIS DOCUMENT.

THE FOLLOWING ORGANIZATION, UNDER CONTRACT TO EPRI, PREPARED THIS REPORT:

DNV Columbus, Inc.

NOTE

For further information about EPRI, call the EPRI Customer Assistance Center at 800.313.3774 or e-mail askepri@epri.com.

Electric Power Research Institute, EPRI, and TOGETHER…SHAPING THE FUTURE OF ELECTRICITY are registered service marks of the Electric Power Research Institute, Inc.

Copyright © 2010 Electric Power Research Institute, Inc. All rights reserved.

Acknowledgments

The following organization, under contract to the Electric Power Research Institute (EPRI), prepared this report:

DNV Columbus, Inc.
5777 Frantz Road
Dublin, OH 43017

Principal Investigator
C. Scott

This report describes research sponsored by EPRI.

This publication is a corporate document that should be cited in the literature in the following manner:

Low-Pressure Steam Turbine Corrosion Mechanisms and Interactions: State of Knowledge 2010. EPRI, Palo Alto, CA: 2010. 1020671.

Product Description

Corrosion, corrosion fatigue (CF), and stress corrosion cracking (SCC) are known issues that affect the service lives of various low-pressure (LP) steam turbine components. Considerable work has been performed to understand the individual mechanisms and the environmental conditions that lead to each of them. However, little progress has been made in understanding the interactions between these damage processes. In particular, little is known about the transition of pits to cracks and the early stages of crack propagation.

Results and Findings

This report provides a summary of the most recent literature on corrosion mechanisms in LP steam turbines. The focus of the study is three main corrosion mechanisms (pitting, SCC, and CF) and interaction between these three mechanisms. Literature from various sources has been reviewed and summarized. Several case studies have been identified in the available literature, and these are also summarized. The literature review was followed with a gap analysis, during which several avenues for future research were identified.

Challenges and Objectives

The objective of the project is to provide guidance for the power generation industry's future research efforts on corrosion damage mechanisms and their interactions in LP steam turbine components.

Applications, Value, and Use

Several test programs have been proposed that would provide the industry with a better understanding of the corrosion and damage phenomena. It is expected that these will lead to better integrity management programs for the turbines and improved operations and maintenance protocols.

EPRI Perspective

The Electric Power Research Institute (EPRI) has taken a proactive approach to address an issue in the industry—corrosion mechanisms in LP steam turbine components. In particular, interactions of mechanisms occurring in service are reviewed. Although the well-characterized mechanisms of corrosion, CF, and SCC have already been reported by EPRI, better knowledge of the interactions between them that lead to pitting, crack initiation, and crack growth is needed.

EPRI is interested in continuing research on damage mechanisms and their interactions in an effort to predict corrosion damage and, ultimately, increase the service lives of the various steam turbine components. To initiate this work, it is necessary for the industry to evaluate the current state of knowledge.

Approach

The objective of the report is to provide guidance for the power generation industry's future research efforts on corrosion damage mechanisms and interactions in LP steam turbine components. The first task was a review of the most recent available literature on corrosion mechanisms in LP steam turbines. The literature was critically reviewed and summarized. A gap analysis was performed, during which several avenues for future research were identified. Several test programs were proposed that would provide the industry with a better understanding of steam turbine corrosion and damage phenomena.

Keywords

Corrosion
Corrosion fatigue (CF)
Pitting
Pit-to-crack transition
Steam turbine
Stress corrosion cracking (SCC)

Contents

1 INTRODUCTION 1-1
1.1 Acronyms, Abbreviations, and Symbols 1-3

2 LITERATURE REVIEW 2-1
2.1 Design Considerations 2-1
2.2 Steam Turbine Components 2-2
2.2.1 Rotors and Disks 2-3
2.2.2 Blades 2-6
2.3 Steam Turbine Materials 2-8
2.3.1 Carbon Steels 2-8
2.3.2 Stainless Steels 2-8
2.3.3 Nonferrous Materials 2-11
2.4 Corrosion Mechanisms 2-11
2.4.1 Pitting 2-11
2.4.2 Stress Corrosion Cracking 2-13
2.4.3 Corrosion Fatigue 2-17
2.4.4 Erosion and EC 2-21
2.4.5 Interaction of Corrosion Mechanisms 2-21
2.5 Steam Turbine Environments 2-22
2.5.1 Temperature and Pressure 2-23
2.5.2 pH 2-23
2.5.3 Oxygen 2-26
2.5.4 Steam Chemistry 2-30
2.5.5 Impurities and Additives 2-35
2.5.6 Static and Dynamic Loading 2-37
2.6 Pit-to-Crack Transitions (Experimental) 2-38
2.7 Pit-to-Crack Transitions (Modeling) 2-41
2.8 Case Studies 2-51
2.8.1 An Investigation of the Failure of LP Steam Turbine Blades 2-52
2.8.2 Turbine Blade Failure in a Thermal Power Plant 2-53
2.8.3 CF Phenomena Learned from Failure Analysis 2-54
2.8.4 Failure Analysis of the Final Stage Blade in Steam Turbine 2-57
2.8.5 Erosion-Fatigue of Steam Turbine Blade 2-58

3 GAP ANALYSIS 3-1

4 PROPOSED TEST PROGRAMS 4-1
4.1 Program One 4-1
4.2 Program Two 4-2
4.3 Program Three 4-2
4.4 Other Considerations 4-3

5 SUMMARY AND CONCLUSIONS 5-1

6 REFERENCES 6-1
6.1 In-Text References 6-1
6.2 Bibliography 6-4

List of Figures

Figure 1-1 A typical tandem compound, single reheat, condensing turbine 1-1

Figure 1-2 Distribution of blade failures in U.S. fossil turbines by row 1-2

Figure 2-1 Three types of rotor construction 2-4

Figure 2-2 Typical locations and orientations of SCC found in LP turbine disks 2-5

Figure 2-3 Typical locations of disk rim cracking 2-5

Figure 2-4 Types of blade root attachments 2-6

Figure 2-5 Typical locations of cracking and localized corrosion on LP turbine rotating blades 2-7

Figure 2-6 SCC growth rates as a function of reciprocal temperature for generator rotor ring steel in water and NaCl solution 2-10

Figure 2-7 SCC growth rates as a function of reciprocal temperature for P900 steels in service 2-10

Figure 2-8 The crack tip electrochemistry for SCC 2-14

Figure 2-9 A typical curve showing CGR versus stress intensity 2-16

Figure 2-10 Stress corrosion behavior of NiCrMoV disk steel vs. yield strength for "good" water and steam 2-16

Figure 2-11 CF (Goodman) diagram for NiCrMoV disk steel tested to 108 cycles 2-18

Figure 2-12 CF (Goodman) diagram for three stainless steel blading alloys 2-19

Figure 2-13 Comparison of S-N curves for UNS S45000-H900 in different environments 2-20

Figure 2-14 Comparison of FCGR curves for UNS S45000-H900 in different environments ... 2-20

Figure 2-15 The measured and calculated CGR as a function of the bulk solution pH at 150°C 2-25

Figure 2-16 The solution conductivity at 150°C as a function of acetic acid concentrations 2-26

Figure 2-17 Elongation of the 3.5NiCrMoV steels as a function of dissolved oxygen tested in water at 150°C with a strain rate of 1 x 10^{-7}/s 2-28

Figure 2-18 Response of corrosion potential to oxygen concentration transients simulating two-shifting operating conditions with pure water for both off-load and on-load chemistry 2-29

Figure 2-19 Response of corrosion potential to oxygen concentration transients simulating two-shifting operating conditions with pure water for the off-load aerated phase and deaerated 300 ppb Cl- solution for the on-load phase 2-30

Figure 2-20 Cross-section of an LP turbine with the locations of moisture formation and deposits 2-31

Figure 2-21 Mollier diagram with LP steam expansion line and thermodynamic regions for impurity concentration and corrosion mechanisms 2-32

Figure 2-22 Crack tip potentials as a function of calculated corrosion potential in neutral NaCl solution 2-33

Figure 2-23 Effect of bulk oxygen concentration on both crack tip and corrosion potentials in Cl- solution at 90°C (K = 40 MPa√m) 2-34
Figure 2-24 Effect of bulk oxygen concentration on both crack tip and corrosion potentials in SO_4^{2-} solution at 90°C (K = 40 MPa√m) 2-34
Figure 2-25 Plot of factor effects with the 95% confidence intervals 2-36
Figure 2-26 Effect of test environment on the fatigue life and cycles to crack initiation at 448 MN/m^2 (65 ksi) 2-39
Figure 2-27 Number of cycles to failure and number of cracks per unit area versus steady-state corrosion potential for Type 403 stainless steels 2-39
Figure 2-28 Aspect ratio of pits as a function of pit depth on the self-loaded specimens tested in aerated 1.5 ppm Cl- solution at 90°C for 9187 h 2-41
Figure 2-29 History of the nucleation and propagation of corrosion damage 2-43
Figure 2-30 Structure of algorithm for prediction of damage function 2-44
Figure 2-31 Calculated concentrations of species down a crack 2-45
Figure 2-32 The effect of loading frequency, f, on crack propagation rate for different corrosion potentials in 0.6 M NaCl with pH = 8 at T = 25°C (77°F) 2-45
Figure 2-33 The effect of loading frequency, f, on crack propagation rate for different bulk concentrations of NaCl with pH = 8 at T = 25°C (77°F) and E_{corr} = -690 mV (SCE) 2-46
Figure 2-34 Pit (P) and crack (C) shapes 2-47
Figure 2-35 The mean depth of the deepest pit as a function of time for 403 stainless steel and 470/471 steel 2-48
Figure 2-36 Calculated failure probability for LP steam turbine blades from CF as a function of different oxygen concentrations in the electrolyte film during the shutdown period 2-49
Figure 2-37 Calculated failure probability for LP steam turbine blades from SCC as a function of different oxygen concentrations in the electrolyte film during the shutdown period 2-49
Figure 2-38 Comparison of integral damage function with that measured on a failed blade from the field 2-50
Figure 2-39 Likelihood of cracks developing from pits as a function of depth for 3NiCrMoV disk steel 2-51
Figure 2-40 The assembly of the blade without the lacing wire that was removed by debrazing 2-52
Figure 2-41 The nature of crack growth behavior 2-53
Figure 2-42 Fraction of intergranular fracture surface vs. K_{max}, aerated 3% NaCl aqueous solution 2-55
Figure 2-43 CF crack initiation and propagation process in association with corrosion pits in 3% NaCl aqueous solutions 2-56
Figure 2-44 General view of two cracked blades (viewed from the LP side), revealing severe plastic deformation and missing material 2-58

Figure 2-45 Detail of two types of severe superficial roughness that were observed on the LP side of the blades 2-59

List of Tables

Table 2-1 A summary of components, materials, and corrosion issues..... 2-2

1 Introduction

Steam turbines are major components in electrical power generating stations. The steam turbine is an efficient engine for converting heat into mechanical energy. Expansion of steam as it cools exerts force on the turbine blades, causing the rotor to turn. The mechanical energy from the turning rotor is then converted into electrical energy through the generators.

Modern turbines vary in size from a capacity of a few kilowatts to approximately 1500 MW. The larger turbines consist of several stages—the high-pressure (HP), intermediate-pressure (IP), and low-pressure (LP) turbines (see Figure 1-1). Steam from the steam generators and the main line enters the HP turbine through stop and control valves and produces mechanical energy in the HP rotor. If a reheater is present in the system, the steam then exits the HP turbine through the cold reheat piping and is re-heated. The reheated steam enters the IP turbine, where more mechanical energy is produced. Finally, the steam enters the LP turbine, where the energy and pressure are further reduced and the steam begins to condense. The now wet steam exits the LP turbine through the exhaust and enters the condenser. The steam cycle then continues as the water is returned to the steam generators.

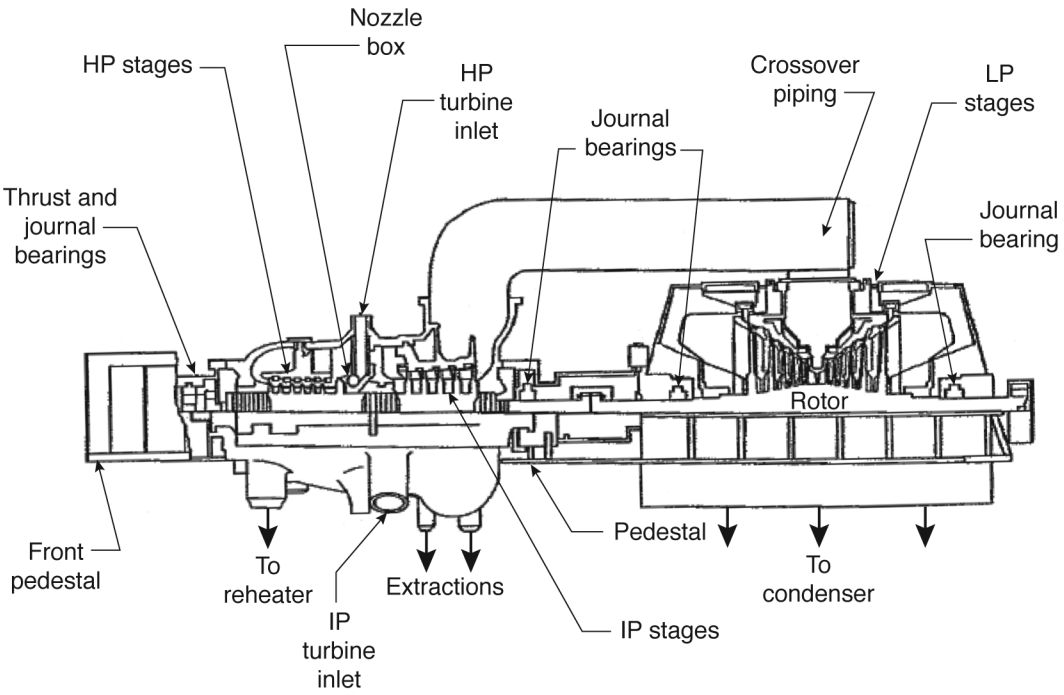


Figure 1-1
A typical tandem compound, single reheat, condensing turbine (The LP turbine of interest is shown on the right.) [1, 2]

The focus of this work is the LP turbine. During the final stages of energy extraction in the LP turbine, the steam pressure and temperature are reduced so that the steam becomes wet. This region in the LP turbine was originally referred to as the *Wilson line*. However, continuing work has shown that the Wilson line is not a defined region in the turbine, and now the region is typically referred to as the *phase transition zone* (PTZ). The region is typically in the last few rows of blades in the turbine, that is, rows L0 and L1 (see Figure 1-2). The moisture present is known to contribute to corrosion issues that are not applicable to the other parts of the turbine.

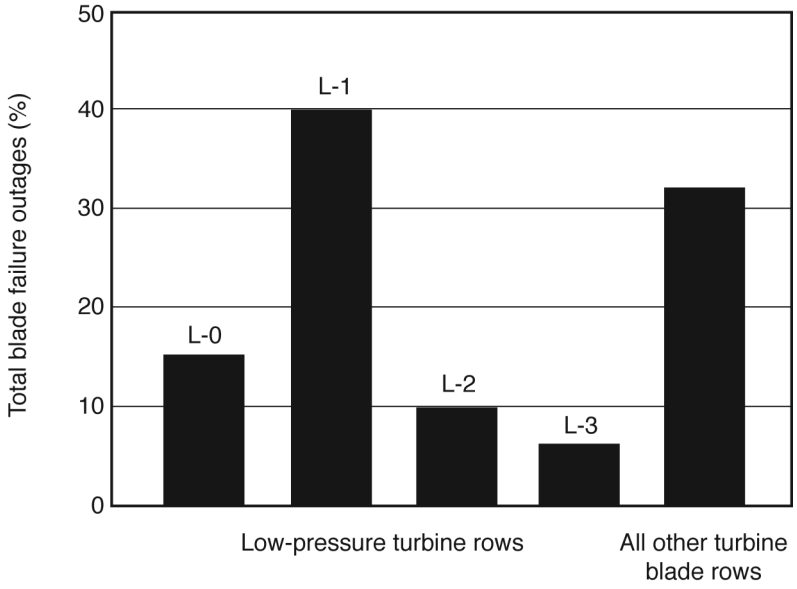


Figure 1-2
Distribution of blade failures in U.S. fossil turbines by row [1, 2]

Several corrosion mechanisms are relevant to the LP turbine, including pitting, stress corrosion cracking (SCC), corrosion fatigue (CF), erosion-corrosion (E-C), and flow-accelerated corrosion (FAC). The mechanisms of concern for any individual component in the turbine are dependent on the materials of which the component is made, its corrosion resistance, the load experienced by the components, and the specific environment. Different materials have varying susceptibility to corrosion in the different environments, and material choices are made accordingly during the turbine design. However, changing conditions and upsets during the life of the turbine can lead to some unexpected corrosion issues that require attention.

LP steam turbines consist of many components. Some of these are more susceptible to corrosion than others because of their construction materials and the specific loading and environments to which they are subjected. The components of specific interest to this work are blades, disks, and rotors; these are the components whose failures lead to the most significant financial losses. The majority of literature identified and reviewed during the course of this work related to these components. Other components in the LP steam turbine are susceptible to various forms of corrosion, but their failures cause less significant damage.

The primary materials used for the blades, disks, and rotors are Cr-Mo-V and Ni-Cr-Mo-V low-alloy steels and stainless steels, particularly 400 series martensitic grades. These materials are used because of their strength and corrosion resistance. However, under certain operating, upset, or outage conditions, the materials can become susceptible to pitting, SCC, and CF. Other materials are used less commonly—for example, 300 series stainless steels for stationary blades and expansion bellows, super-austenitic stainless for blades, titanium alloys for blades and shrouds, and nickel alloys for bolts and expansion bellows.

LP turbine materials are subject to various aggressive environments. Although steam is typically very pure, inadvertent trace impurities or additives can contribute to significant corrosion damage. Pure waters used for power generation typically have less than 50 parts per billion (ppb) impurities, total. Species of concern include chlorides, fluorides, sulfates, carbonates, hydroxides, organic and inorganic acids, and carbon dioxide. In addition, oxygen plays an important role in the corrosion mechanism and must be carefully controlled.

A 1998 survey [3] estimated that the cost of corrosion in U.S. fossil power plants was in the order of $4.6 billion. Of this, approximately $600 million was attributed to SCC and CF issues, $360 million was attributed to oxide particle erosion, and more than $140 million was attributed to copper deposition in LP steam turbines. Corrosion of turbine blades, disks, and rotors can cause catastrophic failures and force unplanned outages. These are considered low-frequency, high-impact events: although they rarely happen, the time and funds required to repair the damage combined with lost production time can cost more than $100 million for a station. For this reason, the U.S. and international power industries have invested considerable funds in research aimed at better understanding and preventing these failures.

The objective of the work described in this report is to evaluate the current state of knowledge of corrosion mechanisms in LP steam turbines. Based on the current state of knowledge, a gap analysis is performed that identifies avenues for future research. Of particular interest is the interaction between the various corrosion mechanisms and pit-to-crack transitions. Considerable research has been performed on individual corrosion mechanisms, but less effort has been invested in identifying interactions between them. If common environmental conditions are known to lead to multiple or synergistic damage mechanisms, research can be funded to mitigate the associated issues and interactions. If pit-to-crack transitions were better understood and could be more reliably predicted, efforts could be made to mitigate SCC and CF issues.

The ultimate goal of the work is to provide guidance to industry participants that helps prevent catastrophic failures in LP turbines, extends the service lives of existing power stations, and contributes to the design and operation of future power stations.

1.1 Acronyms, Abbreviations, and Symbols

AISI	American Iron and Steel Institute
ASM	American Society of Metals
ASTM	ASTM International (formerly the American Society for Testing and Materials)
CF	corrosion fatigue
CGR	crack growth rate
cm	centimeter(s)

DFA	damage function analysis
DFAM	damage function analysis model
EAC	environmentally assisted cracking
E-C	erosion-corrosion
EDS	energy dispersive X-ray spectroscopy
EPRI	Electric Power Research Institute
ETA	ethanolamine
EVS	Extreme Value Statistics
FCGR	fatigue crack growth rate
HCF	high cycle fatigue
HP	high-pressure
Hz	hertz
IP	intermediate-pressure
KI	stress intensity—in this case, Mode I crack opening
KISCC	threshold stress intensity for stress corrosion cracking
ksi	kips per square inch
LCF	low cycle fatigue
LEFM	linear elastic fracture mechanics
LP	low-pressure
min	minute(s)
mm	millimeter(s)
MPa	megapascal(s)
mV	millivolt(s)
MW	megawatt(s)
NHE	normal hydrogen electrode
NPL	National Physical Laboratory (UK)
OT	oxygenated treatment
pH	a measure of acidity, equal to minus the decimal logarithm of the hydrogen activity in aqueous solution

ppb	parts per billion
ppm	parts per million
PTZ	phase transition zone
s	second(s)
SCC	stress corrosion cracking
SCE	saturated calomel electrode
SEM	scanning electron microscope
SSRT	slow strain rate test
ΔK_{th}	threshold change in stress intensity for corrosion fatigue
σ	stress
σ_{SCC}	threshold stress for stress corrosion cracking
µm	micrometer(s)
µS	microsiemen(s)

2 Literature Review

The project began with a review of available literature. The primary sources of information were corrosion science and corrosion engineering journals and corrosion conference proceedings available through NACE International. *PowerPlant Chemistry* also had several relevant articles, and the *Journal of Engineering Failure Analysis* provided several papers that served as the basis for the case studies presented in Section 2.8. And, finally, several Electric Power Research Institute (EPRI) technical reports and workshop proceedings were reviewed. The full list of papers and reports examined during the course of the literature review appears at the end of this report as Section 6.

A brief summary of corrosion mechanisms in steam turbines is available in the American Society of Metals' (ASM's) *ASM Handbook*, Volume 13C. This provides a fairly general overview of the corrosion mechanisms of interest, and it provided a starting point for this work. A recent 2003 EPRI report that considers corrosion in steam turbines provides more detailed information [1]. The present report provides much of that information, but an effort has been made to identify more recent developments that are available in the public literature. In addition, the objective of this work is a better understanding of the interaction of corrosion mechanisms and pit-to-crack transitions; therefore, more focus is placed on these topics where possible.

This report has been organized by the following categories: design considerations, turbine components, materials, corrosion mechanisms, steam turbine environments, pit-to-crack transitions, and failure case studies. For each topic, a general overview is provided, followed by a more detailed review of some of the more recent work (conducted within the last 10 years). More detailed information on specific researchers' work can be found in the references provided.

2.1 Design Considerations

The recognition of various corrosion mechanisms has led to changes in design of LP turbines over the years to minimize these issues. Five main design aspects have been identified as contributors to corrosion [1, 4], as follows:

- **Material selection**. A variety of materials is used for the different components of the LP turbine. In each case, the decision about which material to use depends on the mechanical as well as corrosion properties. Mechanical properties to consider include yield strength, creep, and fatigue resistance. Corrosion properties include corrosion resistance to service environments during both operation and layup periods.
- **Mechanical design**. LP turbine components must be designed to withstand operational stresses, including static and dynamic or vibration stresses. The mechanical design of the turbine will also influence the materials used for the construction. Engineers must consider the threshold stress and stress intensity for SCC and the fatigue limit and threshold stress intensity for CF.
- **Physical configuration**. Design of the various components often leads to unavoidable stress concentrations because of their shape or crevices between adjacent components. Stress concentrations can contribute to crack initiation and make these components susceptible to both SCC and CF. Crevices can allow impurities to concentrate and lead to corrosion issues. This can be a problem in disk bores and keyways.

- **Flow and thermodynamics**. Flow through the LP turbine must be well understood in order to avoid problems associated with vibrational stresses—in the blades, particularly. Flow excitation and resonance can contribute to fatigue susceptibility. The flow of steam through the turbine can also affect the thermodynamics of condensation and moisture formation, which in turn affects the accumulation of impurities.
- **Heat transfer**. The temperature of the various components affects condensation and re-evaporation of moisture on the various components, and therefore affects how salt impurities accumulate.

These considerations must be included in turbine designs. However, many power plants worldwide that are in service were possibly designed without all of these considerations in mind. The lessons learned from previous failures contribute to growth in collective knowledge. Various design considerations will be referred to in the following sections, particularly as these design considerations relate to corrosion mitigation.

2.2 Steam Turbine Components

Steam turbines are made up of hundreds of individual components. Each one has very specific design requirements based on function, loading, and the local service environment. A failure of any component could lead to loss of efficiency of the unit, damage, injury, or an unscheduled and expensive outage. The main components of an LP steam turbine are summarized in Table 2-1. Table 2-1 lists the components as well as common materials of construction and corrosion susceptibilities.

Table 2-1
A summary of components, materials, and corrosion issues [4]

Component	Material	Corrosion Mechanisms
Rotor	Forged Cr-Mo-V or Ni-Cr-Mo-V low-alloy steel	P, SCC, CF, E
Shell	Cast carbon or Cr-Mo-V low-alloy steel, fabricated carbon steel for LP components	SCC, E-C
Disks, bucket wheels	Forged Cr-Mo-V, Ni-Cr-Mo-V, or Ni-Cr-Mo low-alloy steel, 12 Cr weld repair	P, SCC, CF, E-C
Dovetail pins	Cr-Mo low-alloy steels, 5CrMoV, similar to ASTM A681 Grade H-11	SCC
Blades, buckets	12 Cr stainless, 15-5PH, 17-4PH, Ti6-4, PH13-8Mo, Fe-26Cr-2Mo	P, SCC, CF, E-C
Bucket tiewires	12 Cr stainless steels (ferritic and martensitic)	P, SCC, CF
Shrouds, bucket covers	12 Cr stainless, 15-5PH, 17-4PH, Ti6-4, PH13-8Mo, Fe-26Cr-2Mo	P, SCC
Stationary blades	Type 304 stainless steels, other stainless steels	SCC, SCC-LCF
Expansion bellows	Types 321 or 304 stainless steels, Inconel[1] 600	SCC, SCC-LCF

Note:
1 *Inconel* is a registered trademark of Special Metals Corporation.

Table 2-1 (continued)
A summary of components, materials, and corrosion issues [4]

Component	Material	Corrosion Mechanisms
Erosion shields	Weld-deposited or soldered Stellite[2] type 6B, hardened blade materials	SCC, E
Bolts	Incoloy[3] 901, Refactalloy 25, Pyromet[4] 860	SCC, SCC-LCF
Wet-steam piping	Carbon steel	E-C
Valve bushings and stems	13Cr-Mo and other stainless steels	P, OX

Notes:
2 *Stellite* is a registered trademark of Deloro Stellite Group.
3 *Incoloy* is a registered trademark of Special Metals Corporation.
4 *Pyromet* is a registered trademark of Carpenter Technology Corporation.

P = pitting, E = erosion, LCF = low cycle fatigue, OX = oxidation in steam

The great majority of literature identified during the course of this work involved blades, disks, and rotors. These components represent the core of the turbine. Expansion of steam in the unit puts pressure on the turbine blades, which causes the disk and rotor to turn. The turning rotor powers generators, which generate the electricity. Failure of any of these components can lead to an outage.

Much of the research work on LP steam turbine components was initiated following a catastrophic failure at the Hinckley Point Nuclear Plant in England in 1969. An off-line operational test was performed at speeds exceeding the design speeds. A catastrophic failure occurred in which the rotor shaft fractured in five places and three disks were thrown free from the unit. Although there were several workers in the vicinity, there were no casualties associated with the incident.

Investigation of the Hinckley accident concluded that the shrunk-on disks in the unit had suffered SCC. The material used was a 3% Cr-0.5% Mo mild steel. Relatively high phosphorous and sulfur contents and an inappropriate temper led to embrittlement of the material, and the material's susceptibility and corrosive environment led to SCC. The failure was believed to have initiated at a keyway crown in a shrunk-on disk. The corrosive component responsible was suspected to be NaOH in the steam, but this was not verified.

Extensive research on corrosion in steam turbines followed the Hinckley incident. Initial studies indicated that the problem was confined to larger units of more than 500 MW, with high disk-bore stresses in wet steam environments. However, a second major incident occurred in an IP turbine disk in 1987, also in the UK.

2.2.1 Rotors and Disks

Rotors and disks have been the focus of considerable attention following the Hinckley incident in 1969. There are three basic designs: the shrunk-on disk, the solid rotor, and disks welded to form the rotor (see Figure 2-1). The most common design is the solid rotor, which is machined from a single solid piece of metal. The shrunk-on disks have been shown to be more susceptible to SCC, whereas the solid rotor and welded designs do not appear to be as susceptible. There is no apparent effect of rotor and disk design on the susceptibility of blades to SCC or CF.

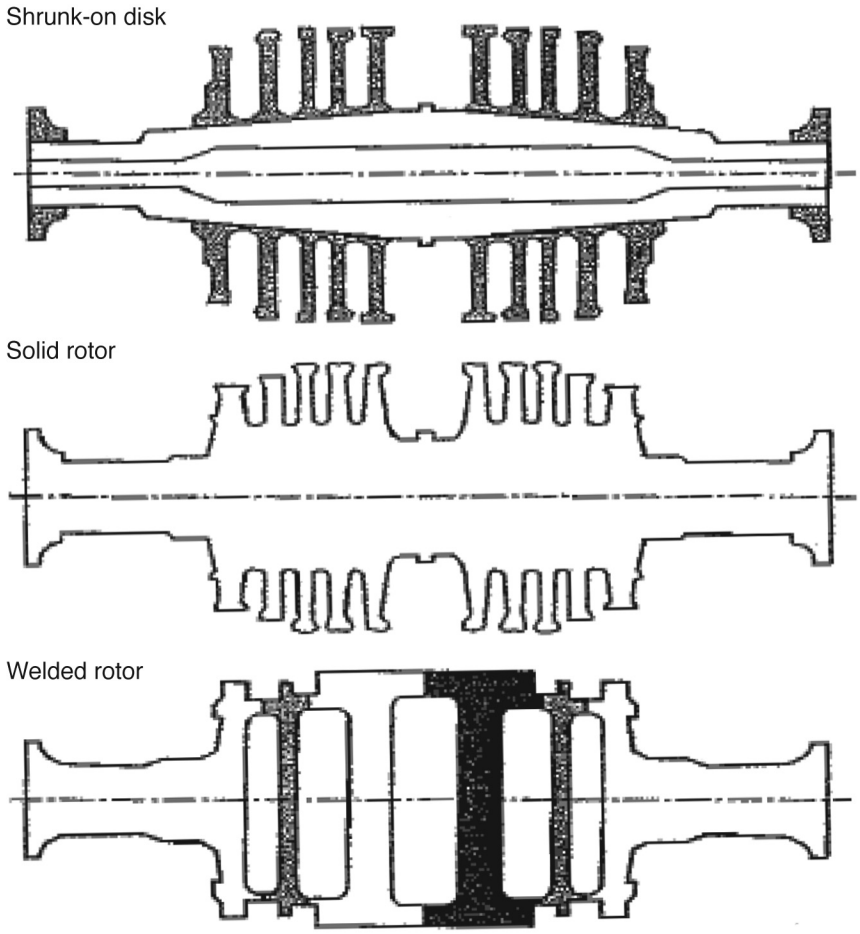


Figure 2-1
Three types of rotor construction [1, 5]

Rotors are typically constructed from ASTM A293 (Classes 2–5) or ASTM A470 (Classes 2–7) steels. The most common are 3.5 Ni-Cr-Mo-V. Shrunk-on disks are typically constructed from ASTM A294 (Class B or C) or ASTM 471 (Classes 1–3) steels. The rotors' steels require the strength and corrosion resistance to operate in the steam turbine environment, and these materials have been found to be appropriate. However, stronger steels are known to be more susceptible to SCC and CF, and strengths are now limited to approximately 130 ksi or less to avoid these issues. Allowable temperatures for these materials are limited to approximately 650°F (343°C) because the materials are susceptible to temper embrittlement.

Several locations on the disks have been observed to be susceptible to SCC (see Figure 2-2 and Figure 2-3). Each location is subject to different conditions of stress and environment, making corrosion management difficult. Some of the cracking problems can be solved by appropriate design of the disk and reduction of local stresses, and some problems can be solved by choosing the appropriate material. However, as with many engineering designs, there are compromises made and it is difficult to completely eliminate the cracking problems. Cracking has been observed near the keyway and shaft of the rotor, on the disk web, on the disk rim, and in the blade attachment areas. Orientations are both axial-radial and axial-circumferential.

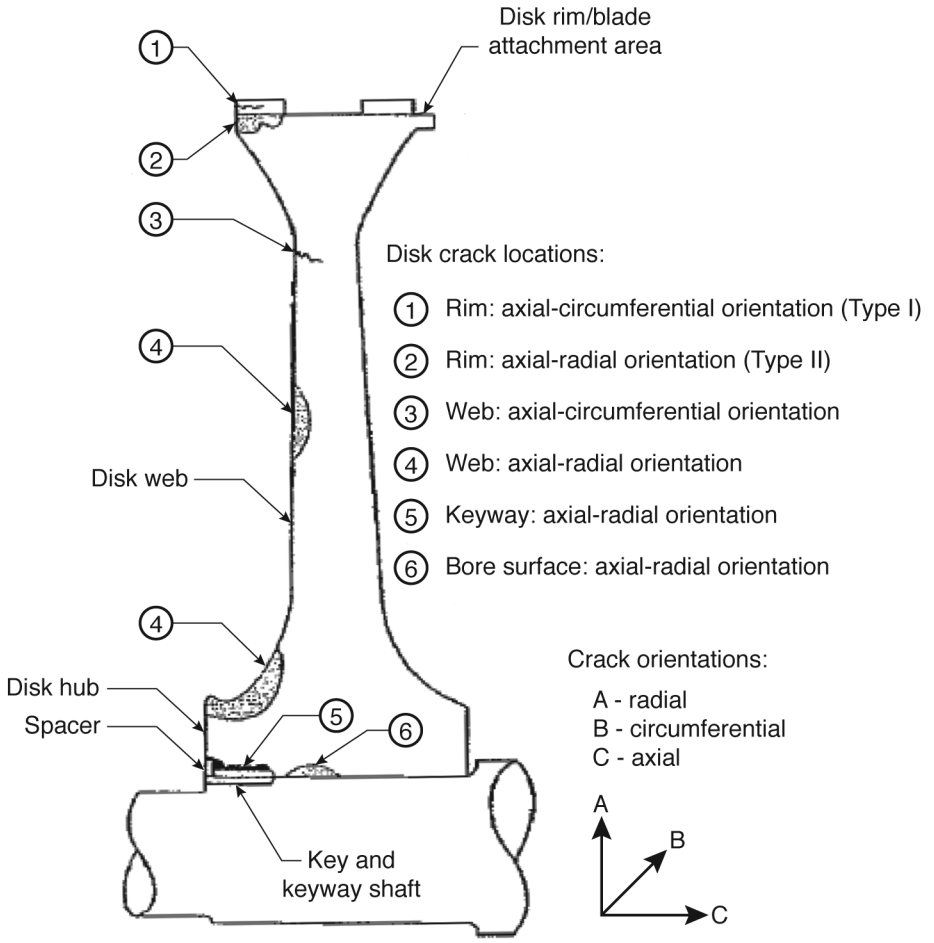


Figure 2-2
Typical locations and orientations of SCC found in LP turbine disks [1, 6]

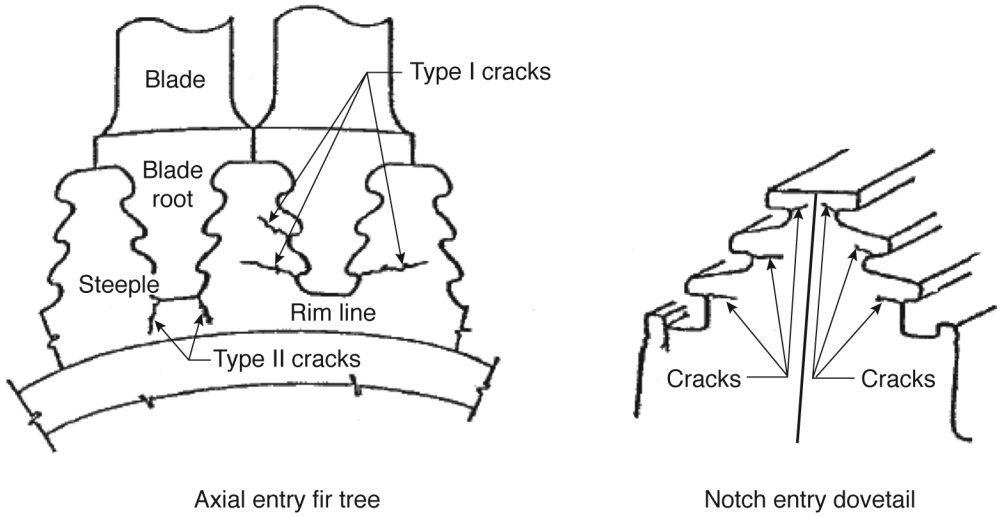


Figure 2-3
Typical locations of disk rim cracking [1, 6]

2.2.2 Blades

Like rotors and disks, there are several designs possible for turbine blades (see Figure 2-4). Differences are common in both the connection points and blade shapes.

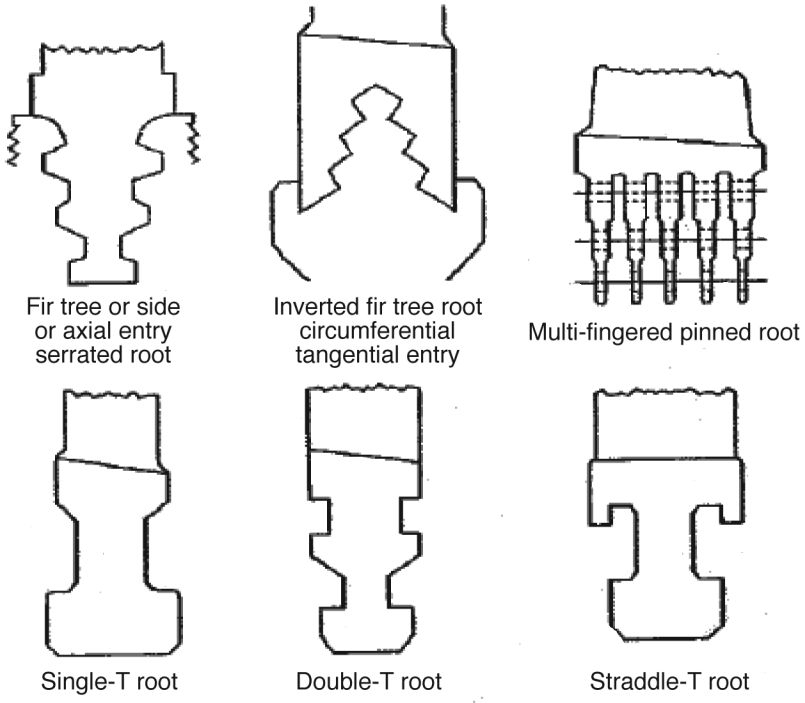


Figure 2-4
Types of blade root attachments [1, 5]

Blade roots are connected to disks by an interlocking structure such as a "fir tree" or a T-shape. The blades fit into slots in the disks that can be either axial or circumferential, depending on the design. The connection points tend to be susceptible to SCC and CF due to the stress concentrations associated with the slots' geometries. Figure 2-5 shows typical locations of SCC and CF in LP turbine blades.

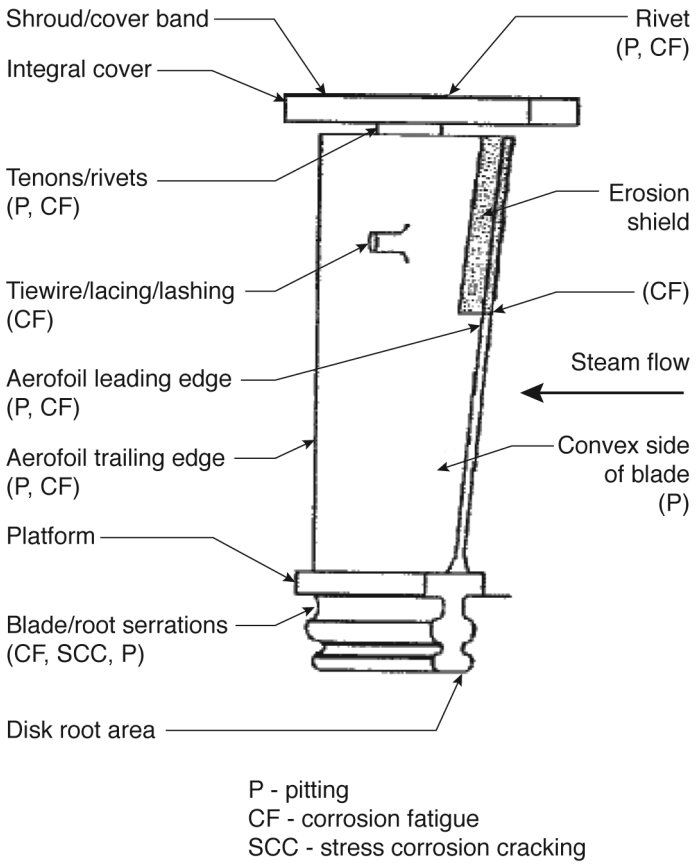


Figure 2-5
Typical locations of cracking and localized corrosion on LP turbine rotating blades (SCC and CF cracking have also occurred in the tiewire holes.) [1, 5]

Blades can be freestanding, or their tips might be continuously connected by a shroud. The connections to the shrouds might consist of tenons that are riveted to shrouds. This allows impurities to concentrate and can lead to localized corrosion issues. Another design involves forged or machined stubs that press against each other during operation and prevent vibration. This design avoids some of the corrosion issues.

Blade shape is important to operation of the turbines. The shape determines the aerodynamic behavior and flow of steam within the turbine, and this contributes to overall turbine efficiency. Shorter blades tend to be of a constant cross-section. Longer blades tend to be of varying cross-section and/or twisted to maximize efficiency. If not designed correctly, blades can suffer from vibration, which can lead to CF. Longer blades are often connected together by lashing wires to reduce the vibration. Blades can be mix-tuned so that adjacent blades do not lead to development of resonant frequencies.

Most turbine blades are constructed from 12 Cr stainless steels—typically, American Iron and Steel Institute (AISI) 403, 410, and 422. Other grades of stainless steels have been used for turbine blades, but there tend to be problems associated with welding or post-weld heat treatments; pitting is also frequently associated with selective dissolution of alloying elements. Titanium alloys, such as Ti-6Al-4V, have been used in the final stages of LP turbines where the environment is wet and there is higher corrosion and erosion susceptibility. Titanium alloys tend to cost more and are more difficult to machine.

2.3 Steam Turbine Materials

2.3.1 Carbon Steels

The material responsible for the failure in the Hinckley unit was 3% Cr-Mo steel. This material has since been demonstrated to have an adverse combination of high strength and poor fracture toughness. Nickel has long been known to increase toughness and decrease impact transition temperatures. It is now recognized that nickel does improve both toughness and resistance to SCC, which explains the development and continued use of 3% Ni-Cr-Mo-V steels. However, although providing some benefits for resistance to SCC, yield strength remains a key parameter in determining susceptibility.

The development of "superclean" steels was expected to further improve resistance to SCC of 3% Ni-Cr-Mo-V alloys by decreasing the number of inclusions that can initiate cracks. However, no significant improvement was observed. In some cases, there were improvements noted in crack initiation but little difference in crack growth rates (CGRs). Testing by Holdsworth and Magdowski and Speidel demonstrated no significant improvement in CGRs [7, 8]. This was attributed to a creep susceptibility in the material at just 95°C. In some cases, initiation resistance was found to be inferior to that of conventional steels of comparable strength. Lyle reported initiation times in the order of 70% of those of conventional steels. Cracks initiated at grain boundaries rather than pits, which was attributed to an oxygen-depleted zone under a crevice corrosion film.

Studies by Holdsworth et al. [7] and Denk [9] reported differences in crack initiation mechanisms in 3% Ni-Cr-Mo-V steels with different yield strengths. The lower-strength steels (<850 MPa) tended to crack near corrosion pits; the higher-strength steels tended to crack at grain boundaries through a film rupture mechanism.

Tsuchiyama et al. [10] studied SCC in 3.5% Ni-Cr-Mo-V steels in carbonated pure water at temperatures up to 157°C. Of particular interest was the role of phosphorous and niobium additions on SCC resistance in both sulfate and phosphate solutions. They performed a series of U-bend tests, slow strain rate tests (SSRTs), Auger electron spectroscopy of fracture surfaces, and electrochemical tests. The electrochemical tests involved a potential-jump method in which a sample was initially cleaned by cathodic reduction at -1300 mV (saturated calomel electrode [SCE]), then the potential jumped to -500 mV (SCE) and the anodic decay currents were measured.

The work concluded that SCC resistance is improved by reducing phosphorous at grain boundaries and thereby decreasing the susceptibility to intergranular SCC. It was also reported that increased niobium content in the steel improves SCC resistance. One hypothesis was that increased niobium results in increased carbide formation in the steel, which then results in grain size reduction. The enlarged grain boundary area results in a lower density of the detrimental phosphorous. The Tsuchiyama work also demonstrated that a phosphate content of more than ~100 parts per million (ppm) significantly increases the passivation rate of a freshly corroding surface, and this has implications on SCC rates when the film rupture model is considered.

2.3.2 Stainless Steels

Ferritic and martensitic stainless steels are used as materials for steam turbine components, including blades, shrouds, and disk weld repairs. The common grades include AIS 403, 410, and 422. Type 422 has poorer resistance to SCC and CF than the 403 and 410, and this must be considered in the design. The ferritic steels are preferred over austenitic materials, which have lower thermal conductivity, higher thermal expansion coefficients, and higher density. In addition, the use of austenitic steels can lead to galvanic corrosion issues caused by dissimilar welds. Recent research on 10–12% Cr ferritic steels has been aimed at increasing high-temperature creep properties.

Austenitic stainless steels are used for secondary components in the steam turbine, such as stationary blades and expansion bellows. Grades used include 304 and 321. These grades might be susceptible to SCC in some environments and subject to LCF conditions.

Considerable work has been done to better understand the kinetics of steam oxidation of ferritic stainless steels [11]. Most of this work has been performed at temperatures of approximately 1000–1500°F (538–816°C) for steam generator components and higher-pressure, higher-temperature steam turbine components. The oxidation kinetics are important to understand because they also affect pitting behavior in these alloys. Various studies have demonstrated that both linear and parabolic oxidation behavior are possible at these higher temperatures. In one study using 2.25% Cr alloy, an apparent change in rate law from parabolic to linear was observed after approximately 8000–10,000 hours of exposure. This indicates a change in oxide formation mechanism that should be considered.

It is known that carbon steels form two different oxides in air at temperatures up to approximately 1000°F (538°C). One is magnetite (Fe_3O_4) and typically forms as an inner layer at the metal-oxide interface. The second oxide is hematite (Fe_2O_3), and it forms at the oxide-air interface. In alloys containing chromium, the Cr forms a variable stoichiometry phase with the inner magnetite spinel. Diffusion of cations through the dense spinel structure is slow, and, therefore, the oxidation kinetics decrease. Increasing the Cr content 2–10% decreases the oxidation rate significantly. Higher levels of Cr can result in an extremely protective Cr_2O_3 layer on the steel. It has been suggested that silicon might contribute to the protective nature of the spinel oxides, though silicon can degrade the long-term creep resistance by accelerating carbide formation in the martensitic alloys.

If steam or water is present, a third oxide phase becomes possible—wustite (FeO). The wustite phase is intrinsically more porous than a magnetite structure, and so the oxide is less protective and supports higher oxidation rates. Studies have also indicated that the kinetics are not necessarily diffusion-controlled and that species are transported through the gas phase in the porous oxide scales.

Steam temperature can also affect oxidation kinetics. Two hypotheses have been put forward. The analysis of one group of researchers indicated that oxide formation follows a parabolic rate law above approximately 1000°F (538°C) and a linear rate law below that temperature. However, further examination by other researchers indicated an equally good statistical fit assuming linear kinetics for all temperatures. Given the uncertainty in the kinetics, complications in analysis because of thermal cycling in service, and the effect of impurities, it is not possible to make accurate and reliable predictions for turbine components.

Speidel and Magdowski [8] attempted to correlate laboratory and in-service data for a variety of SCC phenomena, including cracking in generator rotor retaining rings made from high-strength austenitic stainless steels. They studied SCC in a P900 cold-worked austenitic stainless steel containing 18% Cr, 18% Mn, and 0.6% N. The material was considered resistant to SCC in pure water up to 80°C. However, if the temperature were raised to 100°C or higher, or the steel were tested in 22% sodium chloride solution, CGRs in the order of 100 mm/year or higher were possible (see sample data in Figure 2-6). Speidel and Magdowski reported good agreement between maximum CGRs measured in the laboratory and those measured in service in the Perm, Rjasan, and Porto Tolle units (see data in Figure 2-7).

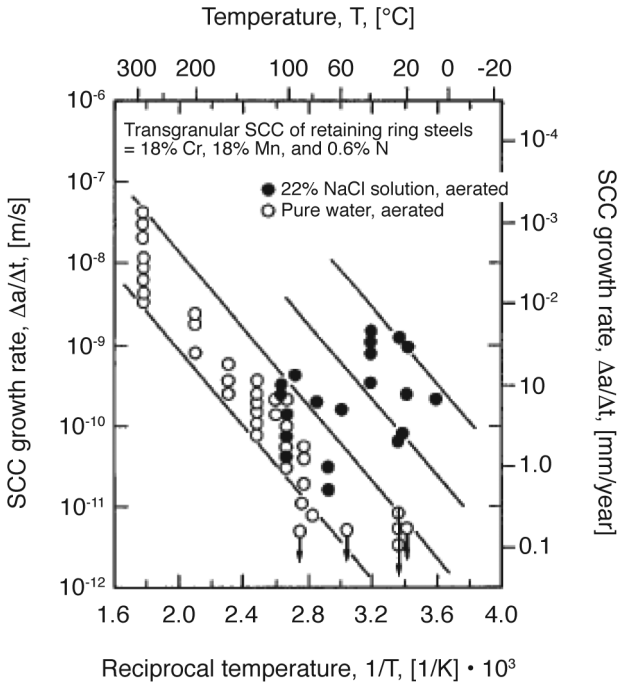


Figure 2-6
SCC growth rates as a function of reciprocal temperature for generator rotor ring steel in water and NaCl solution [8]
Used with permission from NACE International

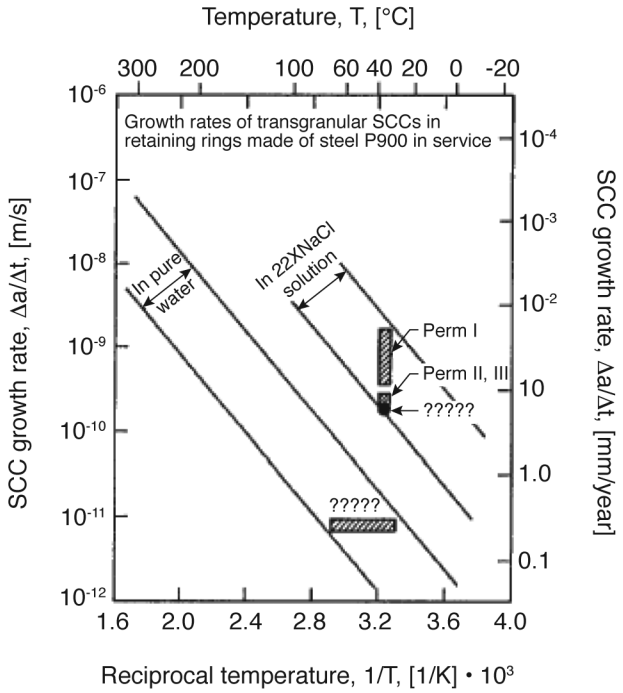


Figure 2-7
SCC growth rates as a function of reciprocal temperature for P900 steels in service [8]
Used with permission from NACE International

Work on Type 410 martensitic stainless steel has demonstrated a susceptibility to SCC in acidic hydrogen sulfide service [12]. Failure analysis following an impeller failure in a hydrogen recycle compressor indicated the importance of austenizing temperature and grain size on susceptibility to hydrogen-induced cracking and the need to test materials in conditions as close to in-service conditions as possible.

2.3.3 Nonferrous Materials

Nonferrous materials have found fewer applications to steam turbine components than have the ferrous materials. Titanium alloys, such as Ti-6Al-4V, have been used in the final stages of LP turbines, where the environment is wet and there is higher corrosion and erosion susceptibility. Titanium alloys have high strength and good corrosion resistance properties. The higher strength at low temperatures allows for their use as longer, last-stage blades. They have good resistance to impact and so are resistant to impact and water droplet erosion. Titanium alloys tend to cost more and are more difficult to machine.

Another alternative to stainless steels in high-temperature service is nickel alloys. The LP steam turbine operates at lower service temperatures, and the cost is not justified. Inconel 600 alloys have been used as expansion bellows.

2.4 Corrosion Mechanisms

The corrosion mechanisms operative on steam turbine components are determined by the materials of construction, the loading experienced by them, and the local corrosive environment. The corrosion mechanisms of most concern in steam turbines are pitting, SCC, CF, erosion, and FAC. These are covered in detail in the following sections.

Although several forms of corrosion have been identified, they are not necessarily operating independently. In some cases, one form of corrosion leads to another. For example, pitting can lead to crack formation and SCC, and erosion can lead to stress concentrations and CF. The interaction of mechanisms is a focus of this report. The few studies associated with these interactions are described in the following sections.

2.4.1 Pitting

Pitting corrosion is a form of localized corrosion attack of a material with an otherwise resistant surface. The number of pits forming on a given surface and their depth and morphology depend on the metallurgy of the material and the specifics of the local chemistry. Pits can be wide and shallow or deep and narrow. Pits can grow subsurface and undercut material. In many cases, the pits are hidden by corrosion products, and their nature is not recognized. Because it can lead to unpredictable failures, this is a particularly insidious form of corrosion.

Pitting corrosion is observed in passive film forming alloys and, in particular, stainless steels in steam turbine environments. Most metals form oxides readily in air environments. The nature of the oxide film that forms depends on the metal and the volume change associated with the oxidation transformation. In some cases, the volume change leads to spalling or cracking of the oxide layer. If the oxide detaches from the metal substrate, further oxidation occurs and the material degrades. In some cases, the volume change in the oxide layer is negligible and the oxide forms an adherent and protective passive film that protects the material from corrosion. Metals that form protective passive films include aluminum, titanium, and stainless steels. The chromium content in stainless steels improves the passivation characteristics of iron and leads to a more corrosion-resistant material.

The design of stainless steels takes advantage of the nature of oxide film formation by chromium alloying. Stainless steels consist of 13% or more chromium. This content allows an adherent chromium oxide film to form, which protects the alloy from general corrosion. In addition, this chromium content stabilizes the ferrite phase. If it is desired for an austenite phase to form a martensitic structure through heat treatments, the chromium content must be decreased or an austenite stabilizer such as nickel must be added.

Passive films can provide improved corrosion resistance to materials but can also make them susceptible to pitting corrosion. In the presence of environmental impurities, such as chlorides and sulfates, the passive films can break down locally. A concentration of these impurities in the defective passive film allows self-sustaining corrosion reactions to develop and a pit to form. Both chlorides and sulfates are known to be detrimental to passive film formation and stability. Because they are possible impurities in steam turbine environments, they are the focus of much research.

The initiation of a pit on a metal surface leads to self-sustaining corrosion reactions. The base of the pit becomes anodic and leads to further dissolution of the metal. The surrounding metal surface becomes cathodic, supporting the reduction of dissolved oxygen or other oxidizers. The pit geometry is sheltered and prevents easy mass transport of species between pit and surfaces, allowing the pit to acidify and further sustain the corrosion. The mechanism is similar to that observed in crevice corrosion.

Electrochemical potential is also a factor to be considered in the susceptibility of materials to pitting corrosion. A small positive potential applied to a metal will typically lead to passivation of the surface. However, if the potential applied exceeds the film breakdown or critical pitting potential, spontaneous pitting can occur. A subsequent decrease of the applied potential can allow the material to repassivate. The difference between the pitting and repassivation (or protection) potentials provides an indication of the sustainability of pits to continue growing. In general, the larger the difference between pitting and repassivation potentials, the greater the susceptibility for continued growth of the pits. A corrosion potential higher than the repassivation potential can also lead to pitting, even if it is less than the breakdown potential. It is also important to recognize that environmental conditions that lead to increased corrosion potential, such as increased oxygen content, can lead to pitting corrosion.

The critical pitting potential is affected by the environment and alloy chemistry. The presence of chlorides tends to increase current densities at all potentials and decrease the critical pitting potential, resulting in increased susceptibility. As chromium content of an iron alloy increases, so does the critical pitting potential, resulting in increased resistance. Manganese sulfide inclusions can also be considered to play a role in pit initiation. Preferential dissolution of the inclusion might lead to a crevice-like geometry and the development of a galvanic microcell. The details of the mechanisms are not fully understood. The specific chemistries of both the environment and the alloy must be considered in determining pitting susceptibility.

Pit growth rates are affected by a variety of factors, including pH, impurity species and concentration, and temperature. Higher concentrations of anions and temperature typically increase pitting growth rates. The higher anion concentrations increase moisture conductivity and support higher current densities and therefore higher corrosion rates. The higher temperatures typically increase rates because the corrosion reactions are thermally activated. If relative humidity reaches 60% and chlorides are present, the pit growth rate can be as quick as that in boiling deaearated sodium chloride solution.

For pits to propagate, both the anodic and cathodic electrochemical reactions must be sustained. The availability of oxidizers can limit the extent of pitting and the spacing of pits. In an environment where oxygen is limited, one would expect widely spaced pits. In an oxygen-rich environment, one would expect a closer spacing of pits because there is more oxygen available to sustain cathodic reactions on the metal surface.

Pitting growth rates typically are not sustained for long periods. As a result of the nature of the pit geometry and mechanism, pitting growth rates generally decrease with time. The growth rate kinetics are complex and subject to the details of the metal, the nature of the passive film, and the environment. For pitting in constant environmental conditions, parabolic rate behavior is expected. For pitting in changing conditions, such as during the startup and shutdown sequences in an operational steam turbine, the kinetics are difficult to predict.

Pitting does not necessarily lead to severe corrosion damage that affects the functionality of components. It can lead to a loss of efficiency by disrupting flow of steam through the turbine. Pitting of a component leads to a minor roughening of the material surface, and the roughness can disrupt steam flow across the surface and therefore disrupt the designed flow within the turbine. This can cause unexpected and detrimental stresses. If the stresses are vibratory, there can be further problems associated with fatigue.

A more significant problem associated with pitting is that a pit can transition into a crack if the stress is sufficient and environmental conditions are satisfied. A crack is then subject to SCC in statically loaded components or CF in dynamically loaded components. Load-bearing capacity and fatigue strength can be significantly reduced. These forms of corrosion can lead to catastrophic failures. The experimental and modeling work performed by EPRI and that described in the open literature are explored further in the following sections.

2.4.2 Stress Corrosion Cracking

SCC is a phenomenon whereby a material can fail at a stress well below its yield strength or with an applied stress intensity acting on a crack well below the typical toughness of the material. The applied stress and corrosion reactions combine synergistically and can result in a time-dependent failure. SCC requires three components to be active: a susceptible material, high stresses, and a corrosive environment. This mechanism was considered responsible for the Hinckley disk failure in 1969. Since then, various research has been performed to design against and mitigate problems associated with SCC. The conditions that tend to lead to SCC include high-yield- strength materials, high stresses, and high temperatures. There is now a tendency to design turbines using lower-yield-strength materials (<900 MPa [<130 ksi]) and to avoid stress concentrations, such as keyways and sharp dovetail designs. The original Hinckley failure was attributed to issues associated with the shrunk-on disks, and so now solid or welded rotors are favored in designs.

The SCC phenomenon is complex and not completely understood. Several mechanisms have been proposed, and some gained general acceptance by academia. Gaining complete understanding is difficult because mechanisms vary with material type and conditions—the mechanisms active in one system might not be applicable to another system. Some of the mechanisms believed to be responsible for SCC cannot be measured directly, and this leaves experimental results open to interpretation.

A generally accepted mechanism of SCC can be simplified as anodic dissolution of the crack tip and passivation of crack walls. A high applied stress initiates the process by locally rupturing the passive film on a metal surface. The bare metal that is revealed is then subject to anodic dissolution, which

extends the crack further. Environmental conditions allow the crack walls to repassivate. Film formed at the crack tip then ruptures, allowing the cycle to continue and the crack to propagate. A simplified schematic of the crack tip electrochemistry is given as Figure 2-8.

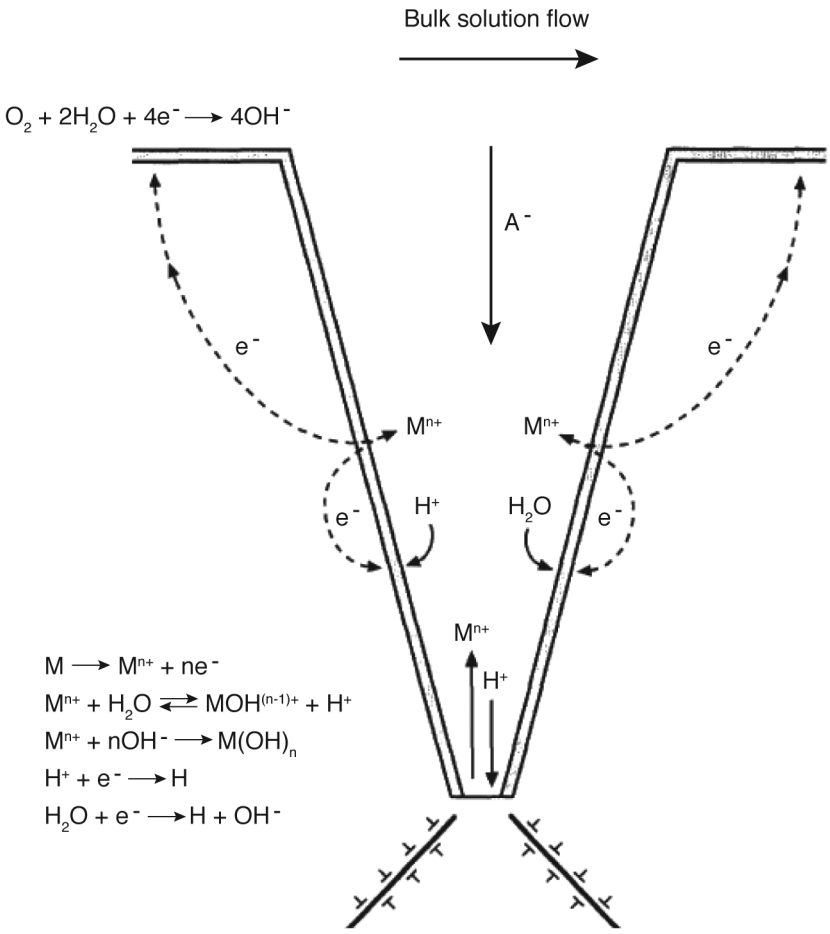


Figure 2-8
The crack tip electrochemistry for SCC [13]
Used with permission from NACE International

The conditions necessary for SCC are different from those necessary for general corrosion. A higher pH is typically required in order to ensure passivation of the crack walls and to allow the film rupture and repassivation to occur. This is the reason that steels are known to be susceptible to SCC in hydroxide environments, including steam turbines under certain conditions. A low pH would destabilize the passive oxide film, and the mechanism would not be operative. In this case, metal dissolution is more likely. There are examples of SCC in neutral pH environments in carbonate-bicarbonate environments. Note that when the SCC becomes active, a pH gradient is set up along the crack length that allows both crack wall passivation and crack tip dissolution.

SCC susceptibility is also dependent on electrochemical potential. Two potential ranges for cracking have been observed. In some cases, the potential range for SCC susceptibility is in the potential range between the passivation and pitting regions identified by polarization scanning. In some cases, the potential range coincides with an active-passive region. In these ranges, both crack tip dissolution and crack wall passivation are possible, allowing the SCC mechanism to become operative. Understanding of the potentials is important in understanding the susceptibility of materials to SCC in various environments. Applying a potential to move the system away from the susceptible potential range might be possible to prevent SCC. The variations in potential occurring in steam turbines during startup and shutdown operations make prevention and control of corrosion challenging.

Materials can be particularly susceptible to SCC in various wet steam environments, including high NaOH, chlorides, sulfides, sulfates, carbonate-bicarbonate, CO_2, and other acids. The concentration of these impurities or additives during condensation of steam is difficult to control and, in some cases, a cause for concern. SCC has been observed in disk rim/blade attachments, the disk web, and rotor keyways, all caused by cyclic evaporation and concentration of impurities.

Plain carbon steels are known to be susceptible to SCC in high NaOH environments. This form of SCC is also known as caustic cracking. There can be carryover of sodium hydroxide into the turbine, raising the pH. If hydroxide concentrates in the wet steam regions of the turbine, caustic cracking can become an issue. Caustic cracking might have been responsible for the Hinckley accident, but this was never confirmed.

Cracking by SCC can be either transgranular or intergranular, depending on the material and environmental conditions. In some cases, different cracking morphologies have been observed in the same failed part in nominally constant conditions. Transgranular fractures typically follow low index crystallographic planes. SCC of plain carbon steels in high NaOH environments is typically intergranular. The intergranular features indicate a susceptibility of the grain boundary chemistry to corrosion relative to the bulk metal. Studies of materials in steam turbine environments indicate that both fracture morphologies are possible and influenced by steam chemistry, potential, and applied stress intensity.

One approach to improving turbine design is to consider the threshold stress or stress intensity necessary to initiate SCC. Data are available for Ni-Cr-Mo-V steels in nominally pure water [14]. Unfortunately, corrosion can occur under a variety of service conditions or upset conditions, and the change in environmental conditions can have a significant effect on SCC behavior. The long times needed for testing and the lack of consistency in experimental techniques used by different researchers can lead to further difficulties. There are no universally accepted techniques for determination of SCC resistance; therefore, designers usually adopt the most conservative options. As a rule of thumb, the SCC threshold stress can be estimated as the elasticity limit at temperature, or approximately 50% of the yield stress.

It is common to plot CGRs as a function of applied stress intensity. The minimum stress intensity for which SCC is possible is the threshold stress intensity K_{ISCC}. For cracking near (but above) this critical value, CGRs typically increase with increasing applied stress intensity. This range is often referred to as *Region I behavior*. As the applied stress intensity increases, there comes a point at which CGRs are limited by corrosion kinetics and the CGR becomes a near constant. This is *Region II behavior*. If the stress intensity is further increased, the corrosion component of the mechanism becomes dominated by the mechanical component, and fracture occurs (Region III). A schematic of this behavior is given as Figure 2-9.

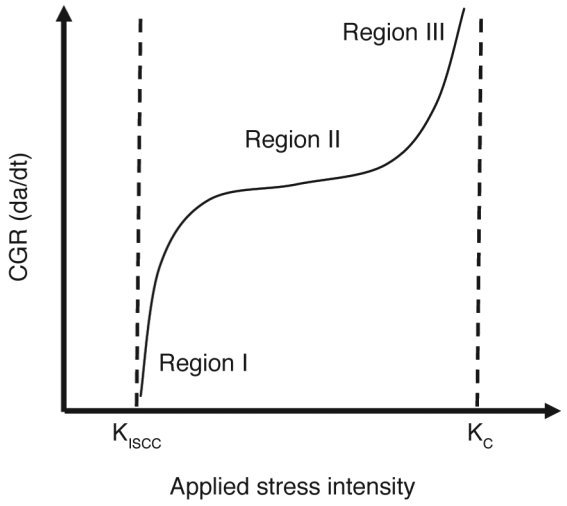


Figure 2-9
A typical curve showing CGR versus stress intensity

Figure 2-10 is an example of SCC data for an Ni-Cr-Mo-V steel in nominally pure water, compiled from published data [14]. The data demonstrate how the threshold stress, stress intensity, and CGR change with the material's yield strength. Lower-strength steels typically have lower threshold stresses and higher threshold stress intensities for SCC. Higher-strength steels tend to have higher threshold strengths and lower threshold stress intensities for SCC. This behavior is recognized by the industry and has led to limiting of yield strengths in new plant designs and avoidance of stress concentrators such as notches and keyways.

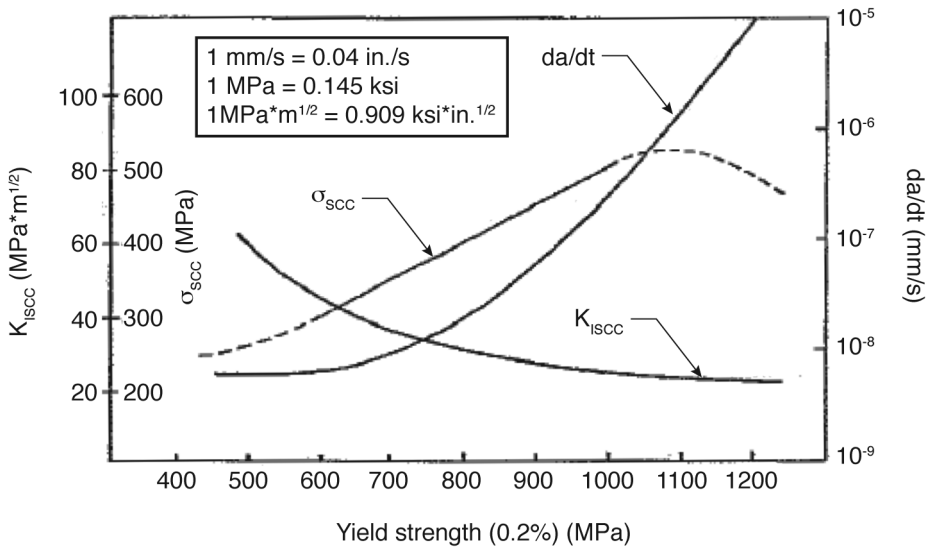


Figure 2-10
Stress corrosion behavior of NiCrMoV disk steel vs. yield strength for "good" water and steam (Compiled from published data. Where K_{ISCC} = threshold stress intensity, σ_{SCC} = threshold stress, and da/dt = Stage 2 CGR.) [1, 14]

Appropriately heat-treated 12% Cr stainless steels used for turbine blade materials have been described as unsusceptible to SCC and CF, and some consider corrosion data unnecessary. Heat treatments limit the yield strength to approximately 85 ksi, which is below the threshold stress for the material. However, this approach to design does not necessarily consider possible upset scenarios.

2.4.3 Corrosion Fatigue

CF is similar to SCC except that a cyclic stress is an active rather than static stress. A susceptible material, a cyclic stress, and a corrosive environment act in combination. Materials that are susceptible to SCC are often also susceptible to CF. As with SCC, various impurities can contribute to CF, including high NaOH, chlorides, carbonate-bicarbonate, CO_2, and other acids. The concentration of these impurities during condensation of steam is difficult to control and, in some cases, cause for concern. An important feature is the details of the design of the components and whether the stresses are cyclic or static.

CF combines the detrimental features of fatigue and corrosion. Fatigue involves cyclic loading of a material that leads to localized plastic deformation and crack initiation. After a crack is initiated, it can propagate relatively quickly with continued loading as stress further concentrates at the crack tip. In the case of CF, the cracking problem is exacerbated by corrosion at the crack tip. The mechanism depends on the material and environment. Acidic environments can lead to enhanced dissolution of materials. Alkaline environments can lead to brittle oxide formation. These oxides are not protective if the cyclic loading causes repeated cracking and damage to them.

Experimental studies often focus on determining the threshold change in stress or stress intensity factor, rather than the absolute values determined for SCC studies. It is common to plot CGRs as a function of change in applied stress intensity, similar to the equivalent SCC plot for static loading conditions. CGRs typically increase with increasing change in applied stress intensity. In the case of fatigue crack growth rates (FCGRs) in inert environments, the relationship is described by the Paris Law, which relates CGR per cycle to the change in applied stress intensity. In the case of CF, the behavior is similar, but CGRs are enhanced by the corrosive reactions at the crack tip. The minimum change in stress intensity for which CF is possible is the threshold stress intensity ΔK_{th}. Similar to SCC, three regions of cracking behavior can be defined. A key difference is that Region II behavior is characterized by Paris Law behavior, typical of fatigue in inert environments, rather than the approximately constant rates typical of SCC Region II behavior. This indicates the higher dependence on the mechanical component in the crack propagation.

FCGRs in inert environments are independent of loading frequency. This enables CGRs to be determined as quickly as mechanical test equipment will allow. However, CGRs in corrosive environments are dependent on loading frequency. A high frequency does not allow enough time for corrosion kinetics to play a role in the fatigue. A low frequency allows enough time for corrosion kinetics to play a role, and it is typically with low frequency that the greatest effect of environment is observed.

CF cracks have notable differences from SCC. CF cracks tend to form more slowly, and there are likely to be corrosion products on the crack surfaces, unlike SCC. CF cracks are often blunted. They are more likely to be transgranular, similar to fatigue cracks in inert environments, but unlike most cracks subject to SCC. Cracks rarely follow grain boundaries.

The main cause of cyclic stresses in steam turbines is vibration in blades associated with mistuning or interrupted flow in the turbine. Considerable effort is made to design and construct turbines in order to minimize these vibrations. Shroud connections or lashing wires can be designed to reduce some vibrations, as noted previously. Blades are tuned to prevent buildup of resonant vibrations. Several

case studies performed by the industry and described in Section 2.8 have demonstrated that failure of lashing wires can lead to the development of vibrational stresses in blades and subsequent failure of the blades. The previous discussion of pitting indicated that pitting of surfaces can lead to interrupted flow in the turbine and detrimental vibrational stresses.

One approach to improving turbine design is to consider Goodman diagrams for materials in different environments. Like threshold stresses, Goodman diagrams provide guidance on the mean and alternating stress limits that are allowable for materials in different environments. However, like the case of SCC, corrosion can occur under a variety of service conditions or upset conditions, and the change in environmental conditions can have a significant effect on SCC behavior. The testing times necessary for reliable experimental data are long, and the differences in experimental techniques used by researchers lead to difficulties in comparison.

Figure 2-11 and Figure 2-12 are Goodman diagrams for Ni-Cr-Mo-V and stainless steels, respectively, in service conditions. Goodman diagrams are plots of mean and alternating stresses for materials in a given environment and surviving a given number of cycles—in this case, 108. Sufficient experimental data allow one to define a safe operating envelope.

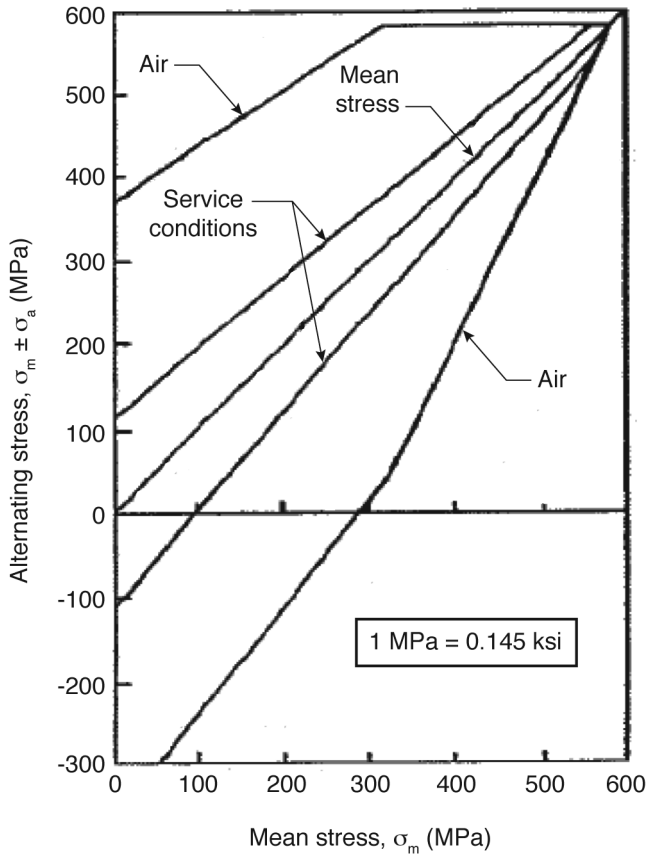


Figure 2-11
CF (Goodman) diagram for NiCrMoV disk steel tested to 108 cycles [1, 15]

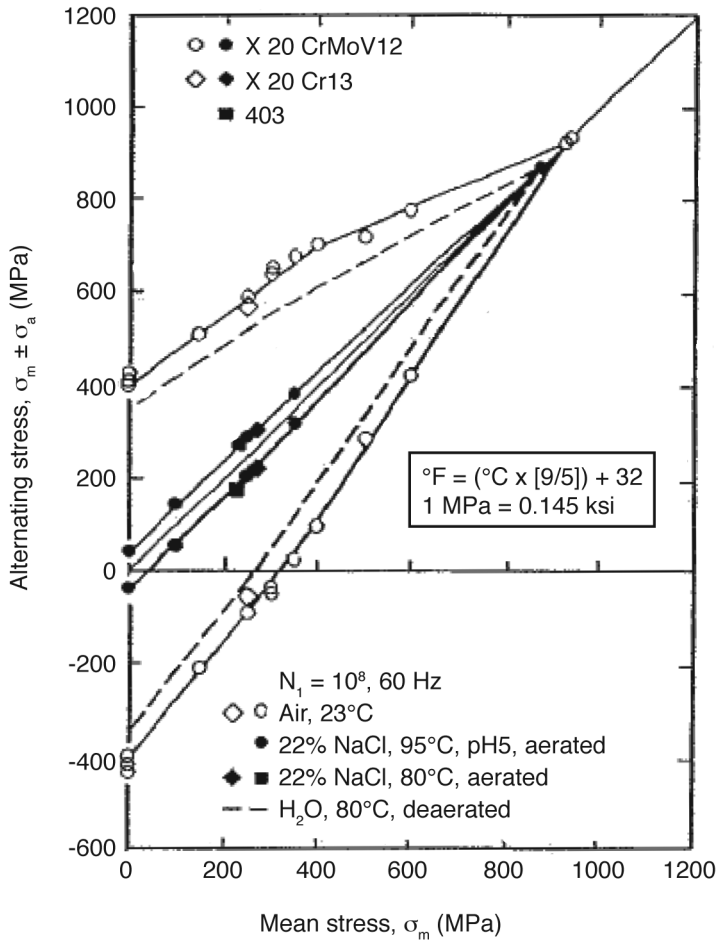
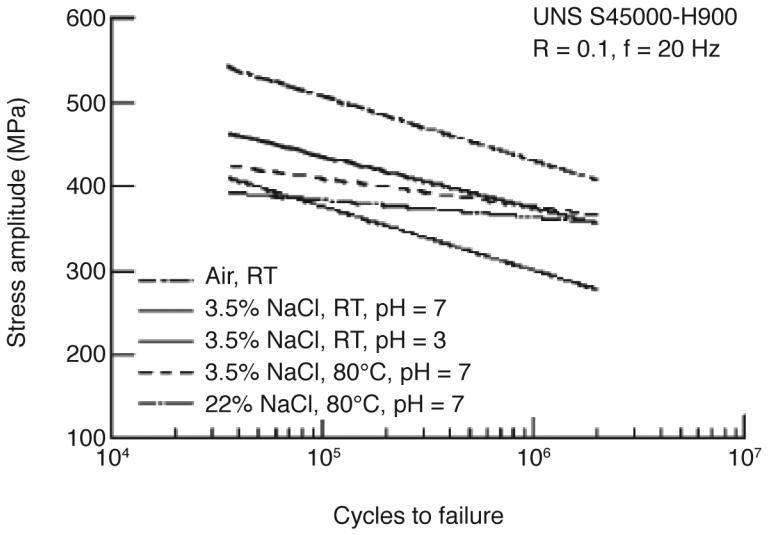


Figure 2-12
CF (Goodman) diagram for three stainless steel blading alloys [1, 16]

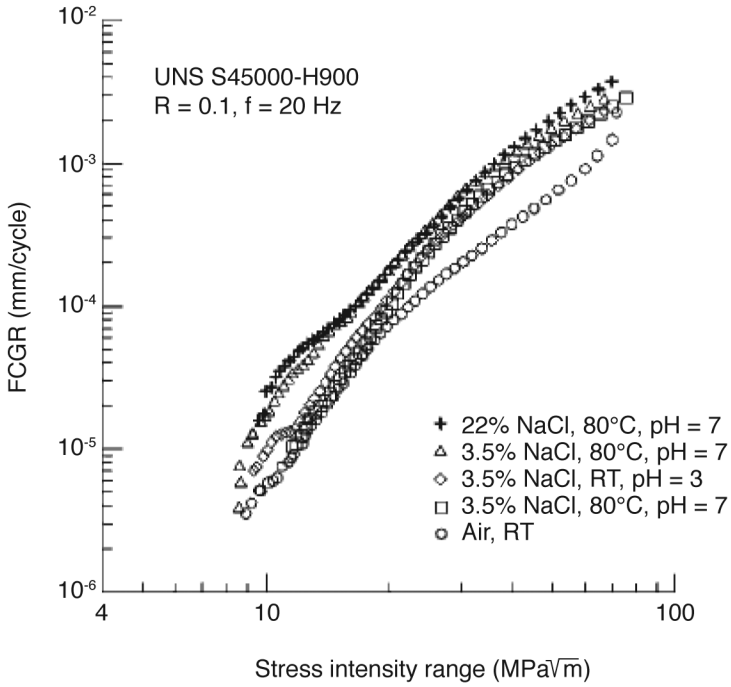
Lin et al. [17] performed a series of experiments to study the fatigue behavior of custom 450 stainless steel in acidic and chloride solutions. The alloy is a precipitation-hardened martensitic stainless steel, similar to a 17-4 pH but developed to avoid the presence of second-phase delta-ferrite stringers. The solution-annealed alloy can be aged to improve toughness and SCC resistance. However, little work has been done on the CF behavior. In the Lin work, both high cycle fatigue (HCF) tests on smooth specimens and FCGR tests on compact tension specimens were performed. S-N curves and da/dN-ΔK curves were developed, and tests were performed in either air or aqueous solutions. The solutions contained either 3.5% or 22% sodium chloride, were either pH 3 or pH 7, and were either at room temperature or heated to 80°C.

Test data from the Lin work are provided as Figure 2-13 and Figure 2-14, which illustrate the effects of various environments on fatigue life and FCGRs. Figures 2-13 and 2-14 show the two different approaches to managing CF. The S-N curves (see Figure 2-13) are plots of cycles to failure of a nominally smooth sample as a function of applied alternating stress. The number of cycles a sample survives is strongly dependent on the environment in which the test is performed, including salt content and pH, as shown Figure 2-13. The CGR curves in Figure 2-14 are plots of CGRs as a function of stress intensity range. As with the S-N curves, they demonstrate the detrimental effect of testing in a corrosive environment relative to air.



°F = (°C x [9/5]) + 32
1 MPa = 0.145 ksi

Figure 2-13
Comparison of S-N curves for UNS S45000-H900 in different environments [17]
Used with permission from NACE International



°F = (°C x [9/5]) + 32
1 MPa = 0.145 ksi
1 mm = 0.4 in.

Figure 2-14
Comparison of FCGR curves for UNS S45000-H900 in different environments [17]
Used with permission from NACE International

The tests demonstrated that low pH, a higher temperature, and/or a high salt concentration led to an increase in FCGR and a decrease in HCF life. For the HCF behavior, it was reported that a decrease in pH had a greater effect than an increase in temperature or salt concentration. This was attributed to formation of corrosion pits in the low-pH solution that initiated CF cracks more quickly than in the neutral solutions. This implies that damage in the neutral solutions initiated in the passive region. Fractography indicated that crack initiation did not occur at corrosion pits and might have initiated at slip bands and inherent defects. However, for the FCGR behavior, it was reported that temperature had a greater effect than pH or salt concentration. It was hypothesized that crack tip acidification and anion concentration might not be affected significantly by changes in the bulk solution and, therefore, the temperature effect is more apparent.

2.4.4 Erosion and EC

Erosion and EC are materials degradation mechanisms that involve mechanical wear. Hard particles rubbing against or traveling past a material can cause surface damage to the material. In the case of soft materials, the result is plastic deformation and might involve some material removal. The deformation can cause an indent to the material and a localized stress concentration. Depending on the material's hardening behavior, there might also be work hardening. In the case of brittle materials, the result of wear can be chipping of the surface and material removal, also leading to stress concentrations or cracks. If the wear occurs in a corrosive environment, the result can be EC. Corrosion exacerbates the damage caused by the wear. Removal of protective oxides on the surface of the materials reveals fresh metal for oxidation, and the cycle of damage and degradation of the material continues.

Erosion problems in LP turbines can be attributed to either water droplets or solid particles. Water droplets forming in the turbine can be traveling at high speeds and form notches in blades that act as stress concentrations or even change resonant frequencies. Fatigue failures have been reported from reversed wet steam flow acting on blades' trailing edges. Solid particles in the form of oxides from corrosion in the steam generator can be passed through to the turbine, also causing damage.

Solid particles, such as silica, have been reported to cause grooving wear to turbine blades [18]. Particles become embedded in the material surface, allowing for the initiation of crevice corrosion. The crevice corrosion allows impurities to concentrate in the interface between material and particle, causing further damage. The stress concentration associated with the groove and/or corrosion can lead to crack initiation, depending on the loading conditions. This can result in CF.

FAC is a related phenomenon caused by high-velocity turbulent flow of a corrosive fluid. As the corrosion occurs, material is removed from components and reaction products are flushed away, leaving fresh surface available for further corrosion. This problem is often related to flow of moistures containing CO2 or other acid-forming anions. The low pH favors dissolution of carbon steel. Passive oxides are unstable at the low pH and prevented from protecting the material.

2.4.5 Interaction of Corrosion Mechanisms

Some of the literature reviewed during the course of this work referred to multiple corrosion mechanisms. These were typically discussions involving the transitions of corrosion or erosion pits to cracks, which then led to SCC or CF. There appears to be no significant difference in the approach to managing these two phenomena, other than consideration of the cyclic or static stresses and reduction of vibrational stresses wherever possible. The concentration of impurities or additives is important to both phenomena if they initiate pitting that leads to crack formation.

Both corrosion and erosion can lead to the formation of pits on a component surface. Corrosion pits form when impurities, such as chloride or sulfate, chemically break down a passive film and result in localized corrosion. Erosion pits form as water droplets or solid particles impact component surfaces, causing localized mechanical damage. These two phenomena can result in pits that act as stress concentrators.

The presence of pits can lead to initiation of cracks in a material surface. The pit geometry concentrates stress in the material. The stress can be either static or cyclic, and, if sufficient, it can initiate a crack. The initiated crack can then propagate by either SCC if the load is static or by CF if the load is cyclic. The conditions necessary to form a pit might be the same as the conditions necessary to propagate a crack in the material. For example, chlorides or sulfates might lead to pit formation, but these species are not necessarily required to propagate SCC of CF cracks. However, the higher conductivity associated with the ion concentration can allow higher current densities to be supported, thereby increasing CGRs.

Similarities in SCC and CF can also be considered. CF crack growth is known to vary with loading frequency and change in stress intensity. SCC can be considered as a special case of CF with a negligible loading frequency and change in stress intensity. Some modeling has been performed using this approach [19]. However, the simplification implies that a true threshold stress intensity range for CF does not exist, or that SCC requires a finite change in stress intensity to be active. In some studies on plain carbon steels in carbonate-bicarbonate environments, it has been shown that SCC requires a fluctuating stress to be operative and that the CGR is a function of the strain rate at the crack tip. The differences in SCC and CF, therefore, can become blurred.

A review of failure analysis case studies indicated that erosion can be a significant problem that can lead to SCC or CF crack formation. Several of these case studies are covered in more detail in later sections.

2.5 Steam Turbine Environments

The corrosion resistance of materials depends on the service environment. Several factors play a role in the corrosion and to varying degrees for each material. The factors of interest include the temperature and pressure of the steam, pH, oxygen content, steam impurities, and loading. The temperature and pressure of the steam are important because they decrease as the steam passes through the turbine. At the PTZ, condensation forms on turbine surfaces, impurities or additives can concentrate, and corrosion might become an issue. The PTZ is at the back of the turbine, typically near the L0 and L1 blades.

The pH, the oxygen content, and the specifics of the steam chemistry all affect corrosion susceptibility and subsequent pitting rates and CGRs. Considerable effort has been put toward understanding how these factors influence corrosion. The details of the more recent studies are presented in the following sections.

Loading of components in the steam turbine can be static, dynamic, or a combination of the two. Static loading can lead to SCC. Dynamic loading can lead to CF. In many components, there is a relatively high static stress and a secondary lower stress fluctuation, and so both forms of damage might be operative. This makes experimentation and modeling for the purpose of predicting in-service corrosion more difficult. Changes in operation resulting from off-load or shutdown scheduling can also contribute to changes in stress conditions that were not necessarily considered in the design of the turbine. Recent changes in industry operation schedules have led to increased interest in understanding the effect of the changing conditions.

2.5.1 Temperature and Pressure

Temperature and pressure vary through the turbine as the steam expands and energy is transferred to the blades. Temperature can change from over 200°C to below 95°C, though this will vary with the specifics of the turbine design. If the unit power is decreased for off-load cycling on evenings and weekends, the temperature might be decreased to approximately 70°C. During shutdown, the temperature is decreased to ambient 25°C.

Temperature is known to affect corrosion rates, and the significant change in temperatures during the course of the turbine's operation must be considered. One would expect higher corrosion rates at higher temperatures. However, one must also consider how the rates are affected by other environmental factors that are sensitive to temperature changes. The reduction in temperature also leads to increased wetness and might allow more impurities to concentrate. When the turbine returns to service, the concentrated impurities can initiate corrosion.

The change in temperature also leads to a change in moisture content. Early condensing steam entering the PTZ would contain moisture in the order of 1%, but moisture increases to 10% as the steam cools and expands. In contrast, the concentration of impurities in the steam effectively decreases. At the inlet end, the concentration of impurities can be in the order of 100 ppb. Near the outlet, this would decease to the order of 10 ppb as the moisture increases. Condensation of steam on the turbine surfaces allows impurities to concentrate in liquid films, thereby decreasing concentrations in the steam.

2.5.2 pH

Acidity plays an important role in the corrosion behavior of many alloys. Low-pH solutions generally thermodynamically favor metal dissolution. Neutral or high-pH solutions tend to thermodynamically favor metal oxide formation and passivation. However, high-pH solutions in some conditions can lead to SCC susceptibility in some alloys—the oxide layer plays a role in the cracking mechanism. Cracking of the oxide layer reveals fresh metal that can dissolve or oxidize. The metal ions precipitate hydroxides at the crack tip and lead to a local acidification. This further drives crack growth.

The pH control in power plants is usually for protection of the preboiler cycle and boiler. The water is typically slightly alkaline, in the pH range 8.5–9.5—this is necessary in order to stabilize magnetite and mitigate against corrosion. However, pH of condensing steam in the turbines is more difficult to control and will increase if hydroxides carry over from the boilers. Temperature, carryover of impurities, and boiler water treatment chemicals can all affect pH of condensing steam in the turbine. Plain carbon steels then become susceptible to SCC. As explained previously, caustic cracking might have been responsible for the Hinckley accident, but this was never confirmed.

The pH of steam condensate in the turbine will decrease if organic acids form from carryover from the boilers. Carbon dioxide might be present in the turbine following ingress of organic matter in the makeup water, decomposing by pyrohydrolysis. Other organic products might be present, including acetic, butyric, formic, and proprionic acids. The CO_2 is of particular interest because it forms mildly acidic carbonic acid that can be corrosive. Previous studies [20] have demonstrated that CO_2 segregates preferentially to the liquid in a two-phase liquid-vapor environment, but the kinetics of the process are believed to limit concentrations in the liquid to less than what thermodynamic considerations would predict.

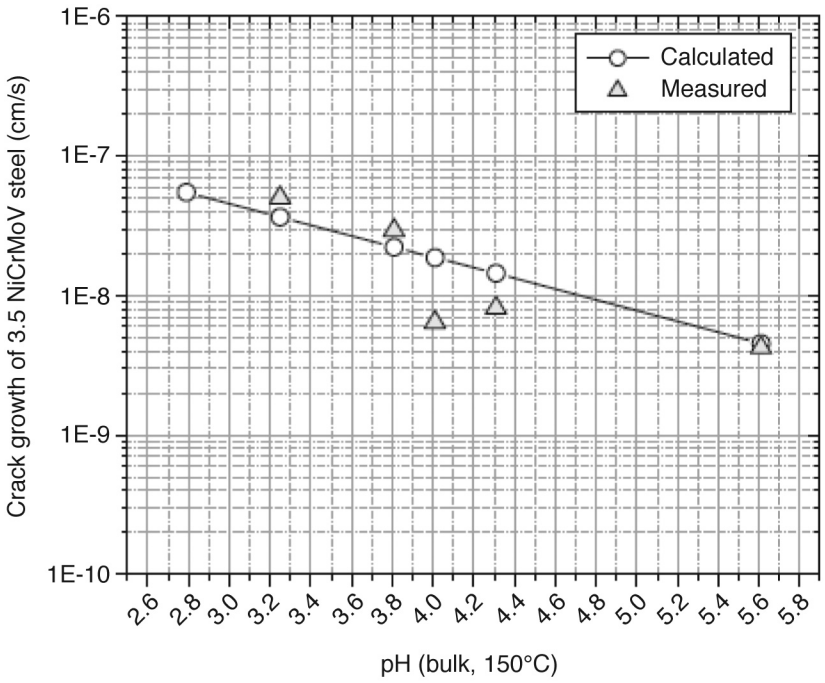
Lyons and Cornish [20] studied the growth of passive oxide films on 12 Cr stainless alloys and the effect of carbonic acid. Carbonic acid is known to form in the wet, final stages of the LP turbine due to the ingress of CO_2 contamination. The acid is weak but might be sufficient to influence the formation of passive films. Stainless steels generally become more resistant to acids with the addition of molybdenum because it affects the formation of the passive films.

The Lyons and Cornish work demonstrated that oxide films tend to form two distinct layers. The inner layer on the metal substrate was shown to be fine-grained, adherent, and rich in Cr2O3. The Cr oxide is advantageous in that it is more resistant to acidic environments. The outer layer was shown to consist of a porous layer of octahedral magnetite (Fe3O4) particles. The second layer was observed only in the in-service testing performed, and it was hypothesized to have been nucleated elsewhere in the turbine.

The inner oxide layers were shown to grow by a parabolic rate law, indicative of a diffusion-controlled growth process. These kinetics were observed only after an initiation time, attributed to a pre-nucleated oxide on unexposed samples. The rate kinetics were shown to be dependent on metal surface preparation. Oxide growth on cold-worked metal substrates, deemed comparable to the surface finish on in-service blades, was higher than equivalent rates on electro-polished lab metal substrates. Crystals were observed to align with polishing grooves, indicating that the grooves provided nucleation sites for the growing oxides. The cold working can also contribute to enhanced diffusion of Cr along grain boundaries and further oxide enrichment.

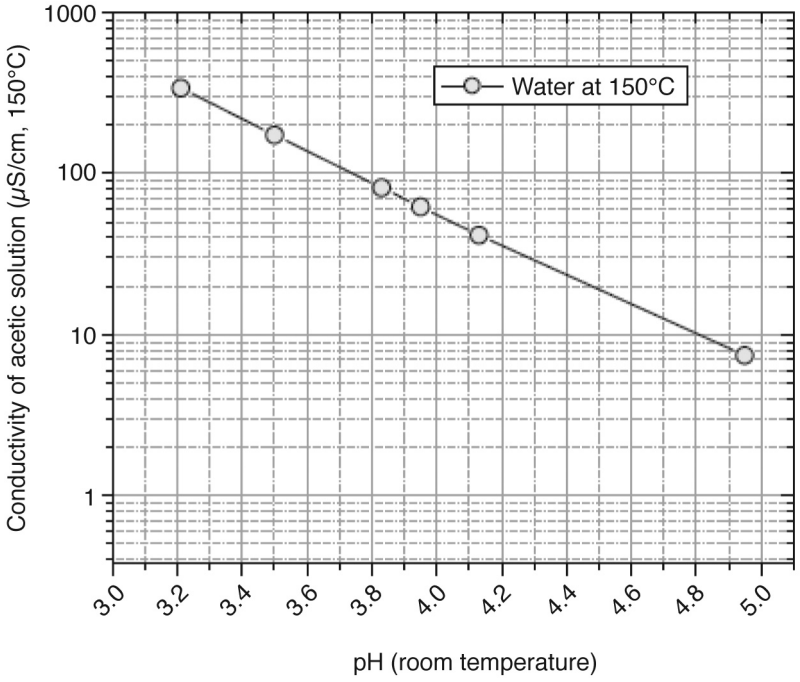
Maeng and Macdonald [21] also consider the effects of organic contaminants on the corrosion resistance of 3.5 NiCrMoV disk and rotor steels. In their study, the organic contaminants were attributed to the thermal decomposition of ethanolamines (ETAs) that are introduced to the steam cycle as pH-conditioning or chelating agents. The ETA is used to reduce sludge buildup and thereby maintain thermal efficiency. However, decomposition can result in the formation of acetic, formic, or lactic acids. Acetic acid concentrations of up to 6000 ppb have been reported in condensates.

The study involved SSRTs using ASTM 470/471 (3.5 Ni-Cr-Mo-V) steels in deaerated waters at 150°C and acetic acid additions to pH 3.21–4.95. The samples tested showed increasing loss of ductility with decreasing pH. The sample tested at pH 3.21 showed severe general corrosion, and it was reported that blunting of the crack tips would have prevented true SCC from occurring. The other samples showed varying degrees of SCC. Calculated CGRs varied from 4.5 x 10-9 to 5.5 x 10-8 cm/s with decreasing pH. Various correlations were made between the CGRs, the pH, and the conductivity of the solution. The correlation considered the most important was the relation between CGR and conductivity, and this was deemed a dominant parameter in the SCC susceptibility (see sample data in Figure 2-15 and Figure 2-16).



°F = (°C x [9/5]) + 32
1 cm = 0.4 in.

Figure 2-15
The measured and calculated CGR as a function of the bulk solution pH at 150°C [21]
Used with permission from Elsevier



°F = (°C x [9/5]) + 32
1 cm = 0.4 in.

Figure 2-16
The solution conductivity at 150°C as a function of acetic acid concentrations (pH at room temperature.) [21]
Used with permission from Elsevier

Maeng and Macdonald also discussed their results with respect to the Coupled Environmental Fracture Model and the Differential Aeration Hypothesis. The crack tips or crevices in the test samples or components are anodic, with limited access to cathodic depolarizers, such as oxygen, water, and hydrogen ions. The external surfaces have more access to these species. A change in the solution pH in the external solution affects exchange current densities and equilibrium potentials of the redox reactions occurring on these surfaces. In addition, the pH affects the conductivity of solution and therefore the "throwing power" of current between the crack tip and external surfaces. The higher the conductivity, the larger the surface area that can support the reactions, and the higher the total current flow. The pH also affects the corrosion potentials at both of the local anodes.

Thermodynamic calculations indicated that the pH of the crack tip can decrease to approximately 1.5 at the conditions studied. This contributes to further acidification of the crack tip because dissolved iron atoms precipitate as hydroxides from the aqueous solution, increasing the local hydrogen ion concentration. The high acidity dissolves any passive oxide films that would form in more neutral solutions. However, the kinetics of the iron dissolution and the effect of pH are unclear. It was recommended that these be topics of future study.

2.5.3 Oxygen

Dissolved oxygen concentration is generally kept at very low levels—typically, less than 10 ppb—in the high-purity waters used in steam turbines. This oxygen can also dissolve in steam condensates forming in the PTZ of the LP steam turbine, and it can be of concern because of its effect on corrosion. High

dissolved oxygen contents can contribute to pitting in stainless steels. Minor oxygen levels, in the order of tens of ppb, lead to passivation of these alloys. The dissolved oxygen contents necessary for pitting are in the order of a few ppm. Chloride or sulfate ionic contaminants are usually required for the pitting to occur. Pitting can then lead to crack formation and SCC. The increased oxygen content raises the corrosion potential and can lead to the pitting or cracking range.

Although oxygen levels are carefully controlled during the operation of most turbines, there are conditions under which oxygen levels can rise to levels that can cause pitting over time. One of these conditions is outages. During non-operational times, the seals preventing oxygen ingress can fail, and oxygen enters the LP turbine through the condensers. The steam is therefore replaced with atmospheric air, unless specifically conditioned with an inert gas. This can be detrimental to turbines that suffer regular startups and shutdowns as a result of power demand and scheduling requirements.

The role of oxygen has been debated among experts in the field of steam turbine corrosion. The reasons for their differences of opinion were freely discussed at an EPRI workshop in 1997 [22]. Initial work demonstrated that turbines in boiling water reactors (BWRs) were more susceptible to cracking than in pressurized water reactors (PWRs), implying that oxygen played a key role in the SCC mechanism. Some researchers (Seidel as well as Holdsworth of GEC-Alstom) have shown that oxygen has little or no effect on initiation or growth of cracks. However, other researchers (Lyle of SWRI and McCracken of Westinghouse) argued that oxygen is deleterious to crack initiation and growth. David (1990) reported no cracking in pure waters up to 100°C and that oxygen levels are not important because of the low conductivity. Arguments have also been made that oxygenated treatments (OTs) of water in fossil power plants lead to no detrimental effects on turbines. Although inlet steam can contain more than 100 ppb oxygen, condensates in the PTZ have been shown to contain no measurable oxygen. Liquid films forming in OT turbines are thinner than usual, and the treatment decreases the concentrating effect of the chloride and sulfide impurities. The debate should be considered in the following discussion.

Otieno-Alego et al. [23] studied the role of oxygen in pitting corrosion using a combination of experimental and modeling work. They performed a series of polarization scans on A470 (3.5 NiCrMoV) steels in simulated steam turbine environments. The simulated environment consisted of 2 ppm NaCl, 2 ppm Na2SO4, 5 ppm SiO2, and 2 ppm NaOH. Dissolved oxygen was varied between 10 ppb and 7.85 ppm. Scan rates of 5–40 mV/min were used. Theoretical analysis of the resulting polarization curves allowed them to deconvolute the anodic and cathodic reactions.

The work demonstrated that increasing dissolved oxygen content or scan rates leads to similar polarization behavior. The net result was that increasing oxygen content led to a change in anodic polarization and increased passivation current density. The analysis allowed for the theoretical prediction of corrosion behavior based on knowledge of steam chemistry. It was demonstrated that only 50 ppb oxygen is necessary for spontaneous passivation and that only 2.50 ppm oxygen is necessary for instantaneous pitting. It was proposed that corrosion behavior could be predicted in a defined system simply by measuring the dissolved oxygen content.

Work by Lyons and Cornish [20] demonstrated that high oxygen content alone is insufficient to increase susceptibility to pitting corrosion. Their work involved testing of 12 Cr stainless alloys with raised oxygen contents up to 200 ppb. No evidence of pitting was observed after 3000 hours, consistent with the accepted view that ionic contaminants, particularly chlorides and sulfates, play a more significant role.

Maeng et al. [24] studied the effects of oxygen content and temperature on the susceptibility of turbine steels to SCC. Oxygen was believed to contribute significantly to SCC, though contradictory results have been reported, as presented previously. Maeng performed SSRTs using ASTM 470 (3.5 NiCr-

MoV) turbine steels in waters with various oxygen concentrations (see sample data in Figure 2-17). Waters were either deaerated or contained up to 8 ppm dissolved oxygen. Oxygen is known to contaminate LP turbines through leakage in the condenser, particularly during outages or startups. In addition, temperatures were varied from 50°C to 200°C, and strain rates were varied between 5 x 10^{-8}/s and 1 x 10^{-6}/s.

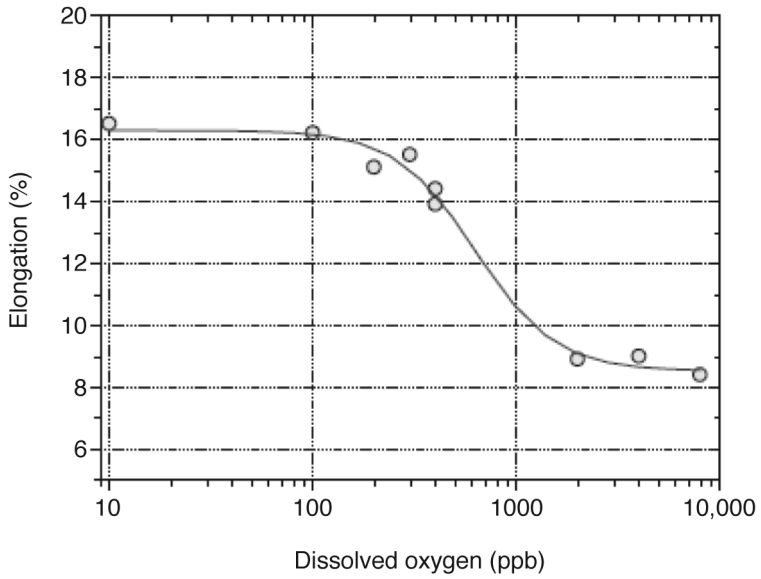


Figure 2-17
Elongation of the 3.5NiCrMoV steels as a function of dissolved oxygen tested in water at 150°C with a strain rate of 1 x 10^{-7}/s [24]
Used with permission from Elsevier

Results of the work demonstrated decreasing ductility and tensile strength with increasing temperature and oxygen content as well as decreasing strain rate. The increase in susceptibility to SCC at high temperature was discussed and two mechanisms proposed. One mechanism considered related to increased anodic dissolution at the crack tips because of increased oxygen mass transport. The increase in SCC susceptibility was attributed to increasing metal dissolution to balance increasing cathodic oxygen reduction. The increasing iron dissolution can also contribute to acidification at the crack tip as iron ions precipitate out as hydroxides. The other proposed mechanism related to kinetics of surface mobility.

Corrosion potentials were observed to increase with both oxygen content and temperature. Differences were also observed in the fracture morphologies. Surface analysis indicated both iron and chromium oxides, with slight variations in the different test conditions.

Work by Zhou and Turnbull [25] considered the oxygen transients associated with the regularly changing operational conditions. They performed a series of corrosion potential measurements on a bainitic 3% NiCrMoV ex-service disk steel. The steel was subjected to alternating conditions to simulate on- and off-load conditions. The on-load conditions were simulated using deaerated high-purity water, and the off-load conditions were simulated using aerated waters containing up to 1500 ppb chlorides or 300 ppb chlorides and 300 ppb sulfate. For each series of tests, the oxygen content and corrosion potential were measured.

The initial corrosion potential in deaerated high-purity water was -0.69 V (SCE). Introduction of the aerated high-purity water increased the potential rapidly to over 0.0 V (SCE), followed by a slower increase over the 8-hour hold. When deaerated water was reintroduced after the hold, the potential decreased immediately by approximately 0.2 V, and it then decayed slowly to close to the original -0.69 V (SCE). However, as cycles were continued, the initial drop in potential following reintroduction of deaerated water decreased to approximately 0.1 V after five cycles. In addition, the corrosion potential decayed to only -0.2 V (SCE). A long-term hold in deaerated conditions allowed the potential to restabilize near -0.69 V (SCE) (see Figure 2-18).

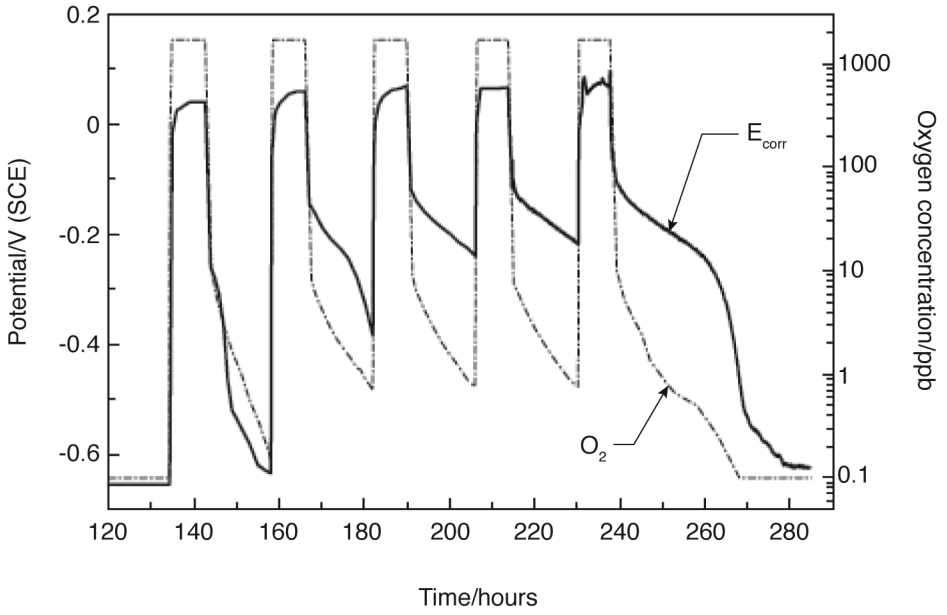


Figure 2-18
Response of corrosion potential to oxygen concentration transients simulating two-shifting operating conditions with pure water for both off-load and on-load chemistry [25]
Used with permission from Elsevier

Tests performed using chloride and sulfate impurities had slightly different results, as shown in Figure 2-19. When deaerated salt solutions were introduced, corrosion potentials decayed to their original levels. The rate of change of corrosion potential decreased with the increasing number of cycles and increased in the sulfate solutions. It was also noted that the corrosion potential in 600-ppb chloride solution was -0.52 V (SCE), which is 0.14 V higher than the -0.66 V (SCE) corrosion potential measured in the solution containing 300 ppb chloride and 300 ppb sulfate. The type of anions in solution affected the corrosion potential as well as the concentration. This difference was attributed to the stability of the passive film in the two environments, and it was recommended that the phenomenon be studied further.

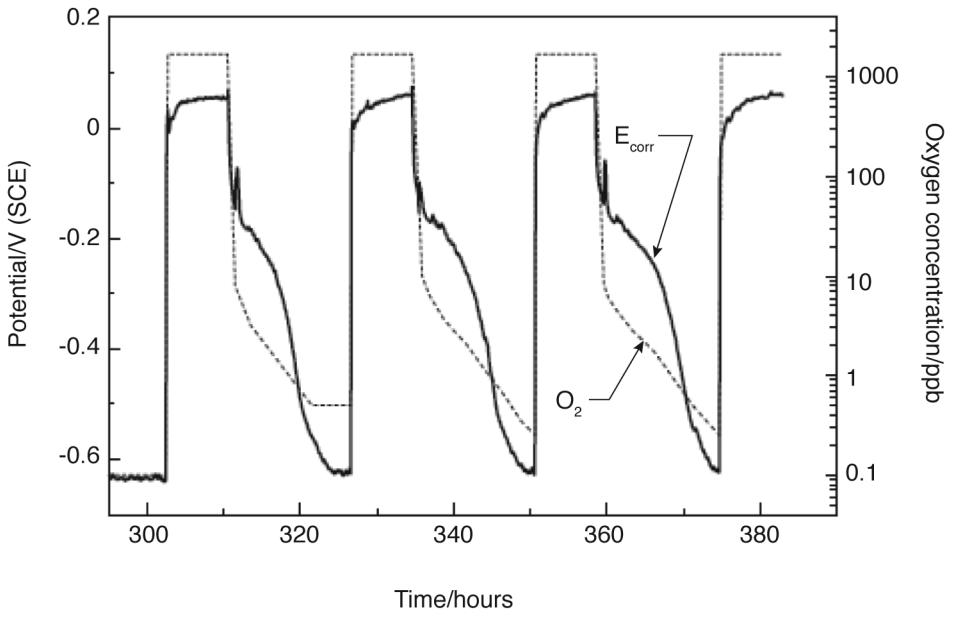


Figure 2-19
Response of corrosion potential to oxygen concentration transients simulating two-shifting operating conditions with pure water for the off-load aerated phase and deaerated 300 ppb Cl- solution for the on-load phase [25]
Used with permission from Elsevier

Zhou and Turnbull concluded that because of the transients in potentials and oxygen and the role of impurities, there were conditions during cycles that would lead to pitting. Nominal on-load conditions would involve deaerated water with anion impurities and low corrosion potentials. Nominal off-load conditions would involve aerated high-purity water with higher potentials. However, when the transients are considered, the slow decay of potential during startup would lead to conditions of anion impurities and higher potentials. These conditions would be aggressive and could cause pitting.

2.5.4 Steam Chemistry

Water chemistry is typically controlled to low ppb impurities in the high-purity waters in order to avoid corrosion issues and to maintain thermal efficiency. Corrosion issues can cause component failures, leading to unforced and expensive outages or personnel injury. Corrosion leading to buildup of corrosion product can affect heat transfer within the unit and result in loss of efficiency. In addition, dissolved ions or particulate from one corrosion reaction can be transferred to other parts of the unit, causing further problems.

Water chemistry impurities and additives are typically maintained below approximately 50 ppb total. Individual concentrations are in the order of a few ppb. Chemistry can be monitored by isokinetic sampling and ionic conductivity measurements. Oxygen levels are maintained below 10 ppb in well-controlled systems. Other species might include chlorides, sulfates, fluorides, iron, copper, or organic materials, all of which can contribute to corrosion issues. The major corrodents—such as chlorides, fluorides, sulfates, and sodium—are kept below the 2–3 ppb range in well-maintained systems, but these concentrations increase during condensation and upset conditions. Conductivity of the inlet steam condensate is in the range of 0.1–1.0 µS/cm.

In addition to the bulk water chemistry, one must consider the localized chemistries in both the water and steam. As dry steam begins to lose heat in the HP and IP turbines and continues to lose heat in the LP turbine, the steam becomes increasingly wet. The final stages of the LP turbine are subject to corrosion that is not considered an issue in the earlier stages of the turbine because the steam is dry. The point in the LP turbine at which moisture forms is the PTZ (see Figure 2-20). As moisture forms in the LP turbine, impurities tend to partition from the gas to the liquid and increase to the order of hundreds of ppb in the early condensates to tens of ppb near the outlet, where moisture contents are higher (see Figure 2-21). These dissolved impurities in the moisture at their higher concentrations contribute to corrosion. The thermodynamics and kinetics of the impurity partitioning are not completely understood.

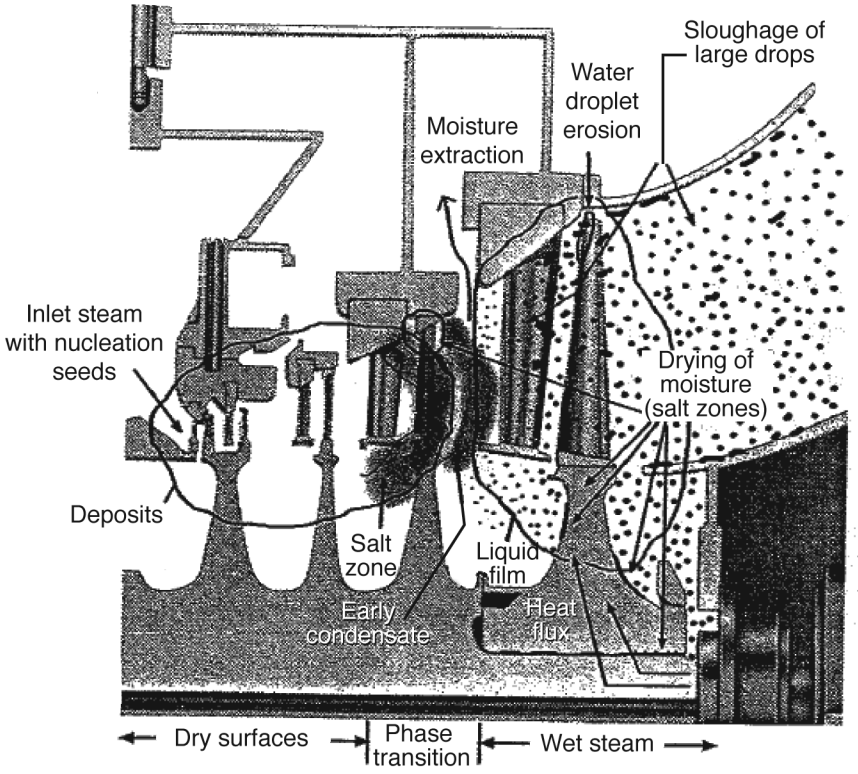


Figure 2-20
Cross-section of an LP turbine with the locations of moisture formation and deposits [1]

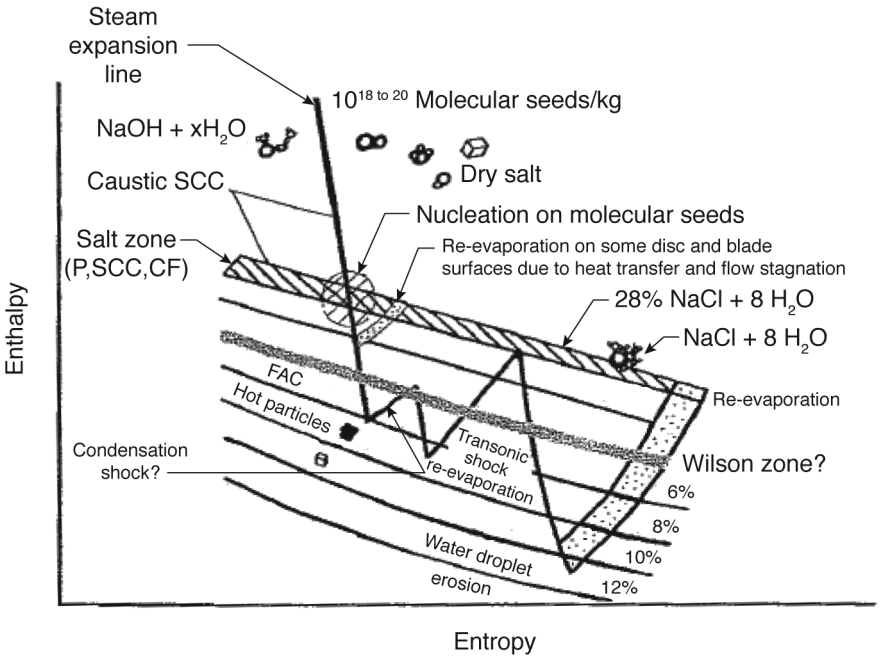


Figure 2-21
Mollier diagram with LP steam expansion line and thermodynamic regions for impurity concentration and corrosion mechanisms [1]

If pits or cracks develop in components because of corrosion susceptibility, one must further consider the water chemistry localized in the crack tip. Due to their crevice-like geometry, crack tips tend to be of lower pH and oxygen content than bulk solutions. This can have a significant effect on the localized pitting and SCC mechanisms.

Turnbull [13] modeled crack tip chemistry to allow predictions as to what conditions were more likely to lead to high SCC growth rates in steam turbine disk steels. He considered applied stress intensity, pH, solution conductivity, and oxygen content. Mass conservation equations were developed, incorporating both diffusion of key species and anode/cathode reaction kinetics.

Results of the modeling predicted a negligible effect of pH on the potential drop between crack tip and mouth. It was considered that any effect of pH would be a result of its influence on solution conductivity. Similarly, little effect of stress intensity was predicted on the potential drop between crack tip and mouth. It was expected that tight control over water chemistry and associated conductivity would decrease CGRs in high-purity waters because low polarization of the crack tip is achievable, even in aerated systems. Figure 2-22 is a plot of crack tip potential data as a function of corrosion potential in neutral NaCl solutions of various concentrations.

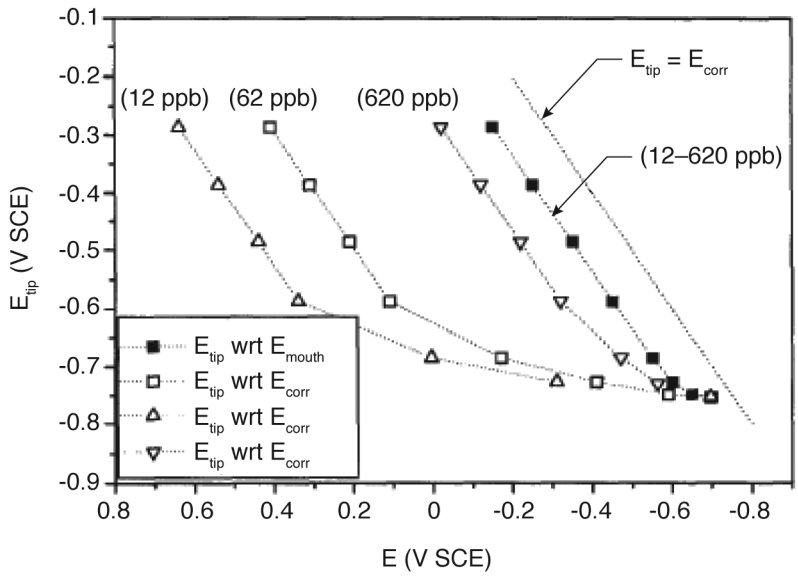


Figure 2-22
Crack tip potentials as a function of calculated corrosion potential in neutral NaCl solution (Concentration of chloride ions in parentheses.) [13]
Used with permission from NACE International

Turnbull et al. [26] performed a series of experiments in which they studied the local crack tip conditions during loading of a 3% NiCrMoV steam turbine disk steel. Of particular interest to their study were the effects of oxygen content, chloride, sulfate, pH, and loading on crack tip potentials. A test rig was developed in which a compact tension specimen was immersed in a solution of known chemistry, the temperature was controlled to 90°C, and the crack tip potential could be measured using a probe embedded in the sample. Solutions were either nominally pure or contained up to 1500 ppb chlorides or 406 ppb sulfates. Oxygen levels were kept <1 ppb for the deaerated tests and estimated as up to 1.7 ppm for the aerated tests.

Turnbull's experiment led to some unexpected results. Crack tip polarization was limited despite relatively high corrosion potentials. As solutions were aerated, corrosion potentials increased by approximately 600 mV, whereas crack tip potentials increased by only 30–90 mV, depending on other solution conditions. The maximum crack tip potentials were achieved with oxygen levels of only 20–30 ppb. When chloride was added to the solutions, there was a negligible change in potential behaviors (see Figure 2-23). When sulfates were added to the solutions, there was a negligible change in crack tip potential measurements, but corrosion potentials were decreased by approximately 300 mV relative to those in aerated pure waters (see Figure 2-24).

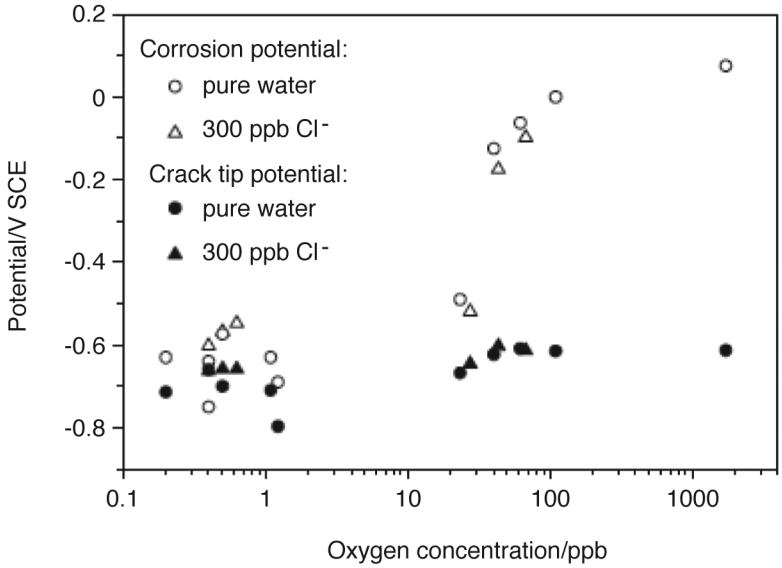


Figure 2-23
Effect of bulk oxygen concentration on both crack tip and corrosion potentials in Cl- solution at 90°C (K = 40 MPa√m) [26]
Used with permission from Elsevier

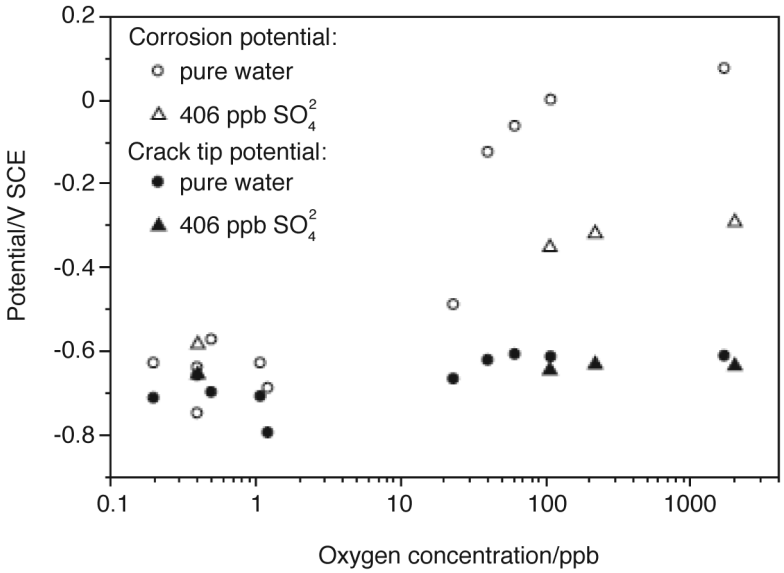


Figure 2-24
Effect of bulk oxygen concentration on both crack tip and corrosion potentials in SO_4^{2-} solution at 90°C (K = 40 MPa√m) [26]
Used with permission from Elsevier

Adjustment of pH between 4.6 using acetic acid and 12.4 using sodium hydroxide had a negligible effect on crack tip potentials in aerated solutions. Increased stress intensity led to decreased potentials at the crack tip in pure waters but increased potentials in solutions containing chlorides.

The Turnbull results were unexpected—conventional thinking is that crack tip conditions are affected by changes in bulk solution. The experimental results were compared to previous modeling work by Turnbull [13] on the same system. The discrepancies were attributed to assumptions involving the long crack model versus the short crack model as well as assumptions regarding the passivation of the crack walls. Further work on growth rates in both long and short cracks was reported as being ongoing.

2.5.5 Impurities and Additives

Although steam turbine chemistry is carefully controlled, it is possible for impurities to be carried over from the boiler water. Each of the impurities can have a detrimental effect on the materials. Chlorides, sulfates, CO_2, and organic acids are known to be issues. In most cases, these impurities are not observed in isolation. Several impurities will exist in combination and will vary by location in the turbine and the turbine design. The particular combination of species might lead to interaction of corrosion mechanisms, though these are difficult to isolate in the laboratory. Following is a review of some of the recent work on the effect of various impurities that might be present in the steam turbine.

Scully and Scully [27] performed a series of experiments to evaluate the susceptibility of AISI 422 stainless steels to environmentally assisted cracking (EAC) in ammonium bicarbonate/ammonium hydroxide solutions. This solution can be used to remove copper deposited on steam turbine blades. Both bicarbonate and hydroxide solutions have been shown to cause EAC of carbon manganese steels at elevated temperatures. The study involved constant extension rate tests and polarization studies of both AISI 422 stainless and commercial purity copper. Tests were performed at 70°C, typical of temperature of the turbine during shutdown. The simulated cleaning solution was pH 9.2.

The work demonstrated that EAC of AISI 422 is unlikely under the conditions tested. The stainless might be susceptible to EAC if the potential is decreased to approximately -0.8 V to -0.7 V (Ag/AgCl), where an active-passive transition was observed during polarization testing. However, the copper deposits have the effect of raising the mixed potential to approximately -0.5 V (Ag/AgCl). It was concluded that cleaning blades in the test solution was appropriate, though there was a low chance of crevice corrosion.

Otieno-Alego et al. [28] performed a comprehensive set of experiments to investigate the effects of chlorides, fluorides, sulfates, and carbonates on the corrosion susceptibility of NiCrMoV alloys. The specific material of interest was A470 turbine disk rotor steel. The base solution selected for experiments contained 2 ppm each of sodium chloride, sulfate, and hydroxide and 5 ppm of SiO2. The base solution contained zero fluorides or carbonates. A two-level full factorial matrix was designed so that the high level of each of the contaminants was set to 2500 ppm. These high contaminant levels were based on reported levels of concern in steam turbines. An anodic polarization scan was performed for each of the 16 (that is, 24 full factorial) high-low impurity combinations. The corrosion potential and breakdown potentials were recorded and analyzed to determine statistically significant effects and interactions.

Statistical analysis indicated that the chlorides, fluorides, and sulfates all contributed to pitting corrosion. These results were calculated as statistically significant. Carbonate was shown to be an inhibitor. Some of the interactive effects were shown to statistically retard the propensity for pitting (see Figure 2-25). For example, Cl-SO4, Cl-F, and Cl-SO4-F all demonstrate antagonistic effects. The conclusion was that high concentrations of these impurities do not necessarily translate to a more aggressive environment. However, it is important to note that the relative effects of each of the individual impurities vary and one might dominate the material's pitting susceptibility.

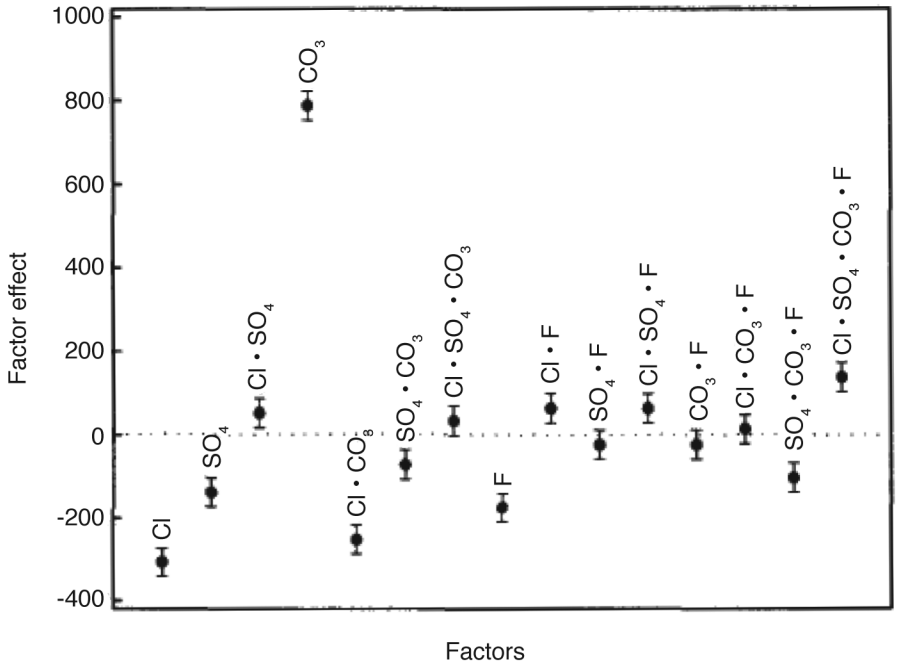


Figure 2-25
Plot of factor effects with the 95% confidence intervals (Positive-factor effects represent inhibition; negative-factor effects represent greater likelihood of pitting.) [28]
Used with permission from Elsevier

A supplementary study to the factorial matrix was an analysis of the effect of dissolved oxygen (DO2) on corrosion behavior. Low levels—up to 0.05 ppm—led to uniform corrosion. Moderate levels—between 0.05 and 0.10 ppm—led to spontaneous film formation. The corrosion potential was reported to increase with increasing oxygen content, as expected. However, at higher oxygen levels of over 2.5 ppm, spontaneous pitting was observed. In these cases, the corrosion potential was increased to values above the breakdown potential. For typical steam turbine service, a low oxygen level of about 0.01 ppm and some uniform corrosion would be expected. During a layup, there can be leakage of air into the system and oxygen levels can exceed 3 ppm. In this case, spontaneous pitting would be predicted, and this might lead to other corrosion issues, such as SCC or CF.

Gonzalez-Rodriguez et al. [29] studied hydrogen embrittlement in Type 410 stainless steels and considered the effects of chloride, sulfate, and hydroxide contents. SSRTs were performed on a series of samples in oil or deaerated salt solutions at 90°C. The 410 steel showed minimal susceptibility to SCC in hydroxide up to 40% NaOH or in sulfate up to 30% Na2SO4. Fractography showed microvoid coalescence and cup and cone fracture, indicative of ductile failure. The 410 steel showed significant susceptibility to SCC in chloride environments between 3.5% and 20% NaCl at a natural pH of 7.6. Fractography showed intergranular features up to 15% NaCl, thereafter regaining ductility. It was also demonstrated, however, that sulfate and hydroxides acted as inhibitors. Tests performed under cathodic polarizing conditions and at low pH 3 showed intergranular, quasi-cleavage features and indicated hydrogen embrittlement as the mechanism.

Gonzalez-Rodriguez et al. [30] also studied chloride-induced SCC of Type 403 martensitic stainless steels and considered the effects of both pH and heat treatments. SSRTs were performed on a series of samples in oil or deaerated 20% NaCl solution at 95°C. Acidity was varied between pH 5 and 7 using hydrochloric acid. The 403 steel was observed to be highly susceptible to NaCl-induced SCC at all pHs tested and in all heat-treated conditions—as-quenched, quenched and tempered, and annealed. Susceptibility was measured by strain to failure. Fractography indicated intergranular fracture for the quenched samples. The SCC was attributed to hydrogen embrittlement, exacerbated by the presence of ε-carbides, high dislocation densities, and coherency strains. Susceptibility decreased with increasing tempering temperature between 200°C and 600°C and increasing pH between 5 and 7. Fractography indicated a transition to transgranular fracture. The annealed sample was found to be susceptible to SCC only at the low pH of 5.

Phosphates have been observed to be beneficial for corrosion resistance. Sodium phosphates are used in boilers, particularly drum boilers. The phosphates cause co-deposits with harmful impurities, effectively neutralizing them while passivating steels. The improvement in corrosion resistance has been confirmed by pitting potential measurements on disk and blade alloys in the presence of sodium phosphate and sodium chloride.

Molybdenum sulfide is considered a corrodent in various turbine components. The sulfide is used as a thread lubricant during disk manufacture; disks are pre-heated and shrunk onto rotors. The MoS_2 oxidizes to form either low-pH molybdic acid or, possibly, ammonium molybdate. The low pH can cause rapid attack of turbine steels. In the presence of steam, MoS_2 has been reported as reducing the notch strength of steels to that of about 30% in air. It has also been reported as having caused failures in bolts and rotor shafts.

2.5.6 Static and Dynamic Loading

The loading conditions experienced by each component in the turbine will determine the design of the component and the material of construction. The material choice is also influenced by the chemical environment and the possibility of corrosion. Components must be able to withstand operational stresses, so both the geometry and material yield strength must be considered. Designs often include stress concentrations in the form of keyways or dovetails for joining of components. These are common in blade-disk attachments. These highly stressed regions become more susceptible to both SCC and CF.

SCC failures are the result of static or sustained stresses. Rotors turning at constant frequencies result in static stresses, although the components themselves are not stationary. Axial stresses in blades caused by centrifugal forces of rotation and bending stresses from steam pressure are examples of static stresses in moving components. However, if rotor speeds change frequently because of repeated startup and shutdown sequences during scheduling, stresses become dynamic. Poorly designed turbines can suffer from problems associated with steam flow that excite blades and cause vibration. In these cases, stresses are dynamic and CF becomes the dominant concern. Given the nature of turbine design and operation, most components will endure both static and dynamic stresses.

One approach used to decrease stresses and therefore decrease susceptibility to SCC and CF is shot-peening. Shot-peening introduces compressive stresses into the surface of materials, thereby decreasing the tension that contributes to cracking. This has been shown to reduce the likelihood of SCC in disks and CF in blades. The compressive surface stress resulting from shot-peening decreases the effective stress acting on the component and can decrease the susceptibility to cracking. However, this compressive surface stress also introduces a tensile subsurface stress. Corrosion pits that grow through the compressive zone might encounter tensile stresses, and there might be a higher propensity for transitioning to a crack.

2.6 Pit-to-Crack Transitions (Experimental)

The pitting, SCC, and CF mechanisms in various steam turbine alloys can be studied individually or in combination. The basic understanding of the three mechanisms was presented previously. However, it is important to recognize that the mechanisms are not necessarily independent of one another. It is accepted that the formation of pits can lead to stress concentrations, which can in turn lead to crack formation. Understanding how these phenomena are related is clearly of interest from the perspective of turbine operation and integrity management.

The concept of pit-to-crack transition can be divided into several stages, each one of which must be considered and well understood to allow damage mitigation strategies to be developed. Initially, one must consider the initiation of pits on a sample surface. This has been studied at length, particularly in passivating alloys and chloride environments. Pits are then assumed to grow. As the pits grow, the local stresses concentrate and the pits can transition into short cracks. The short cracks then grow, transitioning into long cracks. It is important to recognize that short and long cracks are often considered differently, as are the assumptions regarding their growth. Understanding of the pit-to-crack transition is important in understanding the overall life cycle of the corrosion mechanism.

It is also important to note that cracks do not always initiate at corrosion pits. Lyle observed a strong correlation between crack initiation and the presence of corrosion trenches as well as fewer instances of crack initiation from pits, as referenced in Rosario et al. [31]. Studies (Zhou et al. [32]) have also shown crack initiation from inclusions, particularly manganese sulfide. Endo demonstrated a correlation between pits and inclusion content or material impurity in 3.5% NiCrMoV steels. However, this result was in contradiction to work by Siemens (David et al.) that demonstrated that crack initiation was not affected by the cleanliness of the steel. Modeling efforts, which will be described later, have generally focused on the assumption that corrosion pit initiation, growth, and passivation are the primary mechanisms of pit formation.

Shalaby et al. [33] performed an extensive study of crack formation in Type 403 martensitic stainless steel in simulated steam turbine environments. They performed fatigue experiments in solutions containing various combinations of hydroxide, chloride, sulfate, phosphate, and silicate. These species are all known to affect corrosion susceptibility. The work involved fatigue testing of smooth, tapered cantilever beam specimens. Some tests were taken to failure, whereas others were interrupted for examination of surfaces for crack initiation. Fracture surfaces were inspected for failure mode following testing. Figure 2-26 provides sample data that demonstrate the effect of the test environment on fatigue lives.

Shalaby identified four crack initiation modes during the fatigue study—intrusion-extrusion sites, pitting, dissolving nonmetallic inclusions, and emergent etching of grain and platelet boundaries. The crack initiation could be qualitatively correlated to mechanically controlled modes, environmentally controlled modes, or a mixture. The tests performed in air, hydroxide, phosphate, or silicate solutions were observed to be mechanically controlled. Cracks initiated primarily from an intrusion-extrusion mechanism or at nonmetallic inclusions. The fatigue crack propagation was reported as transgranular and resulted in ductile fracture, but with long fatigue lives. The tests performed in chloride or sulfate solutions were observed to be environmentally controlled. Cracks initiated primarily from pits in these aggressive environments, in addition to nonmetallic inclusions and emergent boundary etching. Propagation was reported as being a combination of intergranular and transgranular and resulted in a more brittle fracture and shortened fatigue lives.

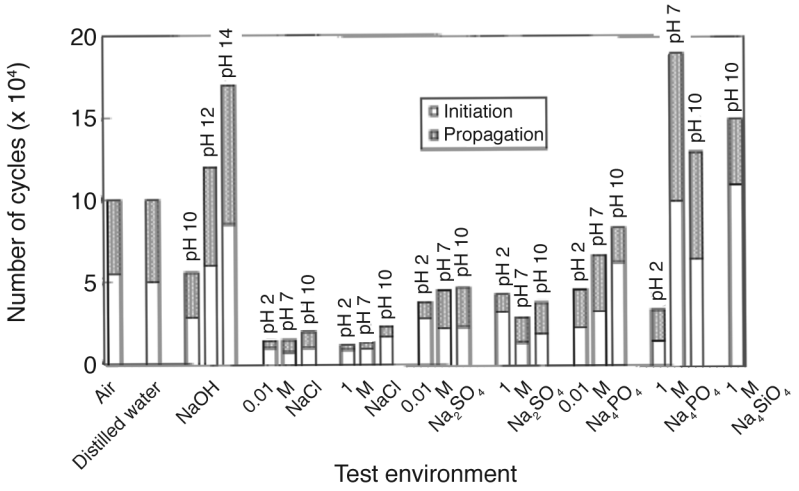


Figure 2-26
Effect of test environment on the fatigue life and cycles to crack initiation at 448 MN/m² (65 ksi) [33]
Used with permission from NACE International

A correlation was also noted between the failure modes and the corrosion potentials measured during the tests. The mechanically controlled mechanisms observed in hydroxide, phosphate, and silicate solutions tended to be at potentials below approximately -350 mV (normal hydrogen electrode [NHE]). The environmentally controlled mechanisms observed in chloride and sulfate solutions tended to be in intermediate potentials between -350 mV and -150 mV (NHE). These tests typically led to the shortest fatigue lives. Mixed mechanical and environmental mechanisms were observed in solutions containing low concentrations of hydroxide or phosphate, and these were at higher potentials, above -150 mV (NHE). These relations are illustrated in Figure 2-27.

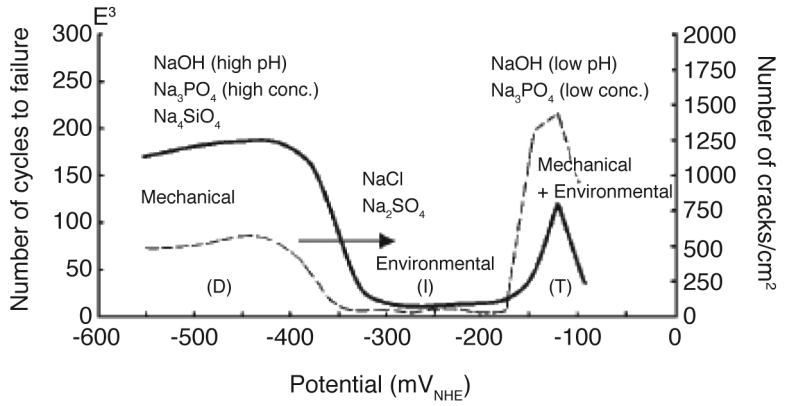


Figure 2-27
Number of cycles to failure and number of cracks per unit area versus steady-state corrosion potential for Type 403 stainless steels (Tested at 448 MN/m² [65 ksi] in dearated aqueous solutions simulating steam cycle environments. D = ductile failure, I = intergranular, T = transgranular, and () = dominant mode.) [33]
Used with permission from NACE International

Zhou et al. [32] studied SCC in various iron alloys in high-temperature water. They performed SSRTs on seven different iron alloys with different size, shape, and density of inclusions. Cracking of steels in lithiated water was shown to increase with increased applied potential or temperature. Cracks were observed to initiate from corrosion pits, film ruptures, and inclusions. In the case of pure irons, crack initiation was observed not at pits or inclusions, but at slip lines, indicating a different mechanism. Cracking in low-alloy steels was found to be associated with inclusions. It was suggested that dissolution of MnS inclusions can result in sulfur species that promoted cracking by either increasing anodic dissolution or enhancing hydrogen entry. The effect of the sulfur might be mitigated by chromium addition to the alloys.

A significant effort in understanding pit-to-crack transitions has been performed by Turnbull and colleagues at the National Physical Laboratory (NPL) in the United Kingdom. Turnbull has performed an in-depth series of experiments, considered modeling of the transitions, and has developed statistical techniques that allow predictions of initiation and growth rates. More modeling-based work has been performed by EPRI and others, and this will be covered in the next section.

Turnbull and Zhou [34] studied pit-to-crack transitions in 3% NiCrMoV alloys in various simulated steam turbine environments. The focus of the study was to understand the effect of both aeration and chloride on the transitions. A series of 35 tensile specimens was used, self-loaded under displacement-controlled conditions to 90% of their 0.2% proof stress. Sixteen of the samples were smooth, and the rest were pre-pitted using a procedure developed at NPL. The samples were immersed in deaerated water, aerated high-purity water, or aerated water containing 1.5 ppm chloride. Temperatures were maintained at 90°C. The samples were left for several months, with removals from the system at various intervals (7, 13, 19, and 22 months) in order to allow for inspection and measurement of pits and cracks.

Turnbull recorded the corrosion potential during the tests. As expected, potentials in the deaerated waters were lower—approximately -0.60 V (SCE)—and potentials in aerated waters were higher at approximately up to +0.10 V (SCE). The effect of chloride in aerated solution was to decrease the potential to approximately -0.20 V (SCE). It was predicted that the pit potentials would be lower and the gradients to the pit mouth influenced by solution conductivity.

At the completion of the tests, the self-loaded samples were unloaded using a mechanical testing machine and their residual stresses were estimated during the process. For the chloride-free waters, the stress was found to have decreased to approximately 80% proof stress (versus the original 90%). The test sample in deaerated water had a shiny black film, whereas the test samples in aerated and chloride solutions had brown films or corrosion product. In all cases, pits were observed, but their density varied with the environment. The pre-pitting procedure was found to be unnecessary. Pits in the deaerated and aerated high-purity waters tended to be shallower and sharper in their aspect ratio. Pits in the aerated chloride solution tended to be both deeper and broader in aspect ratio, and the density was approximately a factor of two higher. In the cases of the aerated tests, both with and without chloride-tested samples, cracks were also observed (see sample data in Figure 2-28). Cracks were reported as having turned toward one another and coalesced. The observation of pits in deaerated chloride-free waters is important from an operational and integrity management perspective. The result is inconsistent with the results of Speidel, in which no pitting was observed in high-purity water.

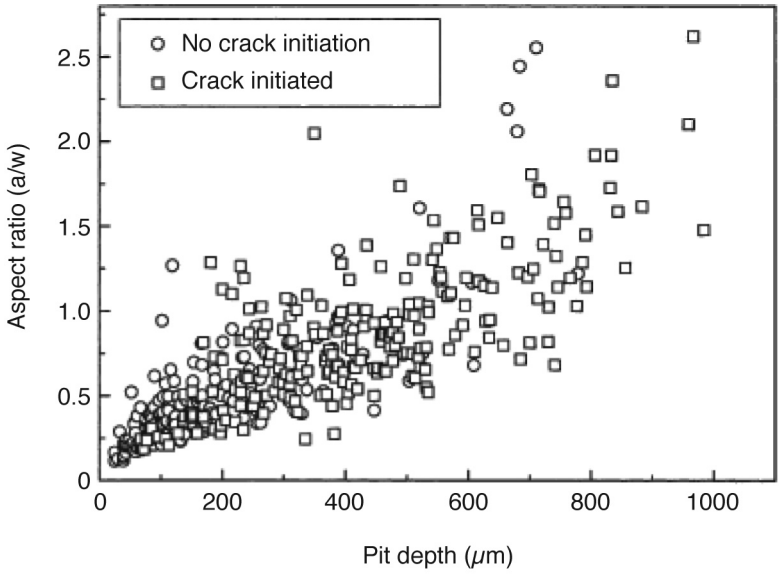


Figure 2-28
Aspect ratio of pits as a function of pit depth on the self-loaded specimens tested in aerated 1.5 ppm Cl- solution at 90°C for 9187 h [34]
Used with permission from Elsevier

Turnbull performed statistical analyses of the pit and crack measurement data. It was determined that the pit growth rates in aerated chloride environments was four to six times higher than the equivalent chloride-free environments and that pit-to-crack transition probability increased with pit depth. There were some uncertainties in the data, and simplifying assumptions were necessary; however, it was also demonstrated that growth rates are approximately four times higher in short cracks than in long cracks. It should be noted that the self-loaded test samples would have experienced displacement-controlled crack propagation and CGRs could be expected to decrease with length. This was not discussed in detail.

Some of Turnbull's analyses were based on the criteria that a pit will transition to a crack if the threshold stress intensity factor is exceeded and the CGR is higher than the pit growth rate. However, several cracks were observed to have initiated either independently of pits or at the side of pits as opposed to at the base of pits. This has implications on the assumptions in the modeling.

2.7 Pit-to-Crack Transitions (Modeling)

A significant effort has been made over the years to develop models that describe the fundamental driving parameters and kinetics of SCC- and CF-related phenomena. A natural central aspect of this work has been the need to better understand crack initiation and subsequent growth. However, the work is not a trivial matter because cracks are known to initiate from nominally smooth surfaces, from erosion pits and corrosion pits. In the case of the carbon and low-alloy steels used for steam turbine applications, pitting occurs; as a result, much of the effort has considered pit formation and subsequent transition to cracks.

The study of crack initiation and growth is complicated by difficulties in defining what constitutes a crack, and there are difficulties in defining at what point in time or under what conditions a crack is considered to have initiated. Various definitions can be considered (Andresen [35]). One option is to

consider an arbitrary length (for example, 50 mm) that is readily detectable by ultrasonic inspection. Another is to consider the minimum depth of pitting at which crack initiation and growth are observed. Some studies have indicated that crack initiation needs to be considered using a probabilistic approach and cracks initiate at dimensions consistent with coalescence of microscopic defect cracks to form an entire crack front. One can also consider that in many fatigue test programs, crack detection is considered a failure of the sample because so much of the lifetime of a component is spent on initiation.

In addition to the debates regarding crack initiation and growth, there are difficulties in defining, and even accepting, the concepts of K_{ISCC} for SCC and ΔK_{th} for CF. Very low K_I or ΔK values are characterized by low applied stresses or by very small crack sizes. The inability to formally define the point of crack initiation also leads to the problem of defining these critical values. Cracks have been observed to initiate at nominal stress intensities below postulated K_{ISCC} values. As the crack size approaches zero, the stress intensity approaches zero, and the definition issue remains. One must also consider the natural defects in materials that lead to crack initiation, even in nominally smooth surfaces. These analysis techniques usually rely on the assumptions of linear elastic fracture mechanics (LEFM), and the concept of stress intensity factor loses validity as crack size decreases to subgrain dimensions.

Much of the work on crack initiation and growth and pit-to-crack transition has recognized a difference between short crack and long crack behavior. Some of the difference can be attributed to the difficulties associated with defining a crack and the assumptions inherent in LEFM. However, there are also studies that have demonstrated differences in mechanisms between the short and long cracks. There have been reports of transitions from transgranular to intergranular fracture mechanism. Short and long cracks can also be considered to have different chemistries; short cracks are expected to have chemistries comparable to the bulk solution, but long cracks might have different chemistries, depending on the crack growth and mass transport–related phenomena occurring along the crack length. These concepts should also be considered in the various analyses and modeling efforts.

It is recognized in many systems that the local crack tip strain rate is a fundamental parameter in understanding environmental cracking systems. Crack tip strain rates cannot be measured directly, and therefore must often be inferred from stress and strain analyses that might suffer the limitations of LEFM. Alternatively, crack tip strain rates can be inferred from complex crack tip creep analyses. The variability in data among experimental test conditions and individual researchers' techniques leads to difficulty in verifying these concepts. It has also been recognized that replicate tests performed under identical conditions do not necessarily guarantee equivalent results. Therefore, it is generally accepted that crack initiation studies in particular should be analyzed using probabilistic techniques.

Early modeling work by Clarke et al. (1981) developed a model that provided a CGR as a function of temperature and material yield strength. The model was accepted by the U.S. Nuclear Regulatory Commission for assessment of turbine disks with cracks. It was later modified to include the effects of manganese content and tempering temperature. The large scatter in the data indicated that further work was necessary.

Life prediction codes have been developed by the Southwest Research Institute (the Lifetime Analysis of Steeples "LAST" program) and EPRI-funded work (the Disk Crack Evaluator "DICE" program). These models take into account stress intensity factors and crack sizes, and they use the Clarke model to estimate remaining life. However, at that time, no codes were commercially available that incorporate all key parameters (stress, temperature, wet surface films, and material properties) into a probabilistic assessment.

In later modeling work, Rau et al. developed an equation to predict normalized initiation time as a function of material yield strength and a calculated CGR, as referenced in Rosario et al. [31]. The CGR was the earlier Clarke model and a function of temperature, yield strength, manganese content, and tempering temperature. A cubic relationship on normalized applied stress was assumed, based on experimental observations. The normalized initiation time model was combined with a Weibull-type equation to give an initiation probability. This early model was based largely on observations and empirical relationships and was nonspecific in the actual transition mechanism.

EPRI funded research work in 2000 [19] to develop techniques for predicting lifetimes of steam turbine components. Englehardt and Macdonald performed much of this work, and they developed the damage function analysis (DFA) technique. The analysis is based on statistics and the electrochemical mechanisms understood to control pit and crack growth. The model is based on the development of a statistical function to describe the frequency and depth of pit or crack events. Pit nucleation rates, pit growth rates, and CGRs are then used to determine how the event distributions evolve with time. A pit reaching a critical value can transition into a crack, and a crack reaching a critical value might fail catastrophically. The work assumed that a pit would transition into a crack if it exceeded a critical length and passivated. The critical length of a crack leading to failure was not discussed explicitly, but it can be determined from independent fracture mechanics techniques. By predicting the evolution of the damage function, one can estimate the condition of a given turbine component and therefore the service life of the turbine. A simplification of the damage evolution sequence is provided as Figure 2-29. An algorithm for predicting damage is provided as Figure 2-30.

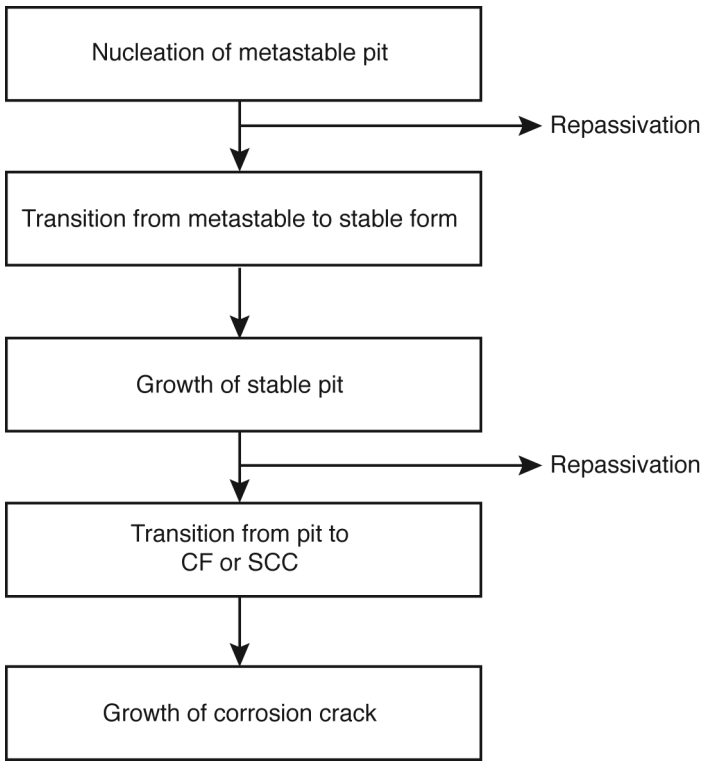


Figure 2-29
History of the nucleation and propagation of corrosion damage [19]

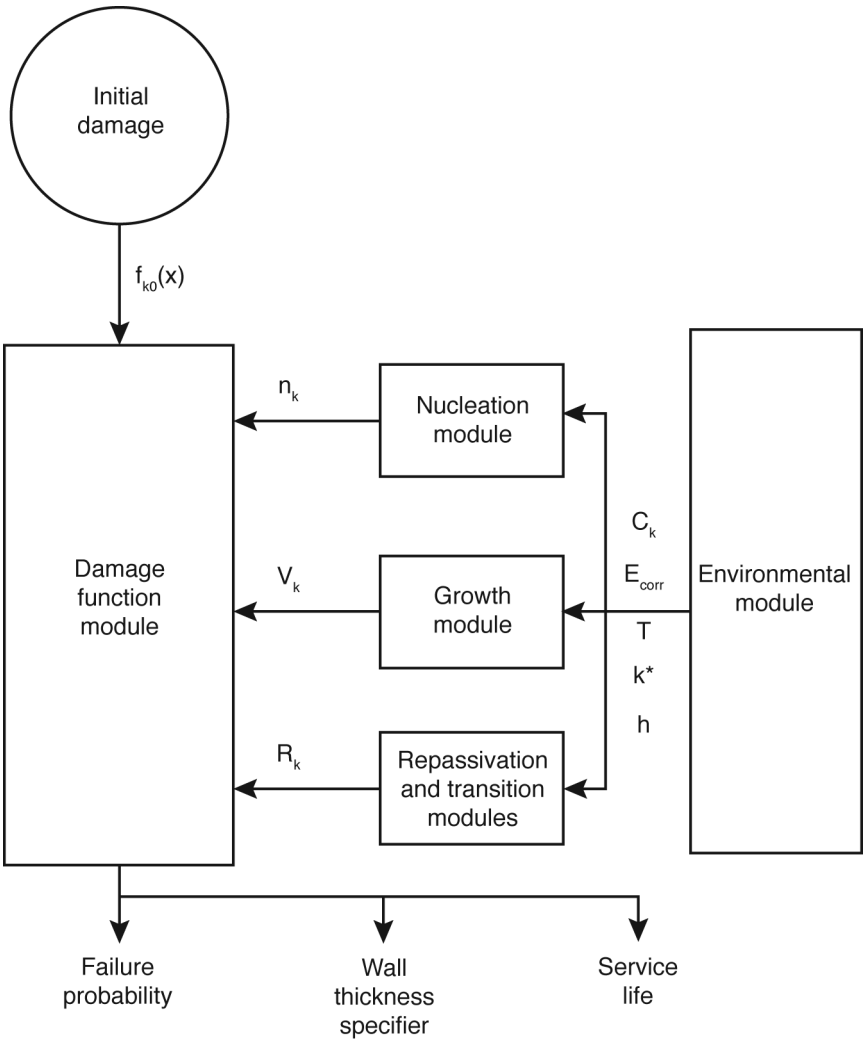


Figure 2-30
Structure of algorithm for prediction of damage function [19]

The DFA technique for predicting damage to steam turbine components provides a variety of predictive capabilities. Figure 2-31 is a plot of the calculated concentrations of species along the depth of a crack. The concentrations of salt, iron ions, and pH are shown to vary by orders of magnitude, in some cases. Figure 2-32 and Figure 2-33 are plots of calculated CGRs as a function of loading frequency. Plots demonstrating the dependence of frequency can be used to demonstrate the relations between SCC and CF behavior. SCC is effectively CF with negligible frequency. The plots show that the CF CGRs become very sensitive to both potential and salt content at the low frequencies, indicating an SCC sensitivity to these parameters. Potential is affected by oxygen content, as previously explained.

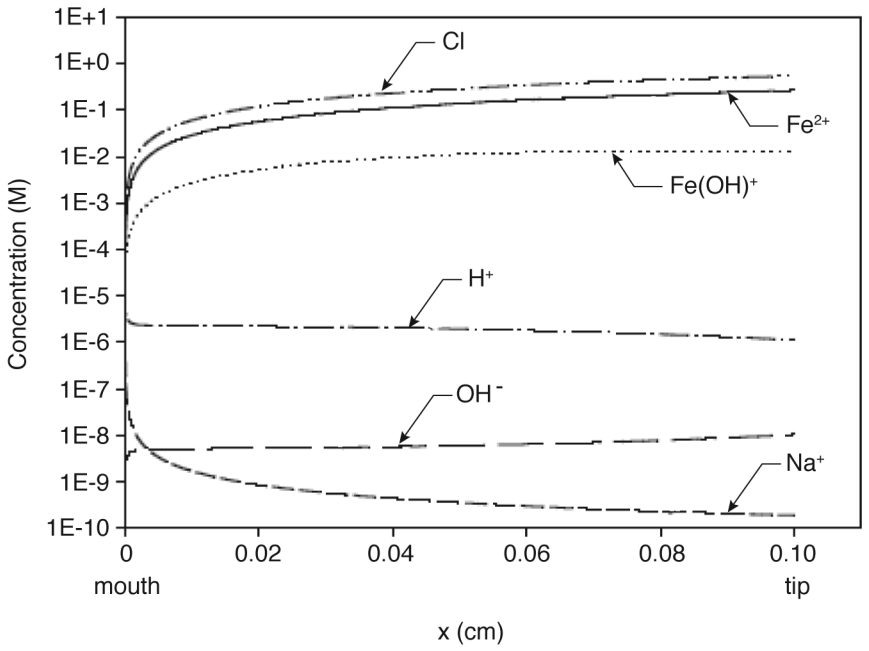


Figure 2-31
Calculated concentrations of species down a crack [19]

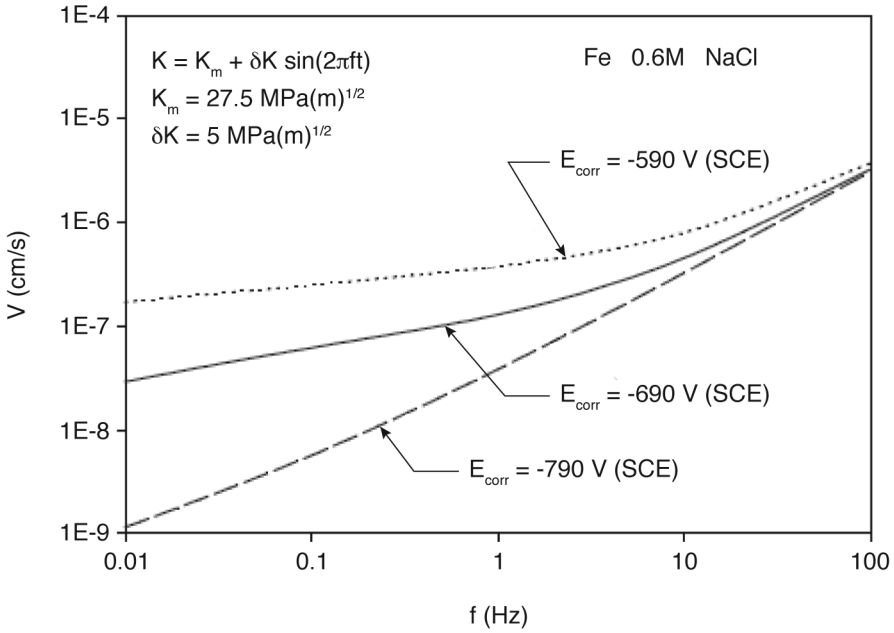


Figure 2-32
The effect of loading frequency, f, on crack propagation rate for different corrosion potentials in 0.6 M NaCl with pH = 8 at T = 25°C (77°F) [19]

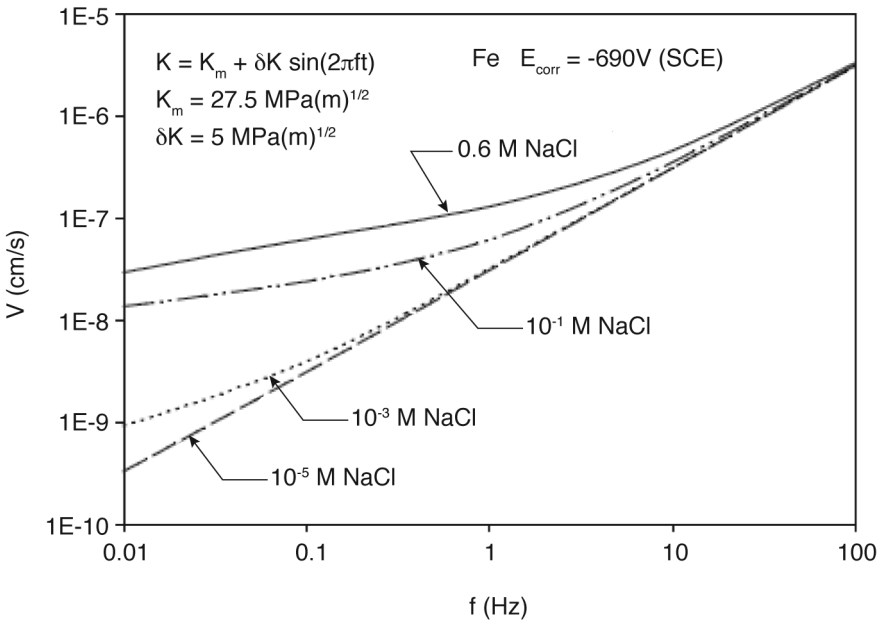


Figure 2-33
The effect of loading frequency, f, on crack propagation rate for different bulk concentrations of NaCl with pH = 8 at T = 25°C (77°F) and E_{corr} = -690 mV (SCE) [19]

A limitation of the technique is that it requires knowledge of pit nucleation and passivation rates, and CGRs are known. Given the sensitivity of these rates to various electrochemical parameters and service conditions, these analyses can be complex. Several parameters are included that describe diffusion of species in the system, the primary anodic and cathodic reactions, and the effect of chloride and oxygen concentrations on damage evolution. Further work that was recommended following the model development included experimental determination of some of these critical model parameters.

The DFA technique was further developed by Englehardt et al. [36]. In this work, the requirements for a pit transitioning to a crack were that (1) either the stress intensity K_I acting on the pit exceeded K_{ISCC} for SCC under static loaded conditions or the change in stress intensity ΔK_I exceeded ΔK_{th} for CF under dynamically loaded conditions and (2) the CGR exceeded the pit growth rate. These conditions were first outlined by Chen et al. (1996). The first condition is related to fracture mechanics, and the second condition is that the crack must be able to outrun the pit. Mathematical analysis of these conditions demonstrated that they are equivalent to those defined earlier by Englehardt and Macdonald in the EPRI 2000 work.

The modeling work was developed, in part, using experimental work from Macdonald and Urduiqi-Macdonald [37]. It was noted that there was a similarity in the percentage of pits with cracks at specific depths, despite differences in environmental conditions. It was also noted that cracks did not necessarily nucleate from the base of pits and might have nucleated alongside them.

One of the conclusions of this modeling work was that the likelihood of pit initiation was sensitive to environmental conditions in the steam turbine during shutdown. The combination of oxygen, chloride, and stress levels during the operation is critical. It was suggested that maintaining a deaearated environment and rinsing the steel surfaces would be beneficial in mitigating the threat of localized corrosion.

Later modeling by Turnbull et al. [34] considered the statistics associated with pit-to-crack transitions during the initiation of SCC. As with the earlier analysis, it was assumed that a pit will transition to a crack if the threshold stress intensity factor is exceeded and the CGR is higher than the pit growth rate. A three-parameter Weibull distribution was used to model an initial stable pit depth distribution. The depth of an individual pit and the evolution of the pit distribution were modeled using appropriate partial differential equations. A crack growth law following transition was assumed that depended on both applied load and crack depth. A random-number generator was then used to simulate the evolution of the pit and crack distributions in a given test case. Previous experimental data were used for the inputs, and predictions were found to be reasonably consistent with available experimental data. Empirical parameters were identified for predictions of pit-to-crack transitions in deaerated pure water, aerated pure water, and aerated chloride water (Turnbull et al. [38]).

The Turnbull modeling provided measurements of crack depth distributions that were unexpected. Inspection of pits and cracks using a novel layer removal technique indicated that 43% of cracks extended beyond the pits and were surface-breaking, as was assumed in the model. However, in 50% of cases, the cracks were shallower than the pits and surface breaking; in 7% of cases, the cracks were shallower than the pits and non-surface-breaking. These observations (see Figure 2-34) were inconsistent with the assumptions of the model and suggest that reconsideration and modification of the approach might be necessary.

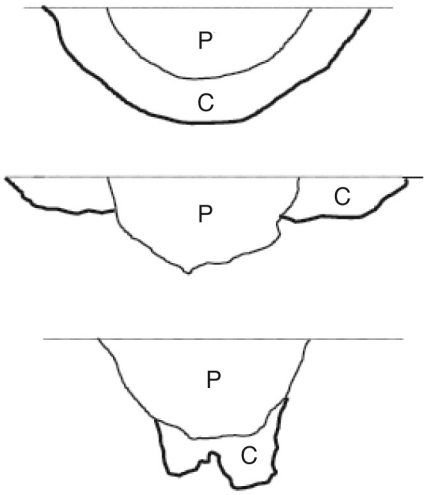


Figure 2-34
Pit (P) and crack (C) shapes (Shown from top to bottom are pits with cracks extending beyond the pit base and breaking surface, pits extending beyond the crack, and cracks just emanating from the pit base but not extending to the surface.) [38]
Used with permission from Elsevier

Turnbull also noted that CGRs decreased during growth, rather than increased with crack depth as would be intuitively expected. He reported difficulty in fitting CGR parameters to the proposed form of the equation [38]. This was attributed to assumptions associated with the behavior of short and long cracks. It should be noted that the self-loaded samples would have been displacement-controlled and CGRs would be expected to decrease. It is also possible that the cracks had entered Region II behavior, in which less effect of stress intensity on CGR would be expected. Turnbull also reported that short

cracks were typically transgranular and long cracks were typically intergranular. This implies a change in mechanism that could lead to a decrease in growth rates. However, it also implies a mechanism becoming more dependent on corrosion than on mechanical fracture processes.

Continued modeling efforts by EPRI [39] were based on the earlier work by Macdonald and Englehardt [19, 40]. The DFA technique was further refined. This approach involves development of a statistical pit distribution and traces its evolution over time using various pit growth rates. In particular, three mechanisms for pit repassivation were included in this most recent model. The three mechanisms are interaction of pits that decreases the potential at the base of the pit below the repassivation value, overlapping of pits, and accidental repassivation of pits. The modified approach allows the number of unknown parameters describing the pit evolution and pit-to-crack transitions to be decreased. Use of the modified model was provided by examples that involved pitting corrosion of aluminum alloys in tap water and pitting corrosion in 403 blade steel and A470 disk steel (see, for example, Figure 2-35).

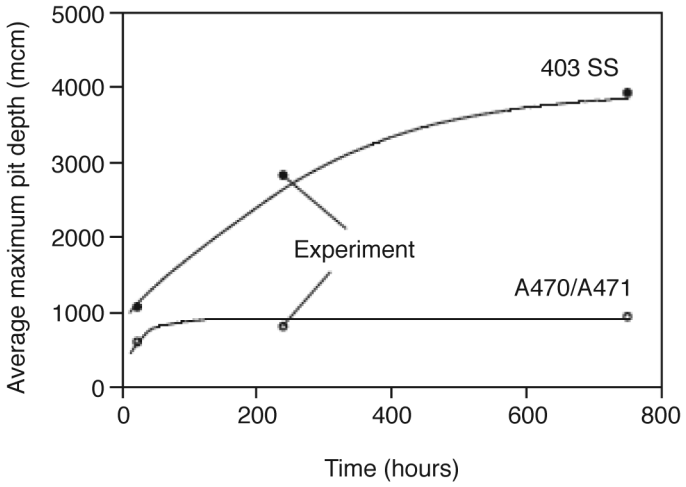


Figure 2-35
The mean depth of the deepest pit as a function of time for 403 stainless steel and 470/471 steel [39]

A further refinement was made to the model in the form of a probabilistic component. The DFA can be related closely to Extreme Value Statistics (EVS). If the damage function is known or can be estimated for defects under known conditions, EVS can be used to calculate the probability of failure by CF or SCC. The model was run for a simulated steam turbine's operational life as an example. Time of operation and shutdown, temperature, loading, pH, and chloride and oxygen concentrations were all defined and the probability of failure calculated. By varying the input chloride and oxygen concentrations, the model demonstrated that failure is very sensitive to these parameters (see Figure 2-36 and Figure 2-37). The result confirmed and highlighted information known from operational experience. It was proposed that turbines be rinsed with chloride-free water during shutdown, under nitrogen blanketing conditions if possible.

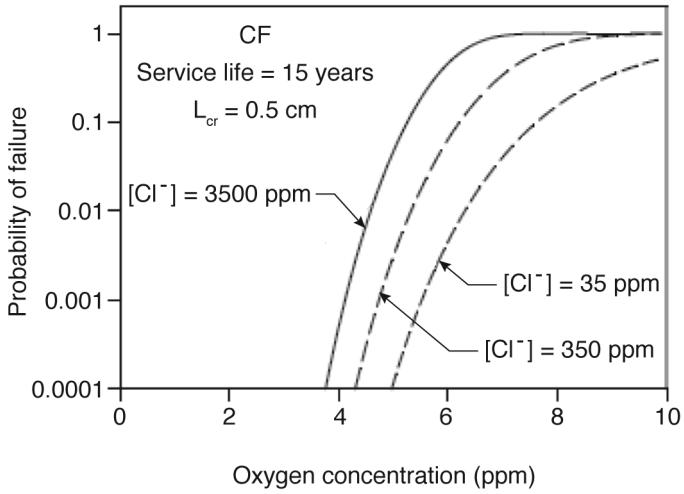


Figure 2-36
Calculated failure probability for LP steam turbine blades from CF as a function of different oxygen concentrations in the electrolyte film during the shutdown period [39]

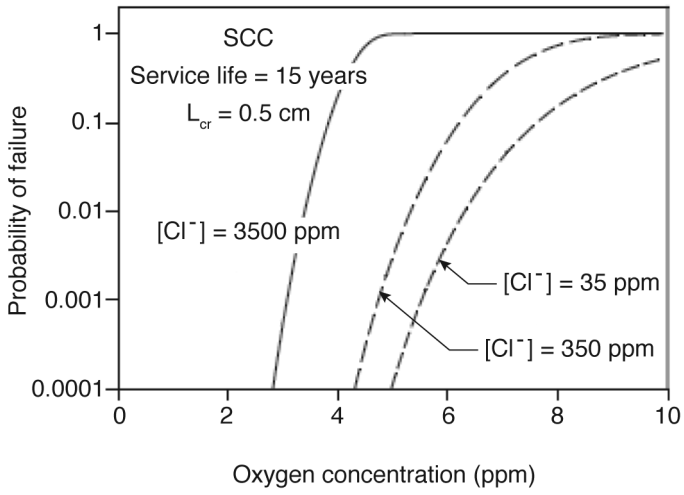


Figure 2-37
Calculated failure probability for LP steam turbine blades from SCC as a function of different oxygen concentrations in the electrolyte film during the shutdown period [39]

The EPRI 2007 work also included the measurement of various parameters necessary for modeling of corrosion in 17-4PH. The corrosion potential and current were measured on 17-4PH steel in sodium chloride solutions as a function of salt concentration, pH, temperature, and dissolved oxygen content. Data were fit to empirical equations with satisfactory agreement. The work demonstrated that the corrosion of 17-4PH proceeds in two stages: 1) uniform corrosion, during which the rates are sensitive primarily to solution concentration, and 2) pitting, during which the rates are sensitive to oxygen concentration. Therefore, two empirical equations for each of potential and current were developed. It was acknowledged that several simplifications were necessary during the analysis.

Several proposals were made for future research and to expand on the current model. It was acknowledged that the model did not adequately account for the mechanical component of the SCC process but was more focused on the environmental components of the process. It was proposed that complementary work on hydrogen-induced cracking and a void nucleation and growth component be considered. In addition, it was acknowledged that some chemical kinetic parameters were not accurately known; it was recommended that these be studied with specific attention to the thin aqueous film conditions expected in the steam turbine. Longer-term studies of the pit propagation rate of 17-4PH steels were recommended.

Zhang et al. [41] used the DFA model to study pitting in an AISI Type 403 stainless steel in chloride environments. Their experimental work involved polarization scanning of test specimens in solutions containing varying concentrations of borate, hydroxide, and chloride. Breakdown potentials were shown to decrease with increasing chloride and increase with increasing pH. These results were used to support the validity of the Point Defect Model for describing passivity breakdown. Parameters determined from the experimental work were input to the model and used to predict pit nucleation numbers. These predictions were then compared to pit numbers measured on an ex-service failed blade. It was noted that none of the pits examined had cracks, and it was inferred that the crack leading to failure of the blade must have occurred from an exceptionally deep pit.

The failed blade was from the Texas Genco W. A. Parish Plant Unit 8 LP steam turbine. It was analyzed by visual examination, stereo-microscopy, and confocal laser scanning microscopy. Pit distributions were measured and related to the DFA model [42]. It was noted that pits without cracks of over 250 μm were present, which is significantly greater than early work by Jonas that predicted that pits of only 25-μm depth could nucleate cracks. Probabilistic analysis indicated that a pit depth of approximately 450 μm was necessary to ensure crack nucleation (see Figure 2-38 and Figure 2-39).

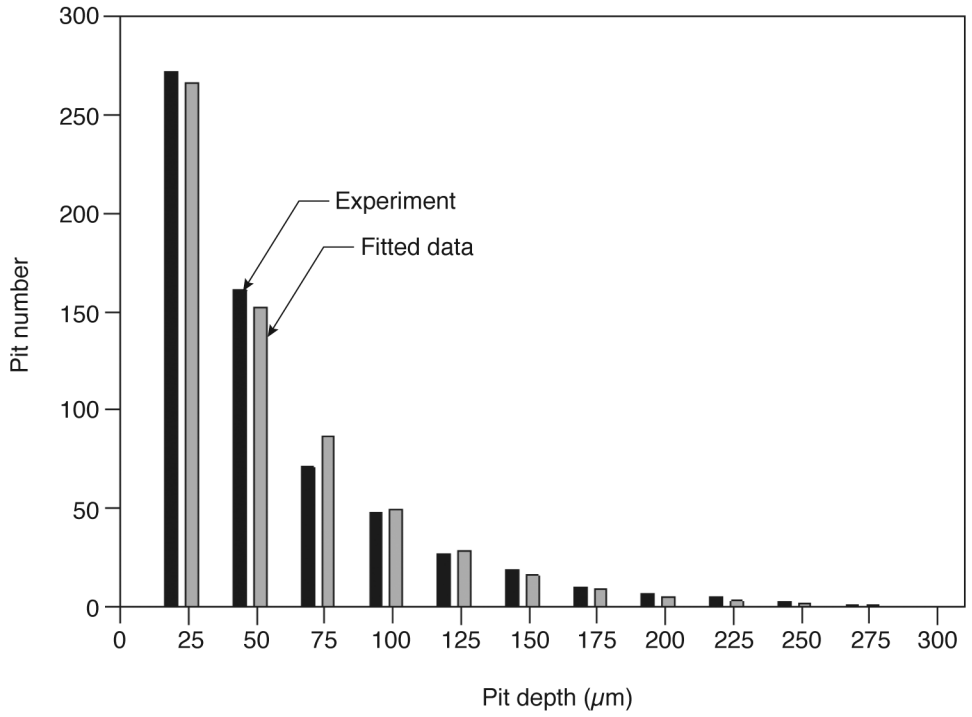


Figure 2-38
Comparison of integral damage function with that measured on a failed blade from the field [42]

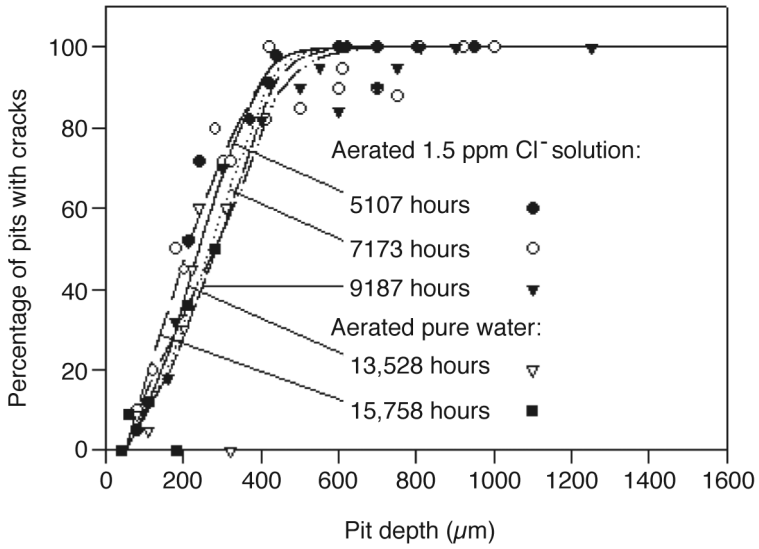


Figure 2-39
Likelihood of cracks developing from pits as a function of depth for 3NiCrMoV disk steel [42]

Englehardt et al. [43] further developed the DFA technique to include a Monte Carlo simulation. The Monte Carlo technique was developed as an alternative to the DFA to better simulate real conditions. In situations where only a few pits or cracks—or even a single pit or crack—lead to failure, the differential equations used to develop the DFA lose their strict physical meaning.

The Monte Carlo simulation was also developed considering the three stages of pitting damage: nucleation, propagation, and repassivation of stable pits. The technique allows one to account for the interaction of pits explicitly, and by doing so to decrease the number of parameters necessary to define the model. As with the DFA, electrochemical arguments are used to define metal dissolution and pit growth. Englehardt demonstrated application of the technique by showing a comparison of model outputs to experimental work performed on aluminum alloys in tap water. In addition, it was shown to reasonably predict the maximum pit depths measured in the previous study on pitting of 403 stainless steels in borate buffer solutions [42].

As with previous modeling efforts and known operations experience, the Monte Carlo simulations were used to demonstrate the importance of controlling conditions during shutdown. Sensitivity analyses were performed to determine which of oxygen concentration, chloride concentration, temperature, and pH have the most significant influence on probability of failure of turbine disks. Modeling demonstrated that oxygen concentration and temperature within certain ranges have the largest influence.

2.8 Case Studies

This section presents summaries of several case studies of failures of components in actual in-service power plants. A review of the literature indicated many steam turbine component failures that were not attributed to cracking associated with corrosion pits. Instead, many failures were attributed to erosion pits or improper joining.

2.8.1 An Investigation of the Failure of LP Steam Turbine Blades (Mukhopadhyay et al. [44])

Mukhopadhyay et al. described a case in which blades in an LP steam turbine in a 210-MW thermal power plant failed. The unit had been overhauled after five years of service but suffered problems two years later. The unit was shut down because of excessive noise and vibration in the LP steam turbine. Four failed blades were identified in the 29th stage. This stage, referred to as one of the Bauman stages, is known to be susceptible to vibration from steam flow. The typical operating frequency of the unit was 50 Hz, but there were some variations between 45.5 Hz and 52.4 Hz because of grid frequency regulation.

Specimens of the failed blade, lacing rods, and brazing alloy were taken for metallurgical analysis. Optical and scanning electron microscopes (SEMs) were used to examine the structure of the materials to determine their quality. Energy dispersive X-ray spectroscopy (EDS) was used to determine chemical compositions. Sections of blade and rod were mechanically tested by tensile testing and fatigue testing, and hardness measurements were performed. The fatigue testing simulated the vibration associated with the steam flow. Because the test was not performed in environment, chemical effects were not included.

Visual examination of the failed blades indicated that cracks had initiated around inner and outer lacing holes (see Figure 2-40). Damage was also observed on the leading and trailing edges of many other blades because of the impact of the broken blades. It was noted that brazed joints were disjoined between rods and lacing holes and contained holes, cavities, and physical discontinuities.

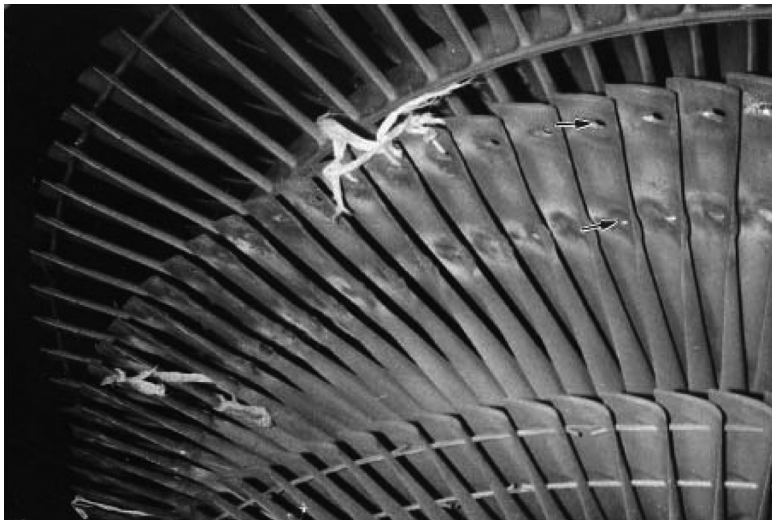


Figure 2-40
The assembly of the blade without the lacing wire that was removed by debrazing (Arrows indicate the position of the lacing holes from where the crack occurred.) [44]
Used with permission from Elsevier

The blade and rod materials were both AISI 400 series stainless steels (0.2% carbon and 12–14% chromium). Chemical analysis by EDS indicated satisfactory specification. Mechanical testing by tensile and hardness testing indicated expected properties. No material degradation was observed in the blade or lacing rod material. Blades were found to be tempered martensite and the rods bainitic, as expected. The brazing wire was found to contain 65% silver, 15% copper, 10% zinc, and 10% cadmium.

Examination of the fracture surface revealed intergranular, quasi-cleavage, and ductile fracture features. Figure 2-41 is illustrates the proposed stages of crack growth that preceded the failure. Some corrosion effects were reported near the thinner edge of blades where the fatigue crack was believed to have initiated. The blades were black, indicating magnetite formation of varying thickness. The failure was attributed to HCF, likely exacerbated by the grid frequency fluctuations that led to excitation frequencies in the blades.

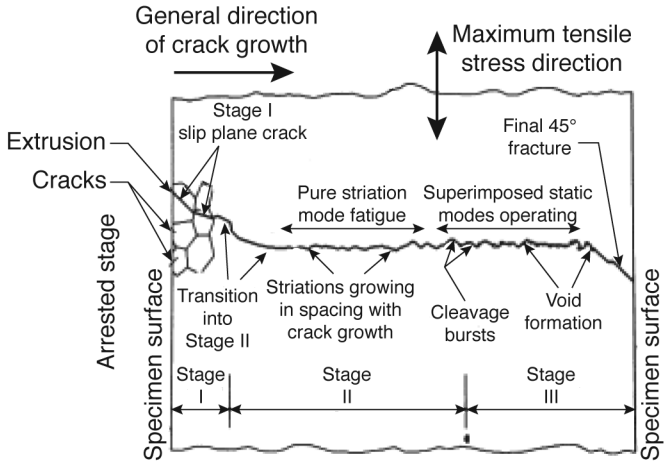


Figure 2-41
The nature of crack growth behavior [44]
Used with permission from Elsevier

An analysis of the brazed joint between lacing rods and the blades indicated the possibility of galvanic corrosion. EDS analysis suggested depletion of zinc from the brazing material near the lacing holes and chromium depletion in the blade material. Interfacial corrosion between the stainless steel blades and brazed alloys is a possibility, as anodic dissolution of zinc is possible in wet steam conditions. It was proposed that improper brazing could have led to failures of the lacing rods, which then contributed to fretting and excessive vibration of the blades. The higher stress concentrations acting on the blades associated with the failed lacing rods allowed fatigue cracks to initiate and propagate to failure. Although corrosion played a role in the failure, it does not appear that corrosion contributed to initiation of fatigue cracks in the blades. Corrosion effects were observed only on the fracture surface at the thinner edge of the blades.

2.8.2 Turbine Blade Failure in a Thermal Power Plant (Das et al. [18])

Das et al. [18] also described a case in which a blade in an LP steam turbine in a 220-MW thermal power plant failed. The turbine and blade had been in operation for approximately 33,000 hours. The unit was shut down because of noise emanating from the turbine. The failed blade was identified in the 29th stage of the turbine. Lacing rods connecting the blades were also reported to have failed.

Sections of the failed blade were cut for chemical, mechanical, and metallurgical analysis. Chemical analysis was performed by a standard wet method. Blade sections were cut for SEM examination, EDS analysis, and metallography. Hardness measurements were made to determine the basic mechanical properties of the material.

The blade material conformed to an ASTM 410 grade martensitic stainless steel. Chemical analysis by EDS indicated that the material satisfied the material specification, and hardness testing indicated a tensile strength within expected values. SEM microscopy revealed a tempered martensitic structure. In summary, there was no evidence that there were any problems associated with the metallurgy of the material or any significant degradation.

Visual examination revealed grooves along the blade, parallel to the fracture surface and along the blade edges. These were attributed to erosion by SiO_2 particles, presumably contamination in the steam. Silicon was identified by EDS.

Examination of the fracture surface of the failed blade indicated striations and intergranular fracture features, indicative of CF. The crack initiation point was traced back to the thinner side of the blade, the aerofoil's trailing edge. A magnetite scale was reported on some areas of the fracture surface. Pits were also observed on (and perpendicular to) the fracture surface. These were attributed to suspected chloride contamination in the steam, likely the result of condenser tube leakage. Chloride was identified by EDS.

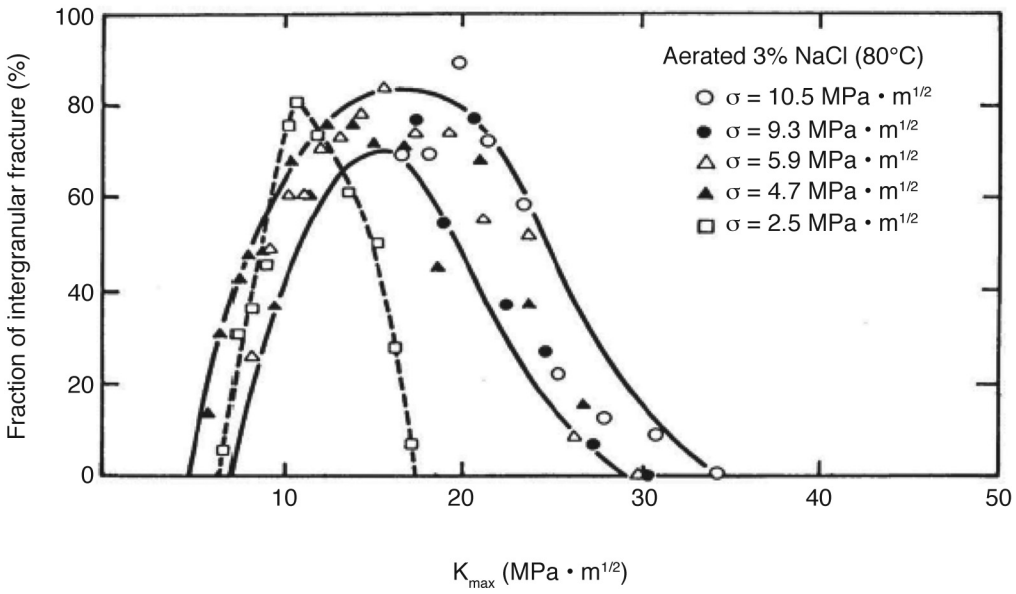
The final conclusion of the study was that there were no problems associated with the quality of the blade material, and that the failure had occurred because of a combination of silica particle impingement and chloride pitting. The silica particles caused repeated strikes on the blades and the grooving. Particles embedded in the blade materials led to some crevice corrosion, exacerbated by chloride impurities. The crevice corrosion on the thinner areas of the blade led to crack initiation. Cyclic wetting and drying of the blades in the PTZ caused further concentration of the chlorides. Oxygen and carbon dioxide present during shutdown might also have aggravated the corrosive conditions.

2.8.3 CF Phenomena Learned from Failure Analysis (Ebara [45])

Ebara studied CF of 12 Cr stainless steels in steam turbine environments through a compilation of failure analysis data. Of particular interest to that study was the effect of chloride and hydroxide impurities on the materials' corrosion susceptibility. It was demonstrated that NaCl and NaOH can have a deleterious effect on turbine blade service lives.

Ebara demonstrated that fatigue cracks initiated and propagated from corrosion pits. Applied stress calculations and pit depth measurements indicated an inverse relationship between stress and fatigue crack initiation depth. More pit depth was necessary to initiate fatigue cracks in samples subjected to lower stresses than those at higher stresses. This observation is consistent with expected trends.

Fractography indicated a varying degree of intergranular features along the fracture surface. Areas near the crack initiation point showed a smaller fraction of intergranular fracture, but the fraction increased away from the initiation point as the K_{max} increased. The fraction of intergranular fracture increased to a maximum of approximately 80% at a K_{max} of 16 MPa√m and then decreased as the K_{max} increased further (see Figure 2-42). This result implies a change in mechanism, which was not fully explored.



°F = (°C x [9/5]) + 32
1 MPa = 0.145 ksi

Figure 2-42
Fraction of intergranular fracture surface vs. K_{max}, aerated 3% NaCl aqueous solution [45]
Used with permission from Elsevier

The pit initiation experiments were performed using chloride solutions up to a concentration of 3% NaCl. Interrupted CF experiments clearly showed that fatigue cracks initiated from the base of corrosion pits and propagated along test sample surfaces (see Figure 2-43). The 3% NaCl solution was shown to decrease the fatigue strength of the material by 75% at 107 cycles with R = -1 and a frequency of 60 Hz. Lower concentrations of chloride had a lesser effect, though even dilute solutions of 3 ppm showed a deleterious effect on fatigue strength. The tests in chloride solutions were completed with CF tests in caustic solutions up to 40% NaOH, and they showed that similar strength reductions were possible. It was concluded that the accumulation of these impurities at the base of corrosion pits and/or fatigue cracks could have significant effects on the service lives of turbine components.

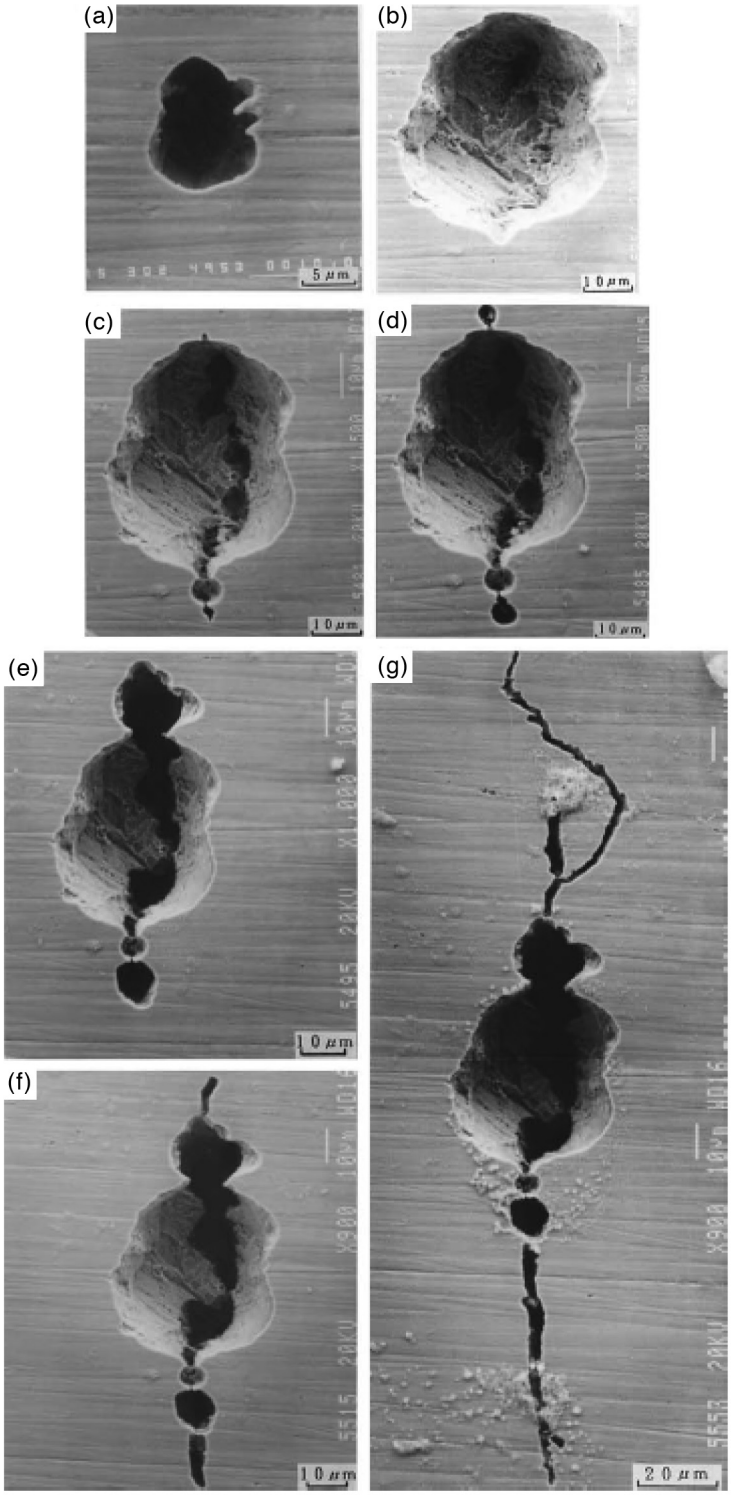


Figure 2-43
CF crack initiation and propagation process in association with corrosion pits in 3% NaCl aqueous solutions ([a] 4.95 x 106, [b] 5.45 x 106, [c] 5.48 x 106, [d] 5.485 x 106, [e] 5.495 x 106, [f] 5.515 x 106, and [g] 5.55 x 106.) [45]
Used with permission from Elsevier

Ebara also briefly discussed other variables that might affect CF of the 12 Cr steam turbine blade materials, though no experimental evidence was reported. The environmental variables of interest were considered to be dissolved oxygen, pH, and temperature, consistent with the earlier findings of other researchers. Metallurgical variables of interest include the microstructure, which is a function of tempering temperature and molybdenum content, and surface roughness. Mechanical variables that affect CF of the alloys include stress concentration factor and mean stress. It was indicated that the most effective way to reduce the susceptibility to CF is to reduce the design stress acting on the blades. This recommendation is consistent with current industry practice. However, some failure analysis examples (such as the ones presented in this section) indicate that failures of other components in the turbine can contribute to increased stresses on blades, exceeding their design stresses. The implication of this observation is that turbines might need to be designed with the potential for these failures in mind and designed so that significant vibratory stresses are avoided even if there are secondary failures in the turbine.

2.8.4 Failure Analysis of the Final Stage Blade in Steam Turbine (Wang et al. [46])

Wang et al. described a case in which steam turbine blade cracking was observed after approximately 13,200 hours of service. A fault tree analysis was performed in order to determine the cause of the failures. Preliminary analysis indicated that fatigue or CF was the cause. Electrochemical corrosion, stress corrosion, and water erosion were ruled out as causes. The continuing investigation included chemical and mechanical analysis, visual examination of the blades, metallography, and fractography. Chemical analysis was performed by EDS during SEM examination of material from the blade root. Mechanical testing included hardness measurements, tensile testing, and impact testing.

The blade material was a modified 12 Cr martensitic steel. The material was heat-treated to provide erosion resistance. The microstructure was observed to be tempered martensite for the quenched region of the blades, and showing no sign of material degradation. Chemical analysis by EDS indicated that the material satisfied specification. Yield and tensile strength measurement also satisfied specifications. However, the area reduction, impact toughness, and elongation were lower than expected. Tempered sorbite (a form of pearlite) microstructure was observed in the blade root region, indicating an insufficient temperature during processing. It was recommended that the tempering temperature be increased.

Visual and microscopic examination of the blades indicated erosion pits on the rearward face of the blades and along the entire length. However, these erosion pits were not considered to have initiated the cracks observed, which appeared to have initiated from the salient face of the blades. This result was unexpected. In addition, no corrosion pits were evident that could have initiated the cracks. Fractographic examination indicated indistinct beach marks and radial striations that confirmed that the crack initiation was not from erosion or corrosion pits. Cracks were described as intergranular and quasi-cleavage. There was no evidence of crack branching that would be expected if the cracks had grown by SCC.

The conclusion of the investigation was that the failures occurred due to fatigue crack growth in the blades. The cracks did not initiate at erosion or corrosion pits, as would be expected, but at a high stressed area near the blade root. Corrosion was believed to have slightly accelerated the fatigue, leading to a decreased service life. The source of the fatigue was attributed to improper assembly of the blade components leading to a vibration. Gaps were reported between laces and bosses that would lead to a detrimental vibration.

2.8.5 Erosion-Fatigue of Steam Turbine Blade (Azevedo and Sinátora [47])

Azevedo and Sinátora described a case in which steam turbine rotor blades had failed prematurely. The blades were components in a 140-MW thermoelectric plant operating in Brazil. During the investigation, it was found that 17 of the 65 blades making up the last stage of the turbine had broken. An investigation was initiated to determine the cause of the failures. Twenty-five of the blades were selected for further detailed analysis. Tests included visual inspection, nondestructive evaluation (magnetic particle and fluorescent liquid dye penetrant), stereo and scanning electron microscopic examination, chemical analysis by EDS and optical emission spectroscopy, metallography, and microhardness measurement.

The blades were forged and heat-treated 12 Cr–NiMoV martensitic stainless steel. Chemical analysis of the blades by optical emission and plasma spectroscopy indicated that the steels were within the specifications of the manufacturer. Mechanical testing of the blades by hardness indentation and tensile testing also indicated that the steels' properties were within specification of the manufacturer. The conclusion was that the blades' failure was not the result of failure of the materials.

Visual inspection of the blades revealed two distinct fracture mechanisms (see Figure 2-44 and Figure 2-45). In some cases, planar fracture surfaces were observed and described as typical of stable fatigue crack growth. In other cases, slant fracture surfaces were reported and attributed to overload failures. Remaining blades had cracks that were identified by either visual inspection or nondestructive testing. Microscopic examination identified several different morphologies associated with erosion wear. Two distinct roughness morphologies were observed on the LP side of the blades. Parallel wear grooves were observed on the lower trailing edge of the blades. Globular wear marks were reported on the leading edge of blades. These two morphologies indicate either a change in erosion mechanism or a change in impingement angle of the blade.

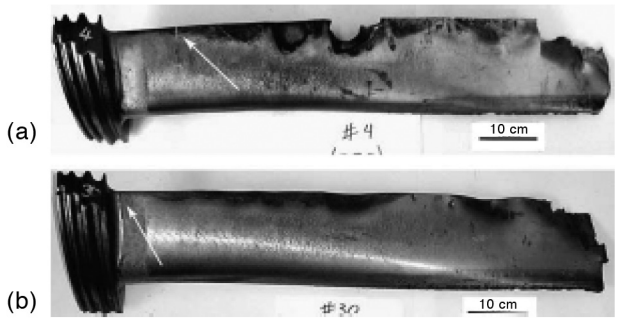


Figure 2-44
General view of two cracked blades (viewed from the LP side), revealing severe plastic deformation and missing material [47]
Used with permission from Elsevier

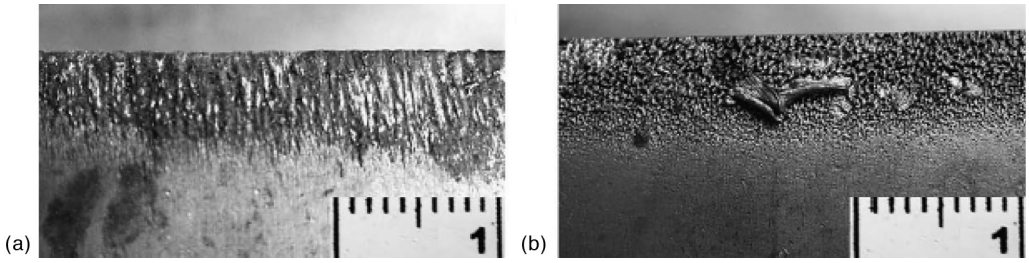


Figure 2-45
Detail of two types of severe superficial roughness that were observed on the LP side of the blades ([a] Lower trailing edge showing parallel grooves and [b] upper leading edge showing globular wear marks.) [47]
Used with permission from Elsevier

Microscopic examination of the fracture surfaces of broken blades revealed fatigue striations, and these were correlated with the wear grooves identified on the trailing edges of blades. Debris on the fracture surfaces of trailing edges was identified as iron-rich. It was hypothesized that they might have been transferred over to the turbine as iron oxide from the steam generator and subsequently reduced. This foreign debris was believed to have caused plastic deformation and material removal from the blades. The morphology of the leading edges was attributed to water droplet erosion. In both cases, the material loss led to stress risers that allowed the nucleation of fatigue cracks. Stable growth of the fatigue cracks ultimately led to blade failures that prompted the investigation.

The study highlighted the importance of erosion on the LP side of the trailing edge of the blades. Water droplets forming in the phase transition point of the LP turbine impact the blades at high speed and frequency and can contribute to significant damage. Operating transients during startup and shutdown can cause turbine vibration and the subsequent initiation of fatigue cracks from the erosion pits, which act as stress raisers. Although there was no acceleration of the fatigue crack growth by corrosive conditions in the turbine attributed to this failure, it is possible in other cases after the cracks have initiated.

3 Gap Analysis

There is a considerable body of work related to corrosion and corrosion mechanisms in LP steam turbines. Much of it has been summarized in handbooks (for example, *ASM Handbook*, Volume 13) and can be considered generic industry knowledge. EPRI has funded a significant portion of the work and is documented in reports and workshop proceedings. EPRI has also produced "State of Knowledge" reports that compile more detailed information on their test programs. Information is also readily available in journal articles and conference proceedings. These documents expand or provide more details on the work summarized elsewhere.

One of the goals of the present work is to review the current state of knowledge in the industry and to identify gaps in the knowledge. These gaps could provide avenues for future EPRI-sponsored research and become the basis for test program proposals. Funding of these programs would provide the industry with better understanding of the corrosion and damage phenomena. It is expected that this will lead to improved integrity management programs for the turbines and improved operations and maintenance protocols.

There is a significant body on work relating to blade, disk, and rotor components and on 3% NiCrMoV and ferritic and martensitic stainless alloys. These topics are of primary interest because their issues can lead to low-probability, high-consequence incidents. There appears to be much less information available on the less commonly used materials and less critical components.

Several researchers have performed work on the various corrosion mechanisms (pitting, SCC, and CF) in simulated steam turbine environments. The work includes studies of pH, effects of oxygen content, potential (both bulk and crack tip), chlorides, sulfates, organic acids, and the conditions under which they can cause corrosion susceptibility problems in the common alloys previously listed. There is little work that specifically discusses SCC-CF interactions. These mechanisms are referred to generally and are typically assumed to follow corrosion pitting.

Several papers have been published regarding pit-to-crack transitions, mostly in the last 10 years. Both experimental and modeling work has been performed. Two main groups have focused on this work—Turnbull and colleagues at the NPL in the UK and Englehardt and Macdonald working largely on behalf of EPRI. The approaches used by these two groups are similar.

One subject that does not appear to be fully addressed by the pit-to-crack transition modeling is that the source of the cracking can be corrosion pits, erosion pits, MnS inclusions, grain boundaries, or even smooth surfaces. The common approach in the modeling is based on the implicit assumption that corrosion pits are the precursor to the crack nucleation. Several of the parameters necessary for the modeling are specific to corrosion—chloride and oxygen concentrations, temperatures, pH, potential, and so on. However, a review of several case studies identified in the open literature indicated that erosion pits are a common source of SCC or CF cracks. Previous work indicated that probability of cracking was a strong function of pit depth, with less influence by environmental factors [36]. This suggests that more focus should be placed on the mechanical aspects of the pit-to-crack transition phenomena.

Current modeling work suggests that a critical crack depth is necessary for crack nucleation. Estimates vary from 25 µm in early work to more than 450 µm in the more recent advanced modeling. More recently, this critical crack depth has been based on K_{ISCC} or ΔK_{th} and predicted growth rates for both cracks and corrosion pits. The stress intensity calculations do not account for the localized stress concentrations associated with pit geometry, which will vary with pit shape and depth. The stress concen-

trations will be important only for short cracks in the order of the depth of the pits, but this is what is relevant to the pit-to-crack transition phenomena. Inclusion of a stress concentration component to the modeling might also allow prediction of crack nucleation at the sides of pits, as opposed to just at the base of pits, which is what is observed in service.

Various experimental work has been performed on SCC and CF, much of it in support of pit-to-crack transition modeling. This work has identified differences in fracture morphology. In some cases, the cracks are observed to be transgranular, and in other cases, the cracks are found to be intergranular. Fracture morphology has been shown to vary with chemistry, potential, and applied stress intensity. The variation in morphology indicates a difference in mechanism that should be considered explicitly in the modeling.

There has been much work investigating the mechanism by which impurities concentrate in steam turbines. Both thermodynamics and kinetics have been considered. There appears to be less experimental consideration of the thin liquid film nature of condensation with respect to corrosion. Given the on-off cycling of units to meet energy demands, the kinetics are increasingly important. There have been studies of transient conditions in the turbines during shutdown; these conditions are important because this is when oxygen can enter the unit and initiate pitting. Fewer studies involving corrosion have taken into account these changing conditions. In addition, the effects of excitation of blades, flow, and heat transfer should be considered.

There has been debate over the role of oxygen in pitting, particularly in initiation. Conventional wisdom is that oxygen contributes to pitting during shutdown; however, some experimental and service data appear to be contradictory. Some researchers have observed no effect of oxygen. This needs to be considered in work going forward.

The effect of pH on electrode reactions is unclear under acidic conditions. Various studies have been performed to better understand changes in environmental conditions at crack tips due to corrosion reactions and local acidification. Some researchers have reported no sensitivity to pH if below ~4. Better understanding of this insensitivity might contribute to better understanding of the corrosion mechanisms.

Currently, there is no universally accepted approach to performing SCC and CF experiments. Researchers have developed some techniques independently in order to study specific phenomena. However, this makes application of some data to service conditions difficult. A common framework of testing would be advantageous. One challenge is that the approaches used to determine theoretical or scientific details of corrosion are not necessarily the same as the approaches used to determine operational requirements.

More data on CGRs under various SCC or CF conditions would be valuable. The effects of K_{max} and ΔK on these rates should be considered. A range of conditions is possible in the turbine, particularly when different designs are considered. It is not feasible to perform testing under all conditions. Testing under more of the expected conditions would provide more statistically reliable data and serve to validate current or future modeling efforts. Current modeling efforts have been difficult to verify because of a lack of data. Ideally, test conditions would be determined in combination with analysis of transients (startup-shutdown cycling) in the turbine.

Several studies on oxide formation and stability have been performed. Oxide film stability is important in understanding corrosion susceptibility of the various alloys used in steam turbines. Also, the breakdown of oxide film and repassivation behavior are important to understanding cracking phenomena. The role of chlorides and sulfates on oxide film stability is of interest, as is oxide morphology.

4 Proposed Test Programs

Three test programs that are intended to augment recent and current research efforts are proposed in this section. There has been a significant body of work performed on corrosion issues in LP steam turbines, particularly since the Hinckley incident in 1969. Most corrosion issues are generally well understood, but some discrepancies in experimental results or expert opinions remain in the literature. It is expected that the test programs proposed herein can help resolve some of these outstanding issues.

4.1 Program One

The first test program involves continued development of the DFA model (DFAM), incorporating a more mechanically based approach in the pit-to-crack transition phenomenon. There has been significant effort over the last 10 years in the development of the DFAM. This model combines statistical arguments and various electrochemical phenomena in its predictions. The current model is based largely on a corrosion pit growth and passivation philosophy. The mechanical aspects of the crack initiation are largely buried in regression parameters.

Fracture mechanics theory indicates that crack initiation will always occur at material defects where stress intensities are high and atomic bonds can be ruptured. A next stage in the development of the DFAM could be to consider these stress intensities more actively. Stress concentrations would be expected at the base of and surrounding corrosion and erosion pits. Elasticity theory indicates that the stress concentration at the base of a pit is three times the far-field stress if the pit is semicircular, or even higher if the pit is sharper. The size of the stressed region is a function of the depth of the pit, and this affects failure probabilities. Turnbull and Zhou [34] demonstrated a variation of pit geometry under different environmental conditions and a variation in CGRs.

Experimental characterization of pits and cracks demonstrates that 50% of cracks are shallower than their associated pits [38], indicating that the pit-extending-into-a-crack approach might need to be re-evaluated. If the stress concentration around a pit is calculated, it would be demonstrated to be high (also three times the far-field stress) at the side and the base of the pits. This approach might be more successful in predicting the location of crack initiation.

Modeling efforts have demonstrated difference between short and long crack growth behavior. This could be explained by the effect of the very localized stress concentration associated with the base of the corrosion or erosion pit where the crack initiates. If this stress concentration and its distance extending into the material are actively not considered in modeling efforts, there can be discrepancies in experimental work. In addition, some researchers have reported differences in fracture morphology with crack length, implying that different crack growth mechanisms might be operative. An approach based more on fracture mechanics that accounts for stress concentration associated with pits might also provide insight on this phenomenon.

It would be possible to continue to consider loading frequency. This allows both SCC and CF to be managed by the same model. FCGRs can be plotted as a function of loading frequency and show linear behavior on a log-log plot. SCC CGRs in oil and gas pipeline steels in carbonate-bicarbonate or acidic service environments have been plotted as a function of loading frequency, and a similar approach can be used for steam turbine conditions.

Experimental work [34] using self-loaded specimens demonstrated an unexpected decrease in CGR. It was reported that data could not be fit to model equations. Incorporation of a stress intensity component might correct this problem and account for stress intensity decrease during cracking under displacement-controlled conditions.

The overall goal of this program would be to further improve the predictive capabilities of the current modeling techniques. Better predictions of pit initiation conditions and nucleation times would allow operators to better manage their inspection schedules and better understand the condition of the turbine under changing operational conditions. Modeling would allow calculation of critical stresses, stress intensities, pH, temperature, and impurity concentrations necessary to significantly decrease the probability of pitting and/or crack initiation.

4.2 Program Two

The second test program involves corrosion testing in simulated operational conditions, with specific attention to impurity concentration and potentials during on-load and off-load conditions, thin-film conditions, and transients.

Considerable progress has been made in understanding condensation of thin liquid films and the composition of impurities within these films. There appears to have been less work on applying this knowledge directly to corrosion testing. Of particular interest to operations of steam turbines is the transients in chemistry, oxygen, and potential that occur during daily or weekend off-load. Preliminary work has shown some unexpected behavior in these transients. In order to prevent corrosion in steam turbines, it is important to have a good understanding of the specific environmental condition during operation cycle, rather than just nominal conditions. If impurity, oxygen, and potential conditions vary, corrosion susceptibility also varies. Zhou and Turnbull [25] demonstrated delayed response of potential during cycling on and off load, and they indicated possible increased pitting susceptibility.

An important aspect of this work might be consideration of thin-film conditions rather than bulk solutions. Corrosion testing in bulk solutions is common for experimental convenience. However, the thin films condensing on steam turbine parts and the kinetics of impurity concentration can lead to different corrosive conditions. It is important that service conditions be replicated where possible—for example, by conducting tests in condensing steam. Bulk conditions are not necessarily valid for all conditions.

The role of oxygen in SCC crack initiation in turbines has been debated. Most researchers have argued that oxygen is detrimental, although a smaller number of researchers have not considered it important. One argument is that oxygen has not been measured in the condensate films. There is also the decreased concentration of impurities to consider when OT is used.

The overall goal of this program would be to confirm that corrosion susceptibility and rates are comparable in thin film and transient conditions, which is more realistic from an operational perspective. Any differences in corrosion behavior between testing in bulk solutions (or nominal conditions) versus thin film (or transient conditions) would be highlighted, and this might allow for improved corrosion management protocols.

4.3 Program Three

The third test program further examines CGRs for SCC and CF conditions, with specific attention to crack morphology (transgranular or intergranular). The program considers short versus long cracks, the effects of oxygen/impurities, and potential.

Some modeling efforts differentiate between short and long cracks. Experimentally, short and long cracks have been shown to have different fracture morphologies [38]. This also indicates that different mechanisms could be considered for the modeling. Proposed Program One suggested that consideration of the local stress concentration associated with pits might provide guidance. Very short cracks, with depth comparable to pit depth, would experience these stress concentrations. Longer cracks would not. One would expect a transition as the crack grows. If one compares the critical stress concentration K_{ISCC} for SCC and the threshold change in stress intensity ΔK_{th} for fatigue, there could be a change in mechanism that explains the change in fracture morphology.

Experiments have demonstrated impurities and their potential effect on fracture morphology [33]. These effects also relate to more environmentally or mechanically driven crack growth conditions. Given the changes in environmental conditions during the lifetime of the steam turbine and differences during operations and shutdown, it is reasonable that the mechanisms of cracking might change. In addition, one could consider the effect of frequency on these cracking mechanisms. A high-frequency fatigue load would be expected to be more mechanically driven than a lower frequency fatigue load, which would likely be driven more by corrosion.

Experiments by Ebara (2004) demonstrated that fracture morphology varies with K_{max} during load cycling. This is an interesting phenomenon that should be considered for modeling and predictive efforts.

The overall goal of this test program would be to clarify understanding of the cracking mechanisms responsible for damage in the turbine. Improved understanding of these mechanisms and the conditions influencing them would lead to better CGR predictions and overall better conditional assessment of the turbine during operations.

4.4 Other Considerations

In addition to the three test programs previously presented, the following tasks need to be considered in order to resolve the outstanding issues on LP steam turbine corrosion mechanisms and their interactions:

- Experimental determination of SCC and/or CF CGRs in environments specifically applicable to startup/shutdown transients
- Experimental determination of threshold stress or stress intensity for SCC in environments specifically applicable to startup/shutdown transients
- Further study on erosion of blades—failure analysis literature indicates that erosion pits are often a precursor to crack initiation
- Development of a standardized test method for SCC and CF susceptibility of turbine materials to allow better comparison of the effects of the environment
- Mitigation or repair technique effectiveness for SCC/CF cracks. For example, a study of shot-peening during fabrication to reduce stresses or grinding of cracks to prevent propagation
- Further study of the role of pH in pitting and crack propagation mechanisms, particularly with respect to pitting and crevice geometries
- A survey of turbine operators to determine more recent issues leading to failures

5 Summary and Conclusions

The work described in this report is a compilation and summary of various research literature on the topic of corrosion mechanisms and their interactions in LP steam turbines. Various aspects have been considered, including turbine design, components, materials, corrosion mechanisms (pitting, SCC, and CF), steam turbine chemistry, and pit-to-crack transitions. Several case studies presented summarize investigations performed following in-service failures.

There is considerable information available to describe the individual corrosion phenomena in environmental conditions relevant to steam turbine operations. However, there is less information available on the interaction of the various corrosion mechanisms. There is also less information available describing corrosion testing in simulated operational conditions, specifically, testing under steam-condensing conditions or with simulated startup/shutdown transients. Given the changing nature of corrosion susceptibility with service conditions, these topics are of interest.

Considerable effort has been put toward modeling of pit-to-crack transitions and damage evolution in steam turbine environments. These models tend to be fairly complex, taking into account specific details of corrosion mechanisms and combining them with various statistical arguments. There are limited data available to thoroughly verify the correctness and applicability of these models to operational service. Evidence from in-service failures indicates that many cracks do not initiate from corrosion pits, and this should be considered in modeling going forward.

Several case studies have been discussed. These cases studies were identified during searches of the available literature (primarily, corrosion engineering and engineering failure analysis journals and conference proceedings). Only one of the case studies specifically identified transitions from corrosion pits to SCC/CF cracks as the failure cause.

Three test programs have been proposed. The goal of these test programs is to better understand the various corrosion mechanisms and their interactions. Better understanding of these mechanisms will lead to improved predictive capabilities and better management of steam turbine corrosion during operation.

6 References

6.1 In-Text References

1. *Low-Temperature Corrosion Problems in Fossil Power Plants—State of Knowledge Report*. EPRI, Palo Alto, CA: 2003. 1004924.
2. "Progress in Understanding Improves Outlook for Control of Turbine-Steam Chemistry." *Power*, March 1981.
3. *Priorities for Corrosion Research and Development for the Electric Power Industry*. EPRI, Palo Alto, CA: 2002. 1007274.
4. O. Jonas, "Corrosion of Steam Turbines." *Metals Handbook* 9th Edition, Volume 13. ASM International, Metals Park, OH: 1987.
5. *Turbine Steam Path Damage: Theory and Practice*. EPRI, Palo Alto, CA: 1999. AP-108943.
6. *Steam Turbine Disc Cracking Experiences—Volumes 1–7*. EPRI, Palo Alto, CA: 1982. NP-2429-LDV1 through NP-2429-LDV7.
7. S. Holdsworth, "Prediction and Prevention of Stress Corrosion and Corrosion Fatigue Cracking LP Steam Turbines." *Proceedings: Advances in Life Assessment and Optimization of Fossil Power Plants*. EPRI, Palo Alto, CA: 2002. 1006965.
8. M. Speidel and R. Magdowski, "Correlation of Laboratory and Field Stress Corrosion Results in the Power Generation Industry." NACE Paper 146 presented at Corrosion 1999.
9. J. Denk, "A New Super-Clean High Pressure, Low-Pressure Rotor Steel for Advanced Combined Cycle Power Plants." Presented at the Prof. Conf. Clean Steel: Superclean Steel, Institute of Materials, London, UK (March 6–7, 1995).
10. T. Tsuchiyama and T. Nakayama, "Stress Corrosion Cracking Behavior of 3.5NiCrMoV Steel in Carbonated Pure Water." NACE Paper 247 presented at Corrosion 1998.
11. I. Wright and B. Pint, "An Assessment of the High-Temperature Oxidation Behavior of Fe-Cr-Steels in Water Vapor and Steam." NACE Paper 02377 presented at Corrosion 2002.
12. R. Setterland, V. Malhotra, and L. Friesen, "Failure of 13% Chromium Stainless Steel Impeller for Hydrogen Recycle Compressor." NACE Paper 00683 presented at Corrosion 2000.
13. A. Turnbull, "Environmentally Assisted Cracking of Steam Turbine Steels—Modelling of Crack Chemistry." NACE Paper 01237 presented at Corrosion 2001.
14. O. Jonas, "Steam Turbine Corrosion." *Materials Performance*, February 1985a.
15. H. Haas, "Major Damage Caused by Turbine or Generator Rotor Failures in the Range of the Tripping Speed." *Der Maschinenschaden*, June 1997.
16. A. Atrens et al., "Steam Turbine Blades." *Corrosion of Power Generating Equipment*, Plenum Press, New York, NY: 1984.

17. C.-K. Lin, W.-C. Fan, and W.-J. Tsai, "Corrosion Fatigue of Precipitation-Hardening Martensitic Stainless Steel." *CORROSION: The Journal of Science and Engineering*, NACE International, Vol. 58, No. 11, pp. 904–12, November 2002.

18. G. Das, S. Ghosh Chowdhury, A. Ray, S. Das, and D. Bhattacharya, "Turbine blade failure in a thermal power plant." *Engineering Failure Analysis*, Vol. 10, pp. 85–91, 2003.

19. *Corrosion of Low Pressure Steam Turbine Components*. EPRI, Palo Alto, CA: 2000. 1000557.

20. J. Lyons and J. Cornish, "The Corrosion of a 12Cr Alloy in a Carbonic Acid Environment in a High-Pressure Steam Turbine." *Corrosion Science*, Vol. 38, No. 8, pp.1331–56, 1996.

21. W. Maeng and D. Macdonald, "The effect of acetic acid on the stress corrosion cracking of 3.5NiCrMoV turbine steels in high-temperature water." *Corrosion Science*, Vol. 50, pp. 2239–50, 2008.

22. *Proceedings: Steam Turbine Stress Corrosion Workshop*. EPRI, Palo Alto, CA: 1997. TR-108982.

23. V. Otieno-Alego, G. Hope, H. Flitt, and D. Schweinsberg, "The Corrosion of a Low Alloy Steel in a Steam Turbine Environment: The Effect of Oxygen Concentration and Potential Scan Rate on Input Parameters Used to Computer Match the Experimental Polarization Curves." *Corrosion Science*, Vol. 37, No. 3, pp. 509–25, 1995.

24. W. Maeng, J. Lee, and U. Kim, "Environmental effects on the stress corrosion cracking susceptibility of 3.5 NiCrMoV steels in high temperature water." *Corrosion Science*, Volume 47, pp. 1876–95, 2005.

25. S. Zhou and A. Turnbull, "Impact of transient chemistry on the corrosion potential of a steam turbine disc steel." *Corrosion Science*, Vol. 49, pp. 2474–85, 2007.

26. A. Turnbull, S. Zhou, and G. Hinds, "Stress corrosion cracking of steam turbine disc steel—measurement of the crack tip potential." *Corrosion Science*, Vol. 46, pp. 193–211, 2004.

27. J. Scully and H. Scully, "Environmental Cracking Susceptibility of AIS 422 Stainless Steel in NH4HCO3/NH4OH Solution at 70°C." *CORROSION: The Journal of Science and Engineering*, Vol. 49, No. 2, February 1993.

28. V. Otieno-Alego, G. Hope, H. Flitt, and D. Schweinsberg, "The Pitting of Low Alloy Turbine Disc Steel." *Corrosion Science*, Vol. 35, Nos. 1–4, pp. 103-9, 1993.

29. J. Gonzalez-Rodriguez, V. Salinas-Bravo, and A. Martinez-Villefañe, "Hydrogen Embrittlement of Type 410 Stainless Steel in Sodium Chloride, Sodium Sulfate, and Sodium Hydroxide Environments at 90°C." *CORROSION: The Journal of Science and Engineering*, Vol. 53, No. 6, June 1997.

30. J. Gonzalez-Rodriguez, V. Salinas-Bravo, and A. Martinez-Villefañe, "Stress Corrosion Cracking of Type 403 Stainless Steel in Sodium Chloride at 95°C Under Different Heat Treatment Conditions." *CORROSION: The Journal of Science and Engineering*, Vol. 55, No. 10, October 1999.

31. D. Rosario, C. Wells, R. Viswanathan, and G. Licina, "Stress Corrosion Cracking of Steam Turbine Rotors." *CORROSION: The Journal of Science and Engineering*, Vol. 54, No. 7, July 1998.

32. X. Zhou, J. Congleton, and A. Bahraloloom, "Mechanisms of Stress Corrosion Cracking for Iron-Based Alloys in High-Temperature Water." *CORROSION: The Journal of Science and Engineering*, Vol. 54, No. 11, pp. 898–910, November 1998.

33. H. Shalaby, J. Begley, and D. Macdonald, "Phenomenological Aspects of Fatigue Crack Initiation and Propagation in Type 403 Stainless Steel in Simulated Steam Cycle Environments." *CORROSION: The Journal of Science and Engineering*, Vol. 52, No. 4, April 1996.

34. A. Turnbull and S. Zhou, "Pit to crack transition in stress corrosion cracking of a steam turbine disc steel." *Corrosion Science*, Vol. 46, No. 5, pp. 1239–64, May 2004.

35. P. Andresen, "Probabilistic Interpretation of SCC Initiation and Growth." NACE Paper 446 presented at Corrosion 1999.

36. G. Englehardt, D. Macdonald, Y. Zhang, and R. Dooley, "Deterministic Prediction of Corrosion Damage in Low Pressure Steam Turbines." *PowerPlant Chemistry*, Vol. 6, No. 11, pp. 647–61, 2004.

37. D. D. Macdonald and M. Urquidi-Macdonald, *Corrosion Science*, Vol. 48, 354 (1992).

38. A. Turnbull, L. McCartney, and S. Zhou, "A model to predict the evolution of pitting corrosion and the pit-to-crack transition incorporating statistically distributed input parameters." *Corrosion Science*, Vol. 48, pp. 2084–105, 2006.

39. *Development of Model to Predict Stress Corrosion Cracking and Corrosion Fatigue of Low Pressure Turbine Components*. EPRI, Palo Alto, CA: 2007. 1012204.

40. D. Macdonald and G. Englehardt, "Towards a Mechanism Based Theory for Crack Initiation." NACE Paper 01116 presented at Corrosion 2001.

41. Y. Zhang, D. Macdonald, M. Urduiqi-Macdonald, G. Englehardt, and R. Dooley, "Prediction of Pitting Corrosion of AISI Type 403 Stainless Steel in Chloride-Containing Borate Buffer Solution." *PowerPlant Chemistry*, Vol. 9, No. 7, pp. 401–8, 2007.

42. *Determination of Damage Function for the Pitting of AISI Type 403 Blade Alloy and 17-4PH Blade Alloy*. EPRI, Palo Alto, CA: 2007. EP-P1150-C434.

43. G. Englehardt, D. Macdonald, and R. Dooley, "The Prediction of Blade and Disc Failures in Low Pressure Steam Turbines." *PowerPlant Chemistry*, Vol. 9, No. 8, pp. 454–62, 2007.

44. N. Mukhopadhyay, S. Ghosh Chowdhury, G. Das, I. Chattoraj, S. Das, and D. Bhattacharya, "An Investigation of the Failure of Low Pressure Steam Turbine Blades." *Engineering Failure Analysis*, Vol. 5, No. 3, pp 181–193, 1998.

45. R. Ebara, "Corrosion fatigue phenomena learned from failure analysis." *Engineering Failure Analysis*, Vol. 13, pp. 515–26, 2006.

46. W.-Z.Wang, F.-Z. Xuan, K.-L. Zhu, and S.-T. Tu, "Failure analysis of the final stage blade in steam turbine." *Engineering Failure Analysis*, Vol. 14, pp. 632–41, 2007.

47. C. Azevedo and A. Sinátora, "Erosion-fatigue of steam turbine blades." *Engineering Failure Analysis*, Vol. 16, pp. 2290–303, 2009.

6.2 Bibliography

D. Bain and D. Christophersen, "Some Common Mechanisms Leading to Failures in Heat Recovery Steam Generators." NACE Paper 03489 presented at Corrosion 2003.

G. Bignold and G. Quirk, "Electrochemical Noise Measurements in a 500 MW Steam Turbine to Maximize Lifetime under Changing Operational Demands." NACE Paper 02333 presented at Corrosion 2002.

B. Brisson, R. Ballinger, and A. McIlree, "Intergranular Stress Corrosion Cracking Initiation and Growth in Mill-Annealed Alloy 600 Tubing in High-Temperature Caustic." *CORROSION: The Journal of Science and Engineering*, Vol. 54, No. 7, pp. 504–15, July 1998.

I. Cotton, "On-Line Dissolved Oxygen Monitoring in Boiler Feedwater Systems." NACE Paper 00661 presented at Corrosion 2000.

D. Domogala, J. Buffa, and D. Nesbitt, "A Case History for the Mitigation of Salt Water Intrusion into a Boiler Steam Cycle." NACE Paper 00435 presented at Corrosion 2000.

G. Englehardt and D. Macdonald, "Modeling the Crack Propagation Rate for Corrosion Fatigue at High Frequency of Applied Stress." Article submitted to *Corrosion Science*, August 2009.

Moisture Nucleation in Steam Turbines. EPRI, Palo Alto, CA: 1997. TR-108942.

Proceedings: Workshop on Corrosion of Steam Turbine Blading and Disks in the Phase Transition Zone. EPRI, Palo Alto, CA: 1998. TR-111340.

Descriptions of Past Research: EPRI Fossil and Nuclear Steam Turbines and Generators— Volume 2. EPRI, Palo Alto, CA: 2006. 1013643.

M. Esmacher, "Stress Corrosion Cracking of Stainless Steel Components in Steam Service." NACE Paper 01496 presented at Corrosion 2001.

D. Gray and C. McDonough, "On-Line pH Measurement for Steam Generating Systems." NACE Paper 00665 presented at Corrosion 2000.

G. Holcomb, B. Covino, D. Alman, S. Bullard, S. Cramer, and M. Ziomek-Moroz, "Supercritical Steam in Power Production—A Materials Review." NACE Paper 04486 presented at Corrosion 2004.

L. Machemer, O. Jonas, and B. Dooley, "Steam Cycle Advisor." NACE Paper 04060 presented at Corrosion 2004.

R. Port, "Flow Accelerated Corrosion." NACE Paper 721 presented at Corrosion 1998.

R. Rebak and Z. Szklarska-Smialoska, "Influence of Stress Intensity and Loading Mode on Intergranular Stress Corrosion Cracking of Alloy 600 in Primary Waters of Pressurized Water Reactors." *CORROSION: The Journal of Science and Engineering*, NACE International, Vol. 50, No. 5, pp. 378–94, May 1994.

J. Robinson and T. Drews, "Resolving Flow-Accelerated Corrosion Problems in the Industrial Steam Plant." NACE Paper 346 presented at Corrosion 1999.

Z. Szklarska-Smialoska, R. Rebak, and P. Skulte, "Susceptibility of Low-Alloy Carbon Steel to Pitting and Stress Corrosion Cracking in Steam Generator Conditions." *CORROSION: The Journal of Science and Engineering*, Vol. 50, No. 4.

A. Turnbull, "Modelling of Environmental Assisted Cracking." Corrosion Science, Vol. 34, No. 6, pp. 921–60, 1993.

J. Jing, Y. Sun, S. Xia, and G. Feng, "A continuum damage mechanics model on low cycle fatigue life assessment of steam turbine rotor." *International Journal of Pressure Vessels and Piping*, Vol. 78, No. 1, pp. 59–64, January 2001.

J. Jing, G. Meng, Y. Sun, and S. Xia, "An effective continuum damage mechanics model for creep fatigue life assessment of a steam turbine rotor." *International Journal of Pressure Vessels and Piping*, Vol. 80, No. 6, pp. 389–96, June 2003.

A. Bagaviev and A. Ulbrich, "Life assessment of turbine components based on deterministic and probabilistic procedures." *International Journal of Pressure Vessels and Piping*, Vol. 81, Nos. 10 and 11, pp. 855–59, October/November 2004.

A. Rusin, Technical risk involved in long term operations of steam turbines. *"Reliability Engineering and System Safety,"* Vol. 92, pp. 1242–49, 2007.

Export Control Restrictions

Access to and use of EPRI Intellectual Property is granted with the specific understanding and requirement that responsibility for ensuring full compliance with all applicable U.S. and foreign export laws and regulations is being undertaken by you and your company. This includes an obligation to ensure that any individual receiving access hereunder who is not a U.S. citizen or permanent U.S. resident is permitted access under applicable U.S. and foreign export laws and regulations. In the event you are uncertain whether you or your company may lawfully obtain access to this EPRI Intellectual Property, you acknowledge that it is your obligation to consult with your company's legal counsel to determine whether this access is lawful. Although EPRI may make available on a case-by-case basis an informal assessment of the applicable U.S. export classification for specific EPRI Intellectual Property, you and your company acknowledge that this assessment is solely for informational purposes and not for reliance purposes. You and your company acknowledge that it is still the obligation of you and your company to make your own assessment of the applicable U.S. export classification and ensure compliance accordingly. You and your company understand and acknowledge your obligations to make a prompt report to EPRI and the appropriate authorities regarding any access to or use of EPRI Intellectual Property hereunder that may be in violation of applicable U.S. or foreign export laws or regulations.

The Electric Power Research Institute Inc., (EPRI, www.epri.com) conducts research and development relating to the generation, delivery and use of electricity for the benefit of the public. An independent, nonprofit organization, EPRI brings together its scientists and engineers as well as experts from academia and industry to help address challenges in electricity, including reliability, efficiency, health, safety and the environment. EPRI also provides technology, policy and economic analyses to drive long-range research and development planning, and supports research in emerging technologies. EPRI's members represent more than 90 percent of the electricity generated and delivered in the United States, and international participation extends to 40 countries. EPRI's principal offices and laboratories are located in Palo Alto, Calif.; Charlotte, N.C.; Knoxville, Tenn.; and Lenox, Mass.

Together...Shaping the Future of Electricity

Program:

Steam Turbines-Generators and Auxiliary Systems

© 2010 Electric Power Research Institute (EPRI), Inc. All rights reserved. Electric Power Research Institute, EPRI, and TOGETHER...SHAPING THE FUTURE OF ELECTRICITY are registered service marks of the Electric Power Research Institute, Inc.

1020671

Electric Power Research Institute
3420 Hillview Avenue, Palo Alto, California 94304-1338 • PO Box 10412, Palo Alto, California 94303-0813 USA
800.313.3774 • 650.855.2121 • askepri@epri.com • www.epri.com